School of Chemical and Petroleum Engineering

Novel Carbon Dioxide Tolerant Ceramic Membrane for Air Separation and Clean Energy Delivery

Kun Zhang

This thesis is presented for the Degree of

Doctor of Philosophy

of

Curtin University

June 2013

Declaration

To the best of my knowledge and belief this thesis contains no material previously published by any other person except where due acknowledgement has been made.

This thesis contains no material which has been accepted for the award of any other degree or diploma in any university.

Signature:……

Date:……...

ABSTRACT

The ceramic membrane with oxygen ion transport ability is drawing ever-increasing attention due to its potential in oxygen production and clean energy delivery. Despite the good progress of the ceramic membrane separation technology, there are still a number of fundamental issues and technological challenges which need to be overcome prior to its further development and commercialization. One of the major hurdles currently impeding the ceramic membrane is its poor material stability under the real application conditions, e.g., with the presence of CO_2 containing atmosphere. Meanwhile, this kind of oxygen selective ceramic membrane is limited only to these high temperature operations and the required qualified sealing technigue is still challenging the membrane module design. Obviously, development of new ceramic membranes that can operate at intermediate temperatures will push the technology closer toward its practical application. The overall objective of this thesis is to develop new robust ceramic membranes with improved stability to be operated in CO_2-containing atmosphere without losing the high permeation flux compared to the existing ceramic membranes.

Based on excellent oxygen ion conducting ability and material stability from fluorite oxides, a new concept for oxygen separation by using the oxygen ion conducting ceramic membrane with external short circuit is successfully developed. In this concept, the mixed conducting function can be realized via the oxygen ion diffusion inside the fluorite (i.e., $Sm_{0.2}Ce_{0.8}O_2$, SDC) bulk and electronic conduction along the external electric circuit, avoiding the mutual obstruction problem often resulted from the conventional dual-phase membrane synthesised by powder mixing. This new membrane concept has been verified by the direct detection and measurement of electrical currents which agree very well with the theoretical calculation based on the equation correlating Faraday constant and oxygen flux. With the strong chemical stability against acid gases like CO_2 and the higher oxygen fluxes at lower temperatures, this novel membrane concept possibly brings in a breakthrough for tonnage oxygen production to improve the viability of these clean energy technologies.

In order to further improve oxygen flux of this novel external short circuiting membrane, and better understand the influence of operation conditions (e.g. the

various CO_2 and H_2O concentrations) on the oxygen flux, e.g., yttria stabilized bismuth oxide (YSB) membranes were examined. The membrane was prepared using a self-made YSB powder under an easy sintering condition with temperatures lower than 850 ^oC and characterized by SEM and porosity measurement. The prepared membranes were tested for air separation under the novel design pure ion conductor with external short circuit. The oxygen permeation fluxes of the YSB membrane decreased with increasing the CO_2 concentration in sweep gas and such flux decline was mainly due to the chemical adsorption of CO_2 to the membrane surface. YSB can withstand the presence of CO_2 atmosphere at high temperatures without causing any reaction between them. More interesting is that, contrary to the negative effect of the water vapor on perovskite membranes, the presence of H_2O is beneficial for oxygen permeation through the YSB membrane. The maximum oxygen flux achieved was 1.33 ml cm^{-2} min^{-1} at 850 ^oC for YSB membrane with a thickness of 1mm. Thin-film membrane technology and surface modification can help to further improve the O_2 fluxes.

Furthermore, to potentially develop oxygen permeable ceramic membrane for portable and high oxygen permeation flux, electrochemical oxygen pump ceramic membranes based on SDC electrolyte and $La_{0.6}Sr_{0.4}FeO_{3-\delta}$ (LSF) electrode were developed. The oxygen electrical permeation behavior of SDC/LSF membrane was investigated under different operating conditions. In consistent with the theoretical prediction from Faraday law, the observed oxygen flux value was closely correlated in quantity with the applied current density. The permeation (or Faraday) efficiency of SDC/LSF membrane could reach above 95% at lower temperatures (600-700^oC). At 700^oC, the oxygen flux through SDC/LSF membrane with 3000 mA·cm^{-2} current density could reach up to 9.97 ml cm^{-2} min^{-1}. It is found that SDC/LSF membrane has excellent structure and permeation stability against CO_2 gas, reflecting its potential applications in oxyfuel technologies or hydrocarbon oxidations.

To further develop ceramic membrane technology with different application purpose, another novel membrane configuration with internal short circuit is proposed for air separation based on the fundamental understanding of the working principles of solid oxide fuel cells. To experimentally demonstrate this novel design, SDC was still used as the membrane material. Oxygen permeation results clearly demonstrated that one internal short circuit in the membrane was sufficient to enable the membrane to

function, thus simplifying the planar membrane design for future scaling up. In addition, the robustness of the membranes was proven by long term exposure to acid gases (CO_2 and CO_2/H_2O) as O_2 fluxes reverted back to original values of 0.4 ml min^{-1} cm^{-2} once these acid gases were switched off. Tested under similar conditions, high O_2 flux through conventional perovskite membranes failed, thus clearly indicating the potential adaptability of the novel SDC membrane to real world industrial application.

In an effort to address the environmental problem from CO_2 emission as well as to achieve high chemical conversion efficiency, membrane reactor based on fluorite SDC utilizing external short circuit concept for oxygen permeation was demonstrated for CO_2 reduction coupled with methane partial oxidation. The fluorite phase was employed to impart its high structural stability while its limited electronic conductivity was enhanced with the help of an external short circuit to function the SDC membrane for oxygen transport. On one side of the membrane i.e. feed side, carbon dioxide decomposition into carbon monoxide and oxygen was carried out with the aid of Pt or Ag catalyst. As such, the required driving force for gas transport through the membrane can be sustained by coupling two different reactions in one membrane reactor. More importantly, we proved the feasibility of highly stable membrane reactor based on external short circuit as evidenced by achieving the reliable performance in CO selectivity, CH_4 conversion, CO_2 conversion and O_2 flux during 100-hour operation along with unchanged membrane structure after this operation together with the coking resistance.

This novel membrane design using short circuit structure in principle can be extended to any other dense mixed conducting oxide membranes for gas separations like mixed proton and electronic conducting membranes for hydrogen separation or mixed carbonate ion and electronic conducting membranes for CO_2 separation. Thus, the improvement of hydrogen flux through proton conducting membranes via the external short circuit was also demonstrated on $BaZr_{0.1}Ce_{0.2}Y_{0.7}O_{3-\delta}$ and $BaZr_{0.3}Ce_{0.6}Y_{0.1}Zn_{0.05}O_{3-\delta}$ oxides.

Finally, to further use the benefit of strong stability of SDC oxide film, a SDC function layer on a conventional perovskite membrane is developed via deposition

method. The SDC shell functions as the protecting layer to strengthen the membrane stability against CO_2 acid gas, but also improve the oxygen permeation flux.

Acknowledgements

Firstly, I would like to express my sincere gratitude to my principle supervisor, Prof. Shaomin Liu, for his continuous guidance, support and inspiration during the course of this work. He has made much valuable help on my life and studies. Without him, my PhD research would not be possible.

I am deeply grateful to my co-supervisor, Prof. Shaobin Wang, and my thesis committee chairperson, Prof. Moses Tade, for their advice, assistance, and help as thesis committee members. I am also very grateful to Prof. Zongping Shao and Prof. Chun-Zhu Li for their useful advice and support of using the equipments during this work.

I would like to thank many members in the department of Chemical Engineering for their friendship and help (in no particular order): Dr. Yi Wang, Dr. Xiang Li, Dr. Xun Hu, Dr. Yun Yu, Dr. Hongqi Sun, Dr. Dezhi Han, Dr. Lihong Liu, Dr. Ling Zhao, Dr. Kongfa Chen, Dr. Na Ai, Dr. Beibei He, Dr. John Bromly, Dr. Dehua Dong, Xin Shao, Zhitao Wang, Yi Cheng, Lei Zhang, Tingting Li, Liping Wu, Shuai Wang, Dr. Huangang shi, Yuan Zou, Dr. Chao Su, Ruijuan Song, Zhangfen Shen, Wentai Wang and Mortaza Gholizadeh.

Most of all, I would like to thank my mothers and fathers for everything they did to support me. Without their selfless love and concern, it would have been impossible for me to have completed this thesis. To my beautiful wife Baoling, words fail me to thank her endless love. My thanks are also extended to all my families and friends who gave me lots of love and supports.

LIST OF PUBLICATIONS

[1] **Kun Zhang**, Jaka Sunarso, Zongping Shao, Wei Zhou, Chenghua Sun, Shaobin Wang, Shaomin Liu, Research progress and materials selection guidelines on mixed conducting perovskite-type ceramic membranes for oxygen production, ***RSC Advances***, 1(2011)1661-1676

[2] **Kun Zhang,** Zongping Shao, Chun-zhu Li, Shaomin Liu, Novel CO_2-tolerant ion-transporting ceramic membranes with an external short circuit for oxygen separation at intermediate temperatures, ***Energy Environmental Science***, 5(2012)5257-5264.

[3] **Kun Zhang**, Yuan Zou, Chao Su, Zongping Shao, Lihong Liu, Shaobin Wang, Shaomin Liu, CO_2 and water vapour-tolerant Yttria Stabilized Bismuth Oxide (YSB) Membranes with External Short Circuit for Oxygen Separation with CO_2 Capture at Intermediate Temperatures, ***Journal of membrane science***, 427(2013)168-175.

[4] **Kun Zhang**, Lihong Liu, Zongping Shao, Rong Xu, João C. Diniz da Costa, Shaobin Wang, Shaomin Liu, Robust ion-transporting ceramic membrane with an internal short circuit for oxygen production, ***Journal of Materials Chemistry A***, Accepted, 2013.

[5] **Kun Zhang**, Jaka Sunarso, Gia H. Pham, Shaobin Wang, Shaomin Liu, External short circuit-assisted proton conducting ceramic membrane for H_2 permeation, ***Ceramics International***, Accepted**,** 2013.

[6] **Kun Zhang**, Lihong Liu, Zongping Shao, Shaobin Wang, Shaomin Liu, CO_2-tolerant ceramic membrane driven by electrical current for oxygen production at intermediate temperatures, ***Journal of the American Ceramic Society***, Under revised, 2013.

[7] **Kun Zhang**, Lihong Liu, R. Xu, Zongping Shao, J. C. D. da Costa, Shaomin Liu, High Performance BSCF Membrane with SDC Shell for Oxygen Production, ***J. Mater. Chem. A***, submitted, 2013.

[8] **Kun Zhang**, Jaka Sunarso, Lihong Liu, J. C. D. da Costa, Shaomin Liu, Highly stable external short circuit assisted-oxygen ionic transport membrane reactor for carbon dioxide reduction coupled with methane partial oxidation, ***Energy & Fuels***, submitted, 2013.

[9] Meng Bo, Hao Guizeng, Qin Jingcan, Tan Xiaoyao, **Kun Zhang**, Shaomin Liu, $La_{0.3}Sr_{0.7}Fe_{0.7}Cu_{0.2}Mo_{0.1}O_3$ perovskite catalyst and its hollow fiber membrane for gas reactions, ***Applied Catalysis-A: General***, submitted, 2013.

[10] S. Zhang, C. Du, Z. Wang, X. Han, **Kun Zhang**, L. Liu, Reduced cytotoxicity of silver ions to mammalian cells at high concentration due to the formation of silver chloride, ***Toxicology in Vitro***, 27 (2013) 739-744.

[11] Xihan Tan, Xiaoyao Tan, Naitao Yang, Bo Meng, **Kun Zhang**, Shaomin Liu, High Performance $BaCe_{0.8}Y_{0.2}O_{3-\delta}$ (BCY) Hollow Fiber Membranes for Hydrogen Permeation, ***Journal of the American Ceramic Society***, Submitted, 2013.

[12] Xiaoyao Tan, Nan Liu, Bo Meng, Jaka Sunarso, **Kun Zhang**, Shaomin Liu, Oxygen permeation behavior of La0.6Sr0.4Co0.8Fe0.2O3 Hollow fibre membranes with highly concentrated CO_2 exposure, ***Journal of Membrane Science***, 389 (2012) 216-222.

Table of Contents

Declarations ····· i

Abstract ····· ii

Acknowledgements····· vi

Publications ····· vii

Table of Contents····· viii

List of Figures····· xii

List of Tables····· xviii

Chapter 1: Introduction

1.1 Background·····1

1.2 Objectives and outline of the thesis·····2

1.3 References·····6

Chapter 2: Literature Review

2.1 Introduction·····8

2.2 Fundamental of ceramic membranes for oxygen production·····10

2.2.1 General characteristics of mixed conducting dense ceramic membranes·····10

2.2.2 Oxygen transport·····12

2.2.3. Oxygen permeation rate determining factors·····13

2.2.3.1 Bulk diffusion·····14

2.2.3.2 Surface exchange·····15

2.2.4 Ceramic hollow fibre membranes·····19

2.2.5 Non-perovskite compounds·····21

2.3 Perovskite compounds·····25

2.3.1 Cobalt-containing perovskites·····29

2.3.2 Cobalt-free perovskites····· 33

2.3.3 Selection of perovskite for oxygen permeation membrane····· 35

2.3.3.1. Contributing aspects to the selection of membrane materials····· 36

2.3.3.1.1 Oxygen migration····· 37

2.3.3.1.2 Stability····· 39

2.3.3.1.3 Guidelines····· 40

2.4 Application of mixed conducting membranes for clean energy delivery·· 42

2.5 Summary and future development····· 44

2.6 References·····48

Chapter 3: Novel CO_2-tolerant ion-transporting ceramic membranes with external short circuit for oxygen separation at intermediate temperatures.

3.1 Introduction····· 60

3.2 Experimental Section····· 64

3.3 Results and discussion····· 66

3.4 Conclusions····· 76

3.5 References····· 77

Chapter 4: Enhanced oxygen permeation performance of CO_2 tolerant ion conducting membrane with easily sintered bismuth-based oxide

4.1 Introduction·····81

4.2 Experimental Section·····83

4.3 Results and discussion·····85

4.4 Conclusions·····97

4.5 References·····98

Chapter 5: CO_2-tolerant ceramic membrane driven by electrical current for oxygen production at intermediate temperatures

5.1 Introduction····· 101

5.2 Experimental Section·····104

5. 3 Results and discussion·····106

5.3.1 Preparation of SDC/LSF EOP membrane····· 106

5.3.2 Oxygen permeation behavior driven by electrical current·····108

5.3.3 SDC/LSF membrane stability in CO_2 atmosphere·····113

5.4 Conclusions·····116

5.5 References·····116

Chapter 6: Robust ion-transporting ceramic membrane with an internal short circuit for oxygen production.

6.1 Introduction····· 119

6.2 Experimental Section····· 123

6.3 Results and discussion····· 124

6.3.1Membrane Preparation and Characterization····· 124

6.3.2 Oxygen Permeation Test ····· 127

6.3.3 Stability Test····· 132

6.4 Conclusions····· 134

6.5 References····· 135

Chapter 7: Highly stable external short circuit assisted-oxygen ionic transport membrane reactor for carbon dioxide reduction coupled with methane partial oxidation

7.1 Introduction·····138

7.2 Experimental section·····141

7.3 Results and discussion·····144

7.3.1Membrane reactor performance using 1-mm thick SDC membrane·····144

7.3.2 Membrane reactor performance using asymmetric SDC membrane·····145

7.3.3 Effects of CO_2 and CH_4 flow rate·····149

7.3.4 Long-term stability·····151

7.4 Conclusions·····154

7.5 References·····154

Chapter 8: External short circuit-assisted proton conducting ceramic membrane for H_2 permeation

8.1 Introduction·····157

8.2 Experimental section·····159

8.3 Results and discussion·····161

8.4 Conclusions·····168

8.5 References·····168

Chapter 9: High performance BSCF membranes shelled by SDC film

9.1 Introduction·····171

9.2 Experimental section·····173

9.3 Results and discussion·····175

9.4 Conclusions·····181

9.5 References·····182

Chapter 10: Conclusions and Recommendations

10.1 Conclusions·····184

10.1.1 Novel CO_2-tolerant ion-transporting ceramic membranes with external short circuit for oxygen separation at intermediate temperatures·····184

10.1.2 Enhanced oxygen permeation performance of CO_2 tolerant ion conducting membrane with easily sintered bismuth-based oxide·····184

10.1.3 CO_2-tolerant ceramic membrane driven by electrical current for oxygen production at intermediate temperatures·····185
10.1.4 Robust ion-transporting ceramic membrane with an internal short circuit for oxygen production·····185
10.1.5 Highly stable external short circuit assisted-oxygen ionic transport membrane reactor for carbon dioxide reduction coupled with methane partial oxidation·····186
10.1.6 External short circuit-assisted proton conducting ceramic membrane for H_2 permeation·····186
10.1.7 Enhanced oxygen permeability and CO_2 stability of BSCF membrane with SDC functional shell for oxygen production·····186
10.3 Recommendations·····186

List of Figures

Figure 2-1 Schematic diagram of two different types of oxygen ionic conducting membranes: (a) mixed conducting membrane; (b) electrolyte membrane. ·····11

Figure 2-2 Diagram of oxygen bulk transport processes through dense membranes, (a) ideal fully dense membrane; (b) membrane with some closed non-connected pores.·····17

Figure 2-3 The structure of perovskite ABO_3, (a) Corner-sharing (BO_6) octahedral with A ions located in 12-coordinated interstices, (b) B-site cation at the center of the cell. ·····27

Figure 2-4 The schematic of the new membrane concept. ·····47

Figure 3-1 Diagrams of various oxygen ionic transport membranes for oxygen separation. ·····63

Figure 3-2 XRD pattern of the SDC powder prepared by the EDTA-citrate method after heat treatment at 700^{o}C in air for 5 hours. ·····66

Figure 3-3 SEM image (A) of SDC membrane surface and its energy-dispersive X-ray spectra (EDXs) (B) before Pt coating, and SEM image after Pt coating (C). ·····71

Figure 3-4 Oxygen permeation fluxes through various SDC membranes with 1-mm-thickness at different temperatures. ·····71

Figure 3-5 Effects of operating temperature on oxygen flux through Sample-III SDC membrane (SDC+ Ag coating + Ag wire) and the electrical current through the external wire with values measured and theoretically calculated. ·····73

Figure 3-6 Effects of helium sweep rate on the oxygen flux through SDC membrane of sample-V with 1mm thickness (SDC +Pt coating+ Ag sealing). ·····73

Figure 3-7 Thickness dependence of oxygen permeation flux through SDC membrane (samples (V to VII) with different thickness (S-V: 1 mm, S-VI: 1.5 mm, S-VII: 0.4 mm). ··75

Figure 3-8 The long term oxygen permeation fluxes through sample-VII (SDC) membrane (0.4 mm) at 600 ^{o}C (A) and sample-VIII (BSCF) membrane (1-mm-thickness) at 850^{o}C (B) under He or He+CO_2 mixture (total sweep gas flow: 100 ml min^{-1}). ·····75

Figure 4-1 The configuration of YSB membrane with external short circuit. ·····85

Figure 4-2 XRD pattern of the YSB powder calcinated at 650 ^{o}C for 5 hours. ·····86

Figure 4-3 SEM morphologies of the YSB membranes sintered from 750^{o}C, 800^{o}C, 850^{o}C for 5 hours and after the oxygen permeation test. ·····87

Figure 4-4 Temperature dependence of the oxygen permeation fluxes through various YSB membrane with 1mm thickness. ·····90

Figure 4-5 Oxygen permeation fluxes through the YSB membrane sintered at different temperatures. ·····90

Figure 4-6 Oxygen permeation fluxes through the YSB membranes sintered at 800^{o}C with different sweep gas flow rates. ·····92

Figure 4-7 Oxygen permeation fluxes through the YSB membrane with different sweep gases (total flow rate is 100 ml min^{-1}). ·····93

Figure 4-8 Diagram of oxygen permeation mechanism of the YSB membrane in the presence of H_2O. ·····96

Figure 4-9 Long term oxygen permeation test of the YSB membranes under different gas atmospheres. ·····97

Figure 5-1 Schematic diagram of the oxygen pump based on SDC/LSF membrane. ·····105

Figure 5-2 XRD pattern of SDC and LSF before and after the CO_2 treatment at 800^{o}C, a: fresh SDC; b: SDC after CO_2 treatment; c: fresh LSF; d: LSF after CO_2 treatment. ·····106

Figure 5-3 SEM images of SDC/LSF membrane cross section (a) and surface area before (b) and after (c) the CO_2 test at 800^{o}C, and energy dispersive X-ray spectrum before (d) and after (e) the CO_2 test at 800^{o}C. ·····107

Figure 5-4 The oxygen flux and voltage with applied current density under various temperature ·····108

Figure 5-5 Schematic diagram of the SDC/LSF membrane working on the SDC electrolyte with a: pure ion conducting; b: mixed ion and electron conducting. ·····110

Figure 5-6 Impedance spectrum of SDC/LSF membrane under the current polarization. ·····111

Figure 5-7 Oxygen permeation (faraday) efficiency of SDC/LSF membrane under different temperatures. ·····113

Figure 5-8 Impedance spectrum of SDC/LSF membrane under CO_2 atmosphere at 800^oC. ····115

Figure 5-9 Impedance spectrum (a) and oxygen permeation test (b) of SDC/LSF membrane after the CO_2 test at 800^oC. ·····116.

Figure 6-1 Working principles of oxygen ionic transporting membranes for solid oxide fuel cell(a), oxygen separation via external short circuit (b) or internal short circuit (c) ·····121

Figure 6-2 the schematic of the SDC membrane with the internal short structure. ·····124

Figure 6-3 XRD pattern of SDC oxide, A: SDC powder prepared by EDTA-citrate method; B: SDC disk sintered at 1350 ^oC. ·····125

Figure 6-4 TEM image of SDC oxide powder prepared by EDTA-citrate method after treatment under 700^oC in air for 5 hours. ·····126

Figure 6-5 Images of SDC membrane, (a) and (b): SEM images for cross section, digital photo images for (c): pure SDC membrane, membrane (d): with internal short circuit and (e) Ag surface modification. ·····127

Figure 6-6 The oxygen permeation fluxes through the SDC membranes with various structures. ·····130

Figure 6-7 The thickness dependence of oxygen permeation fluxes. ·····131

Figure 6-8 The effect of sweep gas rate on oxygen permeation fluxes. ·····131

Figure 6-9 Long term oxygen permeation test of A: SDC membrane with internal short circuit (sample II) at 800 ^oC and B: BSCF membrane (Sample X: Perovskite) at 850 ^oC under He, He+CO_2 or He+CO_2+H_2O mixture. ·····134

Figure 6-10 Oxygen permeation membrane stack system with the internal short circuit structure. ·····134

Figure 7-1 Schematic diagrams of the SDC membrane reactor utilizing asymmetric structure, external short circuit, Pt catalyst in the feed side and $GdNi/Al_2O_3$ catalyst in the permeate side. ·····141

Figure 7-2 Temperature dependent CO_2 conversion; CO_2 with flow rate of 10 ml min^{-1} in mixture with He with flow rate of 30 ml min^{-1} were used as feed gas while Ar with flow rate of 35 ml min^{-1} was used as sweep gas. ·····144

Figure7-3 SEM images of SDC membrane with asymmetric structure; a. cross-section; b. dense thin layer; c. porous layer. ·····146

Figure 7-4 Oxygen flux through SDC membrane with asymmetric structure and dense 1 mm-thick SDC membrane; both utilizing external short circuit. Air was used as feed gas while Ar with flow rate of 100 ml min^{-1} was used as sweep gas. ·····147

Figure 7-5 Temperature dependent CO_2 conversion; CO_2 with flow rate of 10 ml min^{-1} in mixture with He with flow rate of 30 ml min^{-1} were used as feed gas while CH_4 with flow rate of 2 ml min^{-1} and Ar with flow rate of 35 ml min^{-1} were used as sweep gas. ·····148

Figure 7-6 Temperature dependent CH_4 conversion on SDC membrane reactor with asymmetric structure utilizing external short circuit; CO_2 with flow rate of 10 ml min^{-1} in mixture with He with flow rate of 30 ml min^{-1} were used as feed gas while CH_4 with flow rate of 2 ml min^{-1} and Ar with flow rate of 35 ml min^{-1} were used as sweep gas. ·····149

Figure 7-7 The effect of CO_2 flow rate on the membrane reactor performance at 850 ^oC; CO_2 with flow rate of 5-20 ml min^{-1} in mixture with He with flow rate of 35-20 ml min^{-1} were used as feed gas (total flow rate was fixed at 40 ml min^{-1}) while CH_4 with flow rate of 2 ml min^{-1} and Ar with flow rate of 35 ml min^{-1} were used as sweep gas. ·····150

Figure 7-8 The effect of CH_4 flow rate on the membrane reactor performance at 850 ^oC; CO_2 with flow rate of 10 ml min^{-1} in mixture with He with flow rate of 30 ml min^{-1} were used as feed gas while CH_4 with flow rate of 1-5 ml min^{-1} and Ar with flow rate of 36-32 ml min^{-1} were used as sweep gas (total flow rate was fixed at 40 ml min^{-1}). ·····151

Figure 7-9 Long term performance of the membrane reactor at 850 ^{o}C; CO_2 with flow rate of 10 ml min^{-1} in mixture with He with flow rate of 30 ml min^{-1} were used as feed gas while CH_4 with flow rate of 2 ml min^{-1} and Ar with flow rate of 35 ml min^{-1} were used as sweep gas. ·····152

Figure 7-10 Powder XRD patterns of the SDC membranes; A. as prepared; B. after 100 h under CO_2 at 850 ^{o}C, C. after 100 h under CH_4 at 850 ^{o}C. ·····153

Figure 7-11 SEM images of the GdNi/Al_2O_3 catalyst; A. before test; B. after test. ·····153

Figure 8-1 Schematic of the hydrogen permeation membrane utilizing external short circuit. ··160

Figure 8-2 SEM images of BZCY and BZCYZn membranes. ·····161

Figure 8-3 Temperature dependent hydrogen permeation fluxes through basic and external short circuit-assisted BZCY and BZCYZn membranes. Feed gas: 40 ml min^{-1} H_2 + 40 ml min^{-1} N_2; Sweep gas: 100 ml min^{-1} Ar. ·····162

Figure 8-4 Hydrogen permeation fluxes through external short circuit-assisted BZCY and BZCYZn membranes at 950 ^{o}C and different sweep gas flow rate. ·····164

Figure 8-5 Temperature dependent hydrogen permeation fluxes through external short circuit-assisted BZCY and BZCYZn membrane on both membrane sides with and without water vapor (3 vol. % H_2O). ·····164

Figure 8-6 Long term hydrogen permeation fluxes through $BaZr_{0.1}Ce_{0.2}Y_{0.7}O_{3-\delta}$ (BZCY) and $BaZr_{0.3}Ce_{0.6}Y_{0.1}Zn_{0.05}O_{3-\delta}$ membrane (with external short circuit) using different sweep gas at 850 ^{o}C. ·····167

Figure 8-7 Powder XRD patterns of $BaZr_{0.1}Ce_{0.2}Y_{0.7}O_{3-\delta}$ (BZCY) and $BaZr_{0.3}Ce_{0.6}Y_{0.1}Zn_{0.05}O_{3-\delta}$ membrane before/after the stability test under 20 ml min^{-1} pure CO_2 for 10 h at 850^{o}C. ·····167

Figure 9-1 SEM and TEM images for BSCF membrane with SDC protective layer, A: SEM image of pure BSCF membrane surface; B: SEM image of BSCF membrane surface

with SDC layer; C and D: TEM images of BSCF membrane cross section with SDC layer. ·····175

Figure 9-2 Oxygen flux through BSCF membrane with/without SDC layer. ·····176

Figure 9-3 ECR response curves of BSCF membrane with/without SDC layer at various temperatures after sudden change of oxygen partial pressure from 0.05 to 0.2 atm (A&B), and the temperature dependence of the fitted k_{ex} (C). ·····179

Figure 9-4 Long term oxygen permeation test under CO_2 at 850^{o}C, A: pure BSCF membrane; B: BSCF membrane with SDC layer. ·····181

List of Tables

Table 2-1 Oxygen permeation fluxes of mixed conducting membrane materials. ····· 34

Table 3-1 SDC membrane structure, coating material, sealing agent and membrane thickness····70

Table 6-1 Different SDC membranes being tested for oxygen permeation. ·····129

Chapter 1: Introduction

1.1 Background

The cost-effective, large scale oxygen production is of vital importance to the development of the next generation of integrated carbon capture and sequestration power plants based on coal gasification or oxy-fuel coal combustion technologies. In spite of oxygen's rich reserves in the earth's atmosphere, it is very complex and expensive to produce pure oxygen in tonnage scale. Lowering the production cost is a very important issue for many industries, particularly for these clean energy practices where feed gas of pure oxygen is required as the oxidant. Nowadays, tonnage oxygen is still produced by a 100-year-old mature technology-cryogenic distillation, which is capitally expensive and energy intensive, operating at very low temperatures (-200^{o}C) and at elevated pressures. Recently, enormous effort has been placed on these solid oxide materials because of their ability to activate the reduction of oxygen and transport oxygen ions within their lattice [1-2]. These materials hold a particular prospect to be applied as dense ceramic membrane technology for separation of oxygen from air as well as membrane reactors for the partial oxidation of hydrocarbons, oxy-fuel combustion and CO_2 capture [3-5]. However, this technology is still primarily at the laboratory scale at present where the dense ceramic membranes made from doped perovskite materials. There are a number of fundamental and technological challenges that need to be overcome prior to the further development and considerations for commercialization. Although various membrane materials have been tested in different membrane reactor systems, the theory that can be applied to guide the membrane material development is still lacking. Apparently, the perovskite is more reactive due to the preponderance of oxygen vacancies and electron carriers,

but its composition with alkali elements on A site and cobalt at B site renders the material stability intrinsically weak. Therefore, the relationship between the stability (such as chemical stability and phase structural stability) of membrane materials and their oxygen permeation ability should be systematically investigated to clarify these essential factors affecting the performance of the membrane materials. As mentioned above, the current states of the arts of these oxygen permeable ceramic membranes are perovskite oxide. Despite the high oxygen fluxes, the major drawback of these perovskite membranes is their low stability in corrosive environments at the high temperatures, which deteriorates the membrane performance and lifetime. Therefore, it is extremely important to develop new membrane materials or new membrane configurations to improve the membrane stability under the real application conditions. Certainly, these novel membranes must possess sufficiently high oxygen fluxes.

1.2 Objectives and outline of the thesis

The main objective of this thesis is to develop new ceramic membranes to be used for the oxygen production with stable operation in CO_2 containing atmosphere. More specifically, the project has the following objectives:

- Developing a CO_2 tolerant oxygen ion transporting ceramic membrane with external/internal short circuit structure to solve membrane stability problem, and to study the optimum operation conditions.
- Optimizing the oxygen permeation performance at low-intermediate temperatures by: 1) selecting the fluorite oxide with high ion conductivity as bulk membrane material; 2) applying external current across the membrane to drive the high oxygen flux at lower temperatures; and 3) evaluating its oxygen permeation

performance under the CO_2/H_2O conditions to determine the key factors affecting the oxygen permeation.

- Employing this new conceptual short circuiting membrane technique on CO_2 reduction reaction coupled with methane partial oxidation to realize the combination of recation and separation in one unit.
- Extending this new short circuit concept to the hydrogen permeation membrane application, and exploring the potential effect of the short circuit structure on the hydrogen permeation performance of proton transporting membranes.
- Tailoring the conventional perovskite membrane by using highly stable fluorite oxide as surface protective layer to keep high oxygen flux through perovskite membrane as well as with high stability benefited from fluorite protective layer

Based on the specific objectives as listed above, this thesis consists of ten chapters. Chapter 2 is focusing on the literature survey of the state of the art in the filed. The results and discussions of the experimental results are presented in Chapters 3-9, which have been published or submitted to journals for possible publications. In Chapter-10, the thesis has been concluded with some suggestions for future works.

Chapter 1: Introduction

The background of the oxygen permeation membrane is briefly introduced, along with the reasons for doing this research. The objectives and outline of this thesis are also listed.

Chapter 2: Literature Review

Based on an overview of advantages and challenges of the oxygen permeable ceramic membrane technology, the latest development of the ceramic membrane for oxygen production is comprehensively summarized. The principles, advantages or

disadvantages, and the crucial problems of all kinds of membranes are discussed. Materials development and optimisation guidelines for all these different membranes are also included.

Chapter 3: Novel CO_2-tolerant ion-transporting ceramic membranes with external short circuit for oxygen separation at intermediate temperatures

This chapter presents a study of developing a new conceptual external short circuiting ion transporting ceramic membrane with high stability against CO_2 gas and high oxygen flux at the intermediate temperatures. The relationship between the membrane configurations and oxygen permeation performance is also discussed.

Chapter 4: Enhanced oxygen permeation performance of CO_2 tolerant ion conducting membrane with easily sintered bismuth-based oxide

This chapter continues the further study of improving oxygen flux of this new conceptual membrane by applying high ionic conductive fluorite oxides as bulk membrane. The effect of the CO_2 and H_2O on the oxygen permeation performance is systematically investigated

Chapter 5: CO_2-tolerant ceramic membrane driven by electrical current for oxygen production at intermediate temperatures

Based on the concept of short circuiting ion transporting membrane, the high oxygen permeation performance membrane is developed by applying external current across the membrane. The correlation between the applied electrical current density and oxygen performance of the membrane as well as in CO_2 atmosphere is explored in this chapter.

Chapter 6: Robust ion-transporting ceramic membrane with an internal short circuit for oxygen production

In this chapter, another novel membrane configuration with internal short circuit is developed for air separation based on the fundamental understanding of the working principles of solid oxide fuel cells. This further investigation opens the potential for the optimum operational conditions and scaling up oxygen production.

Chapter 7: Highly stable external short circuit assisted-oxygen ionic transport membrane reactor for carbon dioxide reduction coupled with methane partial oxidation

The short circuiting membrane with high stability and oxygen flux is applied into the membrane reactor for CO_2 reduction reaction coupled with methane partial oxidation in this chapter. The effect of the membrane thickness, the oxygen ionic transport rate as well as the CO_2 and CH_4 flow rate to the membrane reactor performance is examined. More importantly, here, we prove the feasibility of highly stable membrane reactor based on external short circuit as evidenced by achieving the constant performance in CO selectivity, CH_4 conversion, CO_2 conversion and O_2 flux during 100-hour operation and unaltered membrane structure after this operation together with the coking resistance.

Chapter 8: External short circuit-assisted proton conducting ceramic membrane for H_2 permeation

Extending from the new short circuit concept, hydrogen permeation membrane with external short circuit is developed in this chapter. The experimental result shows the use of external short circuit improved the H_2 fluxes through proton conducting disk membranes. The hydrogen permeation properties of the resultant proton conducting membranes are also systematically studied.

Chapter 9: High performance BSCF membranes shelled by SDC film

A fluorite function layer on a conventional perovskite membrane is developed with a simple preparation method in this chapter. The function shell can enhance the membrane stability against CO_2 acid gas as well as improved oxygen permeation flux. The effect of function layer on the oxygen permeation performance is systemically characterized.

Chapter 10: Conclusions and Recommendations

The overall achievements of this thesis and the recommendations for future studies are summarized in this chapter.

Reference

1. M.A. Peña and J.L.G. Fierro, *Chem. Rev.*, 2001, **101**, 1981-2017.
2. J. Sunarso, S. Baumann, J.M. Serra, W.A. Meulenberg, S. Liu, Y.S. Lin and J.C. Diniz da Costa, *J. Membr. Sci.*, **2008**, 320, 13-41.
3. W. Yang, H. Wang, X. Zhu and L. Lin, *Topics Catal.*, 2005, **35**, 155-167.
4. Y. Liu, X. Tan and K. Li, *Catal. Rev.*, 2006, **48**, 145-19.
5. X. Dong and W. Jin, *Curr. Opin. Chem. Eng.*, 2012, **1**, 163-170.

Chapter 2: Literature Review

2.1 Introduction

The demand for oxygen generation and removal for different application range has been increased substantially in concurrent trend with the modern society development [1]. Obtaining pure oxygen with low cost is a very important issue in industry. Nowadays, commercial oxygen is still produced by cryogenic distillation and pressure swing adsorption which are energy and cost-intensive technologies. Since Teraoka et al.'s first report [2] on favorable oxygen permeation through dense disk ceramic membranes based on mixed ionic and electronic conducting (MIEC) perovskite oxides of $La_{1-x}Sr_xCo_{1-y}Fe_yO_{3-\delta}$ composition in 1980s, these membranes which posses oxygen ionic in conjunction with electronic conductivity at high temperatures have attracted considerable attention during the past decades. Many related studies and research progress on mixed conducting oxide materials and membranes have been published since then [3-29].

Numerous structures have been reported which exhibit this MIEC properties, such as perovskite, brownmillerite, orthoferrite, K_2NiF_4-type phase and Ruddlesden-Popper series. Among these structures, the perovskite-structured oxides have been studied intensively due to their diverse and controllable properties. The general formula of the perovskite is ABO_3; the properties of which is determined by cations occupying its A and B site lattice. The A-site cations are mainly composed of alkaline earth, alkaline and lanthanide ions while B-site cations are mainly composed of transition metal ions [30]. When the original A-site cation of perovskite is partially substituted by another cation with lower oxidation state than the original cations, the electrical neutrality is normally sustained by the formation of oxygen vacancies or increased oxidation state

of the B-site cations. Accordingly, partial substitution of original cations with another cation having higher oxidation state tends to inhibit the formation of oxygen vacancies or increased oxidation state of the B-site cations. The presence of oxygen vacancies here facilitates the oxygen ion movement which closely affects the oxygen ionic conductivity of the oxide while the electron hopping between the valence-variable metal ions at the B-site make electronic conduction possible. The resulting MIEC properties in turn, have granted these materials a unique separation mechanism, e.g. oxygen permeating through the membrane by dissociating and/or associating in the interface and ionic transport through the bulk instead by way of the conventional molecular diffusion (through micro-pores).

There has been substantial number of articles published on the title subject in the last decade, which highlights the remarkable potential and increasing interest in the field. Several reviews on mixed conducting membranes for oxygen separation are available which provide the main understanding on the material composition, structure, preparation as well as the transport mechanism of oxygen permeable membranes [31-36]. For example, Sunarso et al. [34] reviewed the development of mixed conducting dense ceramic membrane during the past three decades. Yang et al. [35] summarised the development and challenges of perovskite type materials for oxygen transport membrane reactor applications. Liu et al. [36] wrote a review focused on the transport theory of several classes of perovskite compounds including their potential application in different areas and oxygen permeability improvement efforts by doping (e.g. partial substituting of original cations) with various metal oxide elements.

While many perovskite oxide materials have been explored over the past two decades; there are hardly any materials with sufficient practical economic value and performance for large scale applications which justify the continuing search for new materials. Furthermore, there is a lack of systematic studies to assist in materials

selection. To this end, the objective of this review is to provide the recent advances of ceramic membranes for oxygen production, with its main focus on the strategy to systematically select perovskite-type MIEC membrane material composition featuring high oxygen permeability and structural stability. While the overlapping with other available reviews is avoided as much as possible; the basic fundamental aspects are retained and briefly explained to set it as a stand-alone paper which will also facilitate understanding for newcomers in the field. In addition, some perspectives are given in last section to guide the future research in materials development.

2.2 Fundamental of ceramic membranes for oxygen production

2.2.1 General characteristics of mixed conducting dense ceramic membranes

Among dense inorganic membranes, oxygen-ionic conducting membranes have received considerable attention in the past three decades. There are two types of these membranes; the first is the so-called electrolyte membrane, which is a pure oxygen ionic conductor blocking the migration of electron through it [37,38]. Therefore, electrodes on both sides of the membrane are required to separate electron and oxygen ion transport; both of which are also attached to outside electrical circuit to facilitate electron transport. Here, the driving force for the oxygen permeation is the electrical potential. Another type of membranes is the mixed conducting (MIEC) membrane allowing the transport of both oxygen ions and electrons through it. The oxygen permeation is driven by the difference of oxygen partial pressures between opposing sides of membrane. This chemical potential gradient of molecular oxygen creates the opposing direction and inter-correlated flows of oxygen ions (O^{2-}) and electronic charge carriers (electrons and/or holes) through the membrane [39-41]. The difference in transport configuration between an electrolyte membrane and an MIEC membrane is illustrated in **Fig.2-1**.

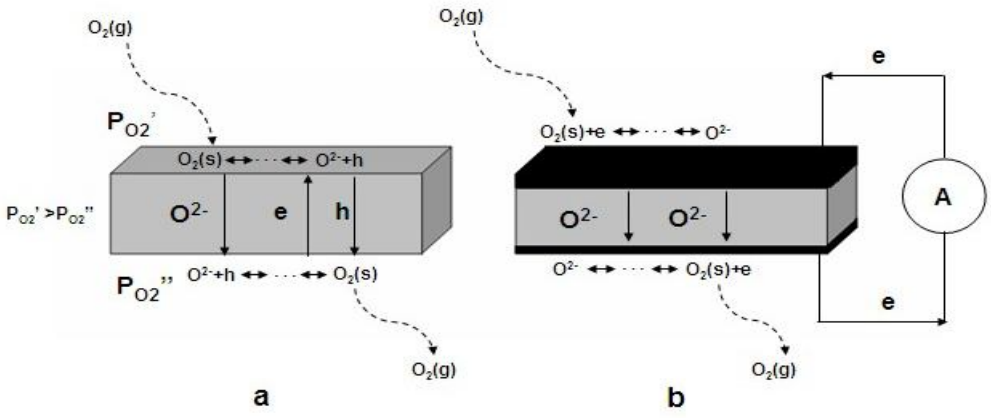

Fig.2-1. Schematic diagram of two different types of oxygen ionic conducting membranes: (a) mixed conducting membrane; (b) electrolyte membrane.

Due to its membrane configuration simplicity, high oxygen permeability, absolute selectivity for oxygen (e.g. only allowing oxygen ions permeation) and catalytic activity; dense MIEC ceramic membranes can also be utilised as catalytic membrane reactors in different petro-chemistry product related processes such as coupling oxidation of methane to C_2 (ethylene and/or ethane) (COM), partial oxidation of methane to syngas (POM), partial oxidation of heptanes to hydrogen (POH), selective oxidation of ethane to ethylene (SOE) and selective oxidation of propane to propylene (SOP) [36,42-48]. In particular, gas conversion to liquids has become more and more important currently for economic and environmental reasons. In contrast with the conventional catalyst operation mode such as packed bed reactor, the direct contact between methane and oxygen is avoided in membrane reactor. As a result, a membrane reactor using a dense oxygen permeable ceramic membrane offers a higher selectivity and yield on the desired products. Moreover, safer operation, simultaneous oxygen separation and catalytic reaction can be realised in a single device. Thus, MIEC membranes for oxygen separation from air and membrane reactor for catalytic oxidation of light hydrocarbons to value-added products (e.g. syngas, ethylene and propylene, etc) have become the hot topic until now [49-55].

2.2.2 Oxygen transport

Several mechanisms such as vacancy mechanism(i.e., via the jump of atom or ion between oxygen vacancies) interstitial mechanism (i.e., via the movement of smaller atom from an interstitial site to one of neighboring interstitial site) and/or their combined mechanisms are available which can explain oxygen ions transport in oxides; depending on the type of existing defects [56]. For perovskite type MIEC material, it is generally known that the oxygen ion conduction is made possible by the existence of oxygen vacancies. Therefore, the following discussion of oxygen transport properties is centralised around the oxygen vacancy mechanism. At elevated temperature, oxygen vacancies are formed in oxides due to the introduction of multivalent cations with redox properties. In the presence of gaseous oxygen, oxygen vacancies react with oxygen atoms resulting in the formation of two electron holes to satisfy charge neutrality criterion.

$$V_O^{\bullet\bullet} + \frac{1}{2}O_2 + \rightarrow O_O^x + 2h^{\bullet} \qquad (1)$$

Oxygen permeation through MIEC membranes involves surface exchange kinetics, bulk oxygen ion and electron diffusion. Firstly, gaseous oxygen in the high oxygen partial pressure side transfers to and adsorbs on the membrane surface. The adsorbed oxygen (at the oxygen vacancies sites of surface layer) is then reduced to lattice oxygen and migrates through the bulk layer to another side of membrane (due to oxygen partial pressure gradient across the membrane). Subsequently, at the low oxygen partial pressure side of membrane, the lattice oxygen reacts with the electron, desorbs from the membrane surface and oxidised to its gaseous form. At the same time, the multivalent metal ions on the B-site experienced reduction or oxidation to compensate the resultant charge from oxygen ions reaction. This leads to electronic conductivity via B lattice cations through strongly overlapping B-O-B bonds by

Zerner double exchange mechanism process [57] which is, typically, 100-1000 times higher than the oxygen ionic conductivity. Normally, the process of adsorption or desorption between gaseous oxygen and membrane surface and the electronic conduction is very fast. Consequently, only bulk diffusion and surface reactions steps need be taken into consideration in major transport resistance evaluation.

2.2.3. Oxygen permeation rate determining factors

Oxygen permeation through MIEC membrane involves oxygen surface exchange reactions and oxygen bulk diffusion. Either or a combination of them could be the rate-determining step(s). A number of reports have investigated the contributions of surface exchange and bulk diffusion at different membrane systems [58-62]. Oxygen permeation rate (fluxes) is not only limited by intrinsic material properties, but also closely influenced by membrane thickness and practical operation conditions. Qiu et al. [58] studies the influence of thickness on oxygen fluxes of $SrCo_{0.8}Fe_{0.2}O_{3-\delta}$ membrane under Ar/He atmosphere. They found that the oxygen permeation is controlled by the slow surface exchange process at the measured operation condition. Chen et al. [59] investigated the oxygen permeability of $La_{0.4}Sr_{0.6}Co_{0.8}Fe_{0.2}O_{3-\delta}$ on which they shows that the permeation process is totally limited by the bulk diffusion when the membrane thickness is between 1.25 and 2.46 mm. However, when the thickness is reduced to 0.62 mm, the permeation is controlled by both bulk diffusion and surface exchange. It is worthy to note that, even for the same material with the same membrane thickness and at similar operating conditions (i.e., oxygen partial pressure gradient and temperature), different oxygen fluxes has been reported by different researchers which reflects the complexity of influencing variables during high temperature experimental permeation measurements. Most likely affecting factors are:

1. The occurrence of non-axial oxygen diffusion due to fringe effects from sealants.
2. Interfacial reaction between the membrane surface and sealing materials.
3. Diffusion and reaction of sealing materials onto/with the oxides' surface.
4. Difficulty to reproduce exactly similar surface morphology for different membrane samples.
5. Inability to determine the real value of oxygen partial pressure on both membrane surfaces.

Understanding the oxygen permeation mechanism through the membrane is important to obtain optimised operation conditions and improved membrane materials. Numerous experimental techniques have been developed to extract bulk diffusion and surface exchange coefficients on MIEC membranes such as transient thermal gravimetric technique, coulometric titration method, isotope exchange combined with secondary ions mass spectroscopy (SIMS) technique and electrical relaxation method [63-68]. Numerous empirical and/or theoretical equations based on various models have also been developed and utilised to model the experimental oxygen permeation results and obtain bulk diffusion and surface exchange information. When the oxygen permeation rate is limited by bulk diffusion, reducing membrane thickness is effective to enhance the oxygen permeation flux. Nevertheless, the flux enlargement cannot be obtained by reducing the thickness when the permeation rate is determined by the surface exchange kinetics. In this latter case, membrane surface modification providing higher surface area or via catalyst deposition is more beneficial.

2.2.3.1 Bulk diffusion

Different oxygen concentration gradient across both sides of MIEC membrane leads to the oxygen ions and electrons flow in opposite direction. Assuming local equilibrium for oxygen ions, electrons and neutral oxygen molecules exist in the

oxide, the bulk diffusion rate of oxygen through membranes can be described as by Wagner equation [69]:

$$J_{O_2} = -\frac{RT}{4^2 F^2 L} \int_{\ln P'_{O_2}}^{\ln P''_{O_2}} t_{el}\sigma_{ion} d\ln P_{O_2} \quad (2)$$

Where σ_{ion} (S cm^{-1}) is the ionic conductivity of the material, t_{el} is the electronic transference number, F (C mol^{-1}) is the Faraday constant, T (K) is the absolute temperature, L (mm) is the membrane thickness, $P'o_2$ and $P''o_2$ (Pa) are the high and low oxygen partial pressure on each membrane side, respectively.

For most perovskite membrane materials, $\sigma_{el} >> \sigma_{ion}$, Equation (1) can be simplified into:

$$J_{O_2} = -\frac{RT}{4^2 F^2 L} \int_{\ln P'_{O_2}}^{\ln P''_{O_2}} \sigma_{ion} d\ln P_{O_2} \quad (3)$$

For the membrane material operated under the bulk diffusion limited condition, reducing the thickness can increase its oxygen fluxes.

2.2.3.2 Surface exchange

Two methods have been developed and utilised to evaluate the effect of surface exchange on the oxygen permeation through MIEC membranes.

1. The ratio of the surface exchange coefficient, K_s and the oxygen ion diffusion coefficient D^*. Low K_s/D^* value implies dominant role of surface exchange reaction.
2. Characteristic (critical) thickness, $L_c = D^*/K_s$, e.g., the membrane thickness when the resistance from surface reaction and bulk diffusion is equal. When $L>L_c$, the oxygen permeation rate is controlled by bulk diffusion. When $L<L_c$, the permeation rate is determined by surface exchange reaction. The characteristic

thickness is governed by the material's nature but also is influenced by the operating conditions like temperature and oxygen partial pressure.

Bouwmeester et al. [70] measured the characteristic thickness of Sr-doped $LaCoO_3$ and $LaFeO_3$, the reported value of which is around 20-500 μm. Kilner et al. [71] pointed out that the characteristic thicknesses for most perovskite oxides are around 100 μm. As a result, it is considered ineffective to reduce the membrane thickness (for improving oxygen fluxes) when the membrane thickness is already less than 100 μm. Moreover, it is worth to notice that occasionally the membrane apparent thickness does not represent the actual oxygen ion diffusion distance in the membrane bulk e.g., the distance (L) used in the calculation of the material's oxygen ionic conducting property. Ideally, the membrane should be fully densified and free of any enclosed pores. However, in most cases, it is difficult to completely avoid the presence of these enclosed pores inside the bulk of the ceramic membrane by simply adjusting the sintering temperatures. **Fig.2-2** compares the different oxygen bulk transport pathways through dense membranes with fully dense structure and porous structure without through connections. Such porous structure containing enclosed pores (**Fig.2-2**) exerts negative effects on the oxygen transport by increasing the transport resistance. There are two possible transport paths for oxygen to pass through these enclosed pores. One is via the more distorted pathway surpassing the isolated cavities. Another is via molecular oxygen gas diffusion which involves several cycles of surface reactions and charge transfer between oxygen ions and molecular oxygen. In both paths, large transport resistance dominates which will definitely slow the oxygen permeation rate.

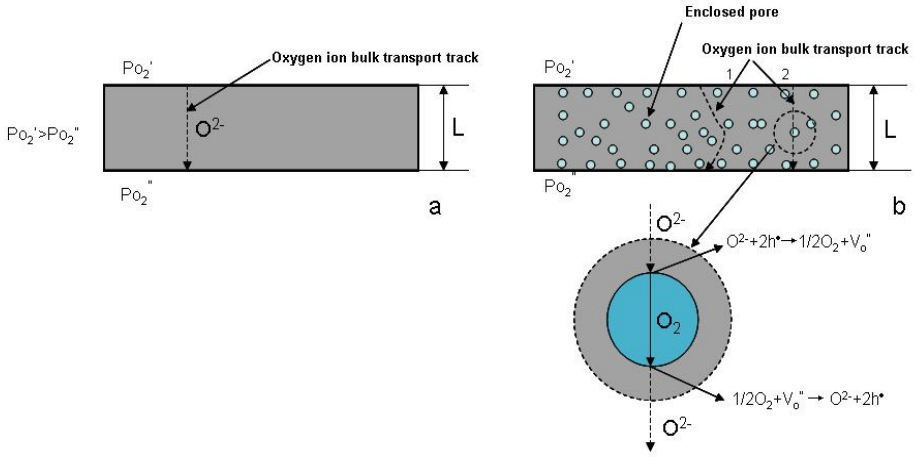

Fig. 2-2 Diagram of oxygen bulk transport processes through dense membranes, (a) ideal fully dense membrane; (b) membrane with some closed non-connected pores.

Accordingly, the reduction or elimination of these isolated pores is expected to improve the membrane performance. A possible reason for these isolated pore formation is the trapped air among the starting ceramic particles. High-energy ball milling procedure can modify the powder properties and to some extent reduce the amount of these pores during the sintering. The resultant membranes with more densified structure demonstrate better oxygen permeation flux (by about 20%) relative to the original BSCF membranes [72]. Another example is on LSCF hollow fibre membranes prepared using phase inversion and sintering. When water is used as the internal and external coagulants, the membrane is characterised by the presence of two arrays of isolated finger-like pores with length up to 30 microns sandwiched by three fully densified layers [73]. Permeability improvement can be obtained by opening these isolated pores onto both membrane surfaces by acid-modification. This increases the permeation flux through LSCF hollow fiber membranes by a factor of up to 18 over the original fibers [73].

Surface treatment and modification are also commonly applied to improve oxygen fluxes in membranes operating in surface reaction dominated regime. In this respect,

surface modification is achieved via a deposition of porous layer or more reactive layer with favorable oxygen exchange properties. Lee et al. [74] enhanced the oxygen permeation fluxes from ~0.33 ml cm^{-2} min^{-1} to ~1.07 ml cm^{-2} min^{-1} at 772 ^{o}C through 0.1 cm thick $SrCo_{0.8}Fe0_{.2}O_{3-\delta}$ dense membrane by depositing porous layer made from the same material. Kharton et al. [75] carried out surface modification by coating Ag onto $La_{0.3}Sr_{0.7}CoO_{3-\delta}$ membrane surface; improving the permeation fluxes from ~0.26 ml cm^{-2} min^{-1} to ~0.34 ml cm^{-2} min^{-1} at 770 ^{o}C.

In practice, it is rare that the oxygen permeation of a certain ceramic membrane in a fixed configuration is controlled only by bulk transport or surface exchange. The combination of both steps normally contributes to the oxygen fluxes. Different operation conditions such as temperature and pressure normally translates to different operating regime. For example, in $La_{0.6}Sr_{0.4}Co_{0.2}Fe_{0.8}O_{3-\delta}$ disk membrane, the oxygen permeation was reported to be governed by the slow kinetics of interfacial exchange at oxygen partial pressure below 1~3 kPa and by bulk diffusion at 10~100 kPa [66]. The controlling step for oxygen permeation through the same membrane is also affected by the operating temperature. For example, at 700 ^{o}C, the permeation fluxes through $La_{0.6}Sr_{0.4}Co_{0.2}Fe_{0.8}O_{3-\delta}$ hollow fiber membranes with Ag coating increase from 0.01 ml cm^{-2} min^{-1} to 0.1 ml cm^{-2} min^{-1} (increased by factor of 10). However, with increasing temperature up to 900 ^{o}C, the increasing factor is only 3 as compared with non-modified sample [76]. This observation may imply that at lower temperature range, the oxygen permeation was largely controlled by slow surface exchange kinetics and surface modification can effectively improve the oxygen permeation flux; nevertheless, when temperature was gradually increased to higher temperatures ($\geq$900^{o}C), the controlling step shifted to bulk diffusion so that the surface modification became less effective.

2.2.4 Ceramic hollow fibre membranes

Most of the currently encountered membrane-based gas separation is performed using molecular sieving membrane, a purely physical process which relies on the relative size of the molecules and the porosity and pore size of the membrane to separate different gas molecules. In contrast, oxygen separation via dense mixed conducting ceramic membranes as discussed here involves the surface ionic reactions and bulk ionic diffusion. Currently, most of the related research work in this area uses disk-shaped or tubular membranes. Although a multiple planar stack can be designed to enlarge the membrane area to afford a plant-scale output production, numerous engineering related problems easily arise from flat designs such as sealing, connection, and pressure resistance. Therefore, tubular membranes have been developed to overcome these problems, nevertheless their small surface to volume ratios as well as their thick bulk transport layer substantially trade-off their advantages particularly towards practical applications. The manufacture of monolith structures with a chessboard arrangement might be considered further to improve the ratio of surface area to volume. Still, the problems related to the manifold complexity and required sealing for different gas streams exists in this particular system design. From another fundamental standpoint of further elucidating the relationship between the membrane structure and properties, these conventional membrane configurations are also considered unattractive. The relatively large membrane thickness (in symmetric structure) utilised in these conventional designs and the fact that they operate in the bulk diffusion regime instead of surface reaction regime means that these membranes are not being operated in possible optimum conditions. In this regard, asymmetric hollow fibre membranes seem to find their niche not only in the membrane fundamental studies but also towards scaling up to industrial applications

due to their very thin transport layer, their large membrane area per unit volume and ease of sealing.

The synthesis method is based on the combined phase inversion and sintering technique where the viscous poly/polyethersulfone solution in NMP (1-methyl-2-pyrrolidinone) and water can be used as the binder and coagulants, respectively [9,77-79]. The resultant hollow fibre membranes with outside diameter of 0.7-2.0 mm and thickness of 0.2 to 0.5 mm featuring thin dense layers supported on porous structures of the same perovskite materials are able to deliver up to 7.6 ml min^{-1} cm^{-2}at 900^{o}C at atmospheric air/helium gradient. The improvement in oxygen fluxes here is due to the thinner thickness of the separating layer in the membrane structure with respect to the conventional disk or tubular shaped membranes.

Depending on the material compositions, some perovskite hollow fibres can be very robust and provides sufficiently high mechanical strength and chemical stability. For example, a proof-of-concept membrane system having maximum capacity of 3.1 L/min O_2 with >99.5% purity using $La_{0.6}Sr_{0.4}Co_{0.2}Fe_{0.8}O_3$ (LSCF) perovskite hollow fibre membranes has been achieved during operation of more than 1000 hours period [80]. Due to the thinner membrane thickness, the perovskite hollow fibres effectively operates on the surface reaction kinetics regime evidenced by the possible improvement of oxygen fluxes by up to a factor of 20 when their membrane surface were etched as well as when the metal catalysts (e.g. Ag, Pt or Pd) were deposited on these membranes' surface [8,76]. All these phenomena were specific to hollow fibre membranes and have been of great substantial value towards elucidating the membrane transport theory and relationship between structure and properties. Notably, the change of binder system and internal coagulant to prepare the hollow fibres, which are often overlooked by researchers, also greatly affects the membrane performance. For example, the usage of sulfur-free polyetherimide (PEI) polymer as a new binder

to replace the polysulfone or polyether avoids the contamination of the hollow fibre membranes by the reaction between sulfur oxide and metal oxides in the perovskite structure, which in turn enhances the membrane purity and translates into high performance with oxygen fluxes higher than 10 ml $min^{-1}cm^{-2}$ possible at atmospheric air/helium gradient [81,82]. Another example is the effect of internal coagulant on the membrane properties. During the phase inversion process, the amount of internal coagulant used to shape the hollow fibre geometry is very minimal, yet playing a vital role in influencing morphology of the hollow fibre. When a mixture of 10% EtOH and 90% NMP replaced DI water as the internal coagulant, a complete new honeycomb structured hollow fibre membrane with a single thin densified layer was produced [83]. This single dense layer hollow fibre membrane delivers much higher O_2 fluxes with improvement factor up to 15 compared to the traditional multi-dense layer sandwiched membrane structure. More interesting is that the hollow fibre membrane delicate architecture is completed in one sintering step in striking contrast to the multi-steps and time-consuming procedures to prepare conventional supported thin asymmetric membranes. All these versatile hollow fibre membrane skills can be expanded directly to any other new ceramic membrane materials and ready to make the contribution towards the future commercial targets in air separation units.

2.2.5 Non-perovskite compounds

There are various mixed conducing materials designed for the potential application of oxygen permeation membrane. In terms of the structure, it can be simply classified into two main groups, non-perovskite and perovskite. For now, most studies put their focus on the oxygen permeation based on perovskite structure because of their excellent oxygen ion and electron conducting capacity. Therefore, in this section we firstly give a brief introduction on the non-perovskite oxides as ceramic membranes.

As well known, the properties of material are closely related to its structure. The structure of material not only determines its performance in practical application but can also provide insight and understanding onto why certain material possesses excellent capability. In the past decades, materials with fluorite, brownmillerite, orthorhombic K_2NiF_4-type and $Sr_4Fe_{6-x}Co_xO_{13}$ structures have shown promises as oxygen transport membranes due to their MIEC properties [84-87]. However, the significant drawback to practical adoption is their lower ambipolar conductivity (with respect to cubic perovskite) [84,88].

Among many structures, fluorite-type structure is one of the most common crystal structures favorable for oxygen ion conduction which is represented by the cubic structure of ZrO_2 at high temperature (in excess of 2370^{o}C) [89,90]. Doping of CaO, Y_2O_3 or some other trivalent metal ions into ZrO_2 has been used to stabilize the cubic structure of ZrO_2 to room temperature. This doping strategy also leads to the formation of oxygen vacancies as a result of the charge neutrality criterion (since Ca or Y has lower valence state than Zr) which further rationalises the oxygen ionic conductivity in this doped fluorite materials. While some transition metal ions, such as TiO_2, CeO_2, $Tb_2O_{3.5}$ and CuO can be introduced into the material to provide electronic conductivity; the oxygen ionic conductivity in fluorite type material is normally accounts for much larger portion of total conductivity (with respect to electronic conductivity) [84,91-93].

Partial substitution of the original A-site and B-site cation with other cations normally leads to the distortion from the cubic symmetry to other structure symmetries, most of which was reported as brownmillerite structure [94]. Further on, when the oxygen vacancy concentration is large at elevated temperature, oxygen vacancies prefer ordered distribution to minimize the free Gibbs energy with consequential structure transition into orthorhombic symmetry as observed in $SrCo_{0.8}Fe_{0.2}O_{3-\delta}$.

Brownmillerite structure is represented by $A_2BB'O_5$ formula. Its crystal lattice can be pictured as an anion deficient perovskite with one-sixth of its oxygen ion empty. Oxygen vacancies are ordered in alternate BO_2 planes of the cubic structure such that the alternate (110) row of oxide anions is missing [30]. In comparison with cubic perovskite, the ordering will result in the unit cell expansion of materials. Since the migration energy for oxygen ions in the ordered structure is substantially higher than that in the oxygen vacancy-disordered structure; the oxygen ionic transport in the former structure is not as mobile as in the latter structure.

A sharp change in the oxygen flux behavior with temperature change has been commonly noted mostly on the mixed conducting membrane containing brownmillerite structure at specific temperature range, due to the effect of the order-disorder transition of oxygen vacancies on the oxygen ion transport in such oxides. The relationship between oxygen permeability and phase transition in mixed conducting membranes are of interest. The transport of oxygen ions in the perovskite-related mixed conducting oxides is also affected by the distribution state of oxygen vacancies. In parallel with a structural transition from cubic perovskite to brownmillerite, the oxygen vacancies change its packing state from disordered into ordered arrangements. In the latter state, in particular, oxygen ions are hardly mobile because of the ordering and pinning states of the oxygen vacancies; to the extent that transport is restricted in a two-dimensional ac plane instead of three dimensional bulk phase in the former state [95]. Bouwmeester et al. [96,97] observed that $SrCo_{0.8}Fe_{0.2}O_{2.5}$ experienced a zero oxygen release process because of the formation of the vacancy-ordered brownmillerite phase. The absence of ordered vacancy in $Ba_{0.5}Sr_{0.5}Co_{0.8}Fe_{0.2}O_{3-\delta}$, on the other hand leads to its higher oxygen permeation fluxes. Nevertheless, some materials with brownmillerite structure still show considerable oxygen permeability. Eltron Research [98-100] reported oxygen conducting capability

for some brownmillerite materials which are equivalent to or exceed the value for perovskite materials, the highest flux of which under syngas production can reach 10-12 ml cm^{-2} min^{-1}. The reason for the high oxygen permeation through the brownmillerite oxides is likely to be related to their high concentration of intrinsic oxygen vacancy and low activation energy for ionic conductivity. Moreover, it is interesting that not only the order-disorder of oxygen vacancies, but also the order-disorder of A site cation in perovskite-related oxide can influence the oxygen permeability. Recently, numerous A-site ordered perovskite has attracted a considerable attention as potential alternative mixed conducting materials [101-103]. Due to the ordering of A-site cations, these materials have an ordered layered structure which reduces the strength of oxygen binding and provides disorder-free channels for oxygen transport. In spite of significantly fast oxygen exchange and diffusion kinetics, the oxygen permeation flux of A-site ordered layered membranes, i.e., $LnBaCo_2O_{5+\delta}$, is much lower than that from the highly-permeable $Ba_{0.5}Sr_{0.5}Co_{0.8}Fe_{0.2}O_{3-d}$ membranes under similar operating conditions. It is well known that the layered material distributes the oxygen vacancies in the LnO_δ planes. In such structure, oxygen ions can transport quickly but their transport is only limited to a confined two-dimensional plane of the single crystals of the oxides. When oxygen permeates through the dense polycrystalline ceramic membrane, the oxygen ion transport will not be a straight path but a detoured or round about path due to the random crystal orientation in the ceramic bulk. In this case, the actual oxygen diffusion distance will be much longer than the real membrane thickness [104]. Therefore, $LnBaCo_2O_{5+\delta}$ oxides should be more appropriate for usage as thin catalyst coating layer to improve the surface exchange kinetics rather than as bulk dense membrane materials [105-106].

Dual-phase membranes have also been widely investigated [107-111]. The dispersion of a metallic phase electronic conductor phase into an oxygen ion conducting phase, e.g.

Pd metal into stabilised zirconia allows oxygen ion and electron transport through separate phases. Unfortunately, such membranes usually demonstrate low oxygen permeability which might be due to the non-ideal mixing of the two phases. Chen et al. [110] reported preparation of dual phase membrane using several dual phase composites such as erbia stabilized bismuth silver or gold. It was observed that in order to form an electronically conducting phase network, around 40% volume of metal is required. The oxygen transport was controlled by bulk diffusion of oxygen ions in the oxide phase for membranes with a thickness equal to or more than 1.0 mm. As the membrane thickness decreases further, both bulk diffusion and surface exchange determine the oxygen permeation rate. Dual phase membranes have also been prepared using two ceramic materials phases with one provides large ionic conductivity and another offers large electronic conductivity. For example, dual phase membrane with the fluorite type material, $Ce_{0.8}Gd_{0.2}O_{2-\delta}$ as the oxygen ion conducting phase and the perovskite type material, $La_{0.7}Sr_{0.3}MnO_{3-\delta}$ as the electron conducting phase have been prepared by Kharton et al. [111]. The utilisation of perovskite structure in this latter system which is less stable than the fluorite structure alone especially in long term and harsh operating condition normally limits the stability of these membranes. The advantage of dual phase membrane concept nevertheless lies on the possibility to tune its stability by choosing proper phase component; both of which contribute its stability. Very recently, a dual phase membrane consisting of alkaline earth free CO_2-stable spinel-type material, $NiFe_2O_4$ and Co-free fluorite type material like $Ce_{0.9}Gd_{0.1}O_{2-\delta}$ have been developed which demonstrates very stable fluxes during 100 hours of operation when CO_2 is used as sweep gas [112].

2.3 Perovskite compounds

In broad definition, perovskite is any material with the same crystal structure type as calcium titanium oxide, e.g. $CaTiO_3$, which has face cubic centered structure with the oxygen occupies the face centers. Perovskite derives their name from this compound, which was first discovered in Ural Mountains in Russia by Gustav Rose in 1839. Around 90% elements in the periodic table can form the perovskite structure. The ideal perovskite structure is cubic with structure formula of ABO_3 on which A is the larger cation and B is the smaller cation [30]. Perovskite can also be regarded as a framework structure (ReO_3-type framework), constructed from corner-sharing BO_6 octahedra with A ions located in twelve-coordinated interstices, as shown in **Fig.2-3**. Alternatively, the structure can be viewed with B cation in the center, as shown in **Fig.2-3** on which each oxygen ion is coordinated with two B ions and four A ions. It was pointed out that the most important pre-requisite for a stable perovskite structure is the existence of a stable BO_3 skeletal sub-lattice. From the geometric point of view, ionic radius of B cation should be larger than 0.051 nm to achieve stable octahedral coordination in perovskite oxides. BO_3 skeletal sub-lattice can be further stabilised by putting large A site cation at the center of eight BO_6 octahedral. The presence of the A site cation generally distorts BO_3 skeletal sub-lattice while it tries to attain optimal A metal cation-oxygen ion bond length whereby the lowest radius of A cation is 0.09 nm [113]. When the distortion is very large, non-cubic crystal geometries such as orthorhombic or rhombohedral are preferred. The relationship between the tolerance limits and size of ions are defined as follows [114,115]:

$$t=(R_A+R_O)/\sqrt{2}(R_B+R_O) \quad (4)$$

Where R_A, R_B and R_O represents the ionic radius of A-site cation (12-coordination), B-site cation (6-coordination) and oxygen ion (1.40Å), respectively. Ideally, t should be equal to 1 for the cubic structure to form. In practice, cubic structure exists in

between the limits of 0.75<t<1.0; particularly when t = 0.8 and 0.9. If the resultant t is lower than 0.9 but larger than 0.75, a cooperative buckling of the corner shared octahedron takes place, leading to orthorhombic distortion. It is obtained by tilting BO_6 octahedra so that the A atoms are displaced along (1 1 0) pseudo-cubic directions or (0 1 0) direction. When there is no octahedral buckling, a small deformation from cubic to rhombohedral symmetry might take place. This occurs for t between 0.9 and 1.0. In perovskite oxides, the difference in the ionic radiuses of dopants and outer electronic structure can easily cause the distortion from ideal cubic structure.

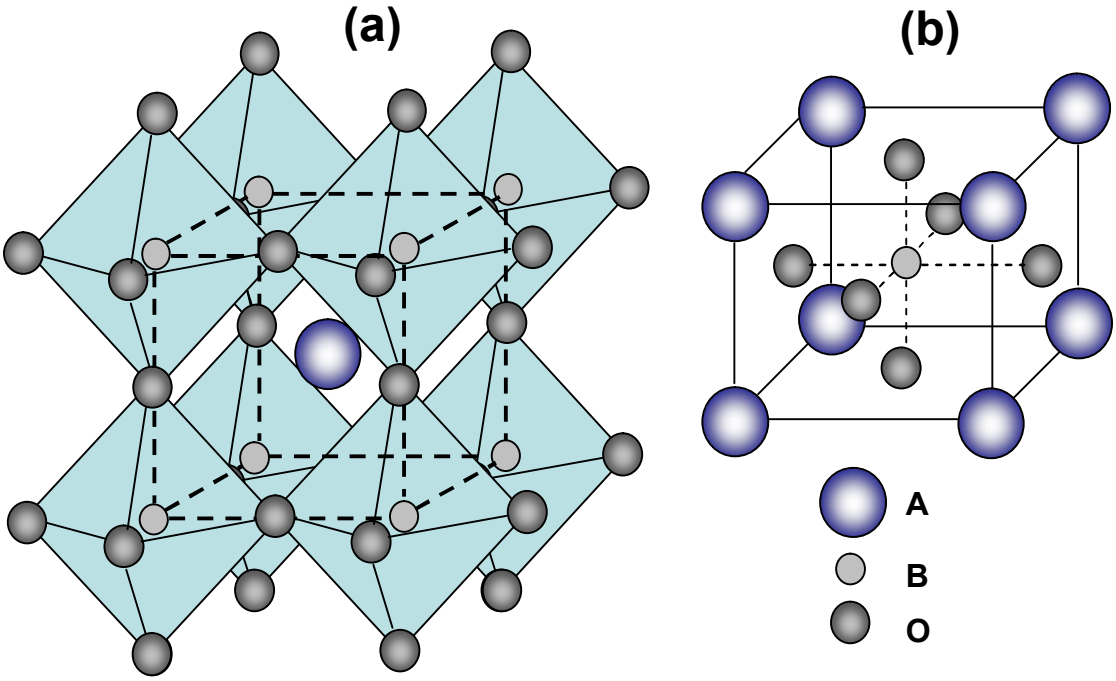

Fig. 2-3 The structure of perovskite ABO_3, (a) Corner-sharing (BO_6) octahedral with A ions located in 12-coordinated interstices, (b) B-site cation at the center of the cell.

It must be noted that the total charge of A and B cations should be equal to the total charge of oxygen ions for the electrical neutrality criterion to be maintained. This can be obtained by different means of charge distribution on the form of $A^{1+}B^{5+}O_3$, $A^{2+}B^{4+}O_3$ or $A^{3+}B^{3+}O_3$. For that reason, partial substitution of A and B cation by other cations with different ionic radius size and oxidation state is made possible while

maintaining perovskite structure. A relatively wide range of allowed t value (between 0.75 and 1.0) also means that nonstoichiometry is normally observed in perovskite oxides by the result of either A-site or B-site cation deficiency, oxygen anion deficiency or excess. In cation deficiency case, A-site cation may be partially empty without the occurrence of perovskite network collapse due to the support from BO_3 skeletal lattice. In contrast, B site cation vacancies are not favorable energetically due to the large formal charge and the small size of B cations in perovskites. As a rule, in perovskite oxides, oxygen vacancy is more easily created and reported than cations deficiency. To some extent, the oxygen vacancy amount is particularly important and can be adjusted to control the oxygen ionic conduction. This can be accomplished for example by doping with ions of similar size but having different valence state. For example, some La^{3+} ions in $LaBO_3$ can be replaced by Sr^{2+} to form $La_{1-x}Sr_xBO_{3-\delta}$ which results in the additional formation of oxygen vacancies [16,116,117]. When B cations can adopt a mixed-valence state, charge neutrality can be achieved by simultaneous formation of oxygen vacancies and change in the valence state of B cations. Therefore, perovskite oxides are capable to demonstrate both high oxygen ion conductivity attributed to high oxygen vacancies concentration and high electronic conductivity from mixed-valence state of B-site cations. The concentration of oxygen vacancies can also be increased by partially substituting the original B site cation with other lower valence state cations such as Cu or Ni ions which naturally exhibit divalent oxidation state. In case the valence state of B cations is fixed, charge neutrality can only be maintained by the formation of oxygen vacancies rendering the oxides being predominantly ionic conductors.

In practical applications, the oxygen permeation performance depends on several factors such as the materials' nature, the membrane thickness and operating conditions. It was firstly reported by Teraoka et al. that membranes based on La_{1-}

$_xSr_xCo_{1-y}Fe_yO_{3-\delta}$ having cubic perovskite structure showed oxygen permeability at elevated temperature [2]. Since then, Co-based perovskite oxides have attracted considerable interest as oxygen membranes especially due to their very high oxygen fluxes although their chemical stability to resist reducing gases and CO_2 is low. Nevertheless, Co-free oxides have been pursued intensively since the last decade due to their substantially better stability in long term and harsh condition operation [118,119]. At this point; it is worth mentioning that a trade-off occurs between oxygen permeability and stability. On introducing cobalt which is redox reactive, oxygen permeability is improved with stability being compromised. Therefore, in this section, the oxygen permeation performance of both compounds might be of interest for readers which will be expanded in two different subsections.

2.3.1 Cobalt-containing perovskites

Numerous MIEC materials with high oxygen permeability come from cobalt containing perovskites such as $SrCoO_{3-\delta}$ based oxides [120-126]. The oxygen permeation fluxes through $SrCoO_{3-\delta}$ based membranes are one or two orders of magnitude greater than those through stabilised ZrO_2. However, pure $SrCoO_{3-\delta}$ does not exhibit cubic structure; instead displays the typical 2-H type hexagonal structure regardless of the preparation methods and operation conditions used. It will experience structure transformation from hexagonal (during which no oxygen permeation is observed) to defect cubic at about 900^{o}C. It has been widely known that partial substitution of A or B site cations in cobalt-based perovskite oxides with other metal cations can stabilize the cubic structure to room temperature; thereby improving the oxygen permeability at low temperature. Teraoka et al.[2] investigated the oxygen permeation based on $La_{1-x}Sr_xCo_{1-y}Fe_yO_{3-\delta}$ perovskite systems. They found that the oxygen permeation fluxes constantly increases with increased Sr and Co content in parallel with increasing

oxygen vacancies concentration in the oxide. The A site or B site doping effect on the oxygen permeability was further studied on cobalt containing perovskite [127,128]. For A site doping on $La_{0.6}A_{0.4}Co_{0.8}Fe_{0.2}O_{3-\delta}$ materials with fixed cations at B site, the oxygen permeation fluxes decreases in the sequence of Ba>Ca>Sr>Na. For B site doping on $La_{0.6}Sr_{0.4}B_{0.8}Fe_{0.2}O_{3-\delta}$ materials, the oxygen permeation flux decreases in the sequence of Cu>Ni>Co>Fe>Cr>Mn but again with fixed A site cations.

Following this, many investigations on the oxygen permeation through $SrCo_{0.8}Fe_{0.2}O_{3-\delta}$ membrane were performed [96,129,130]. The permeation results under various temperatures and oxygen partial pressures in conjunction with the modeling results devised that the oxygen permeation rate through 1.5 mm thickness $SrCo_{0.8}Fe_{0.2}O_{3-\delta}$ oxide is controlled by surface exchange [58]. Its very high oxygen permeability mainly results from the high oxygen vacancy concentration as reflected by the oxygen content (3-δ) between 2.33 and 2.58 under a wide temperature and pressure range from 1173 K and 0.05 kPa to 873 K and 100 kPa. However, high oxygen vacancy concentration also brings excessive free energy into the oxygen vacancy disordered system. To dissipate this extra free energy, the oxygen vacancies tend to associate with each other and the ordered form is generated, leading to the structure transition from cubic to orthorhombic. Therefore, at temperatures less than 1073 K and pressures lower than 10 kPa, oxygen vacancy ordered orthorhombic brownmillerite phase, $Sr_2Co_{1.6}Fe_{0.4}O_5$, was observed in the $SrCo_{0.8}Fe_{0.2}O_{3-\delta}$ oxide [131]. The oxygen vacancy ordering not only inhibits the oxygen permeation through membranes but also induces cracks in the membrane due to the internal stress in the membrane as a result of the phase transition and the volume change. To improve the structural stability of $SrCo_{0.8}Fe_{0.2}O_{3-\delta}$ and stabilize its cubic structure to lower temperature (<800 ^{o}C) and oxygen partial pressure (<10 kPa), partial substitution of

Sr^{2+} at A site by other metal ions such as La^{3+} and Ba^{2+} has been performed successfully [13, 127,128, 132].

Prado et al [132] reported that the increase of La content in $La_xSr_{1-x}Co_{0.8}Fe_{0.2}O_{3-\delta}$ results in the decrease of valence state of Fe and Co ions and the increase of oxygen ions content. At x=0.4, e.g. represented by $La_{0.4}Sr_{0.6}Co_{0.8}Fe_{0.2}O_{3-\delta}$ compound, no brownmillerite phase exist in the oxide; only cubic perovskite structure was observed under the experimental condition (20 $^oC < T < 900\ ^oC$, 1×10^{-3} kPa $< P_{O2} < 1\times10^{-3}$ kPa). This study demonstrates that doping a certain amount of La into A site can enhance the stability of $SrCo_{0.8}Fe_{0.2}O_{3-\delta}$ oxide. Limitations however exist in here since increasing La content leads to apparent decrease in its ionic conductivity. Shao et al. [12] developed $Ba_{0.5}Sr_{0.5}Co_{0.8}Fe_{0.2}O_{3-\delta}$ on which 50% mole of Sr at A site is substituted by Ba. This compound has improved stability and oxygen permeability (with respect to $SrCo_{0.8}Fe_{0.2}O_{3-\delta}$). They also investigated the Ba doping effect at A-site (at different amount of Ba) on the oxygen permeation performance of $SrCo_{0.8}Fe_{0.2}O_{3-\delta}$ [13]. By introducing proper amount of Ba into $SrCo_{0.8}Fe_{0.2}O_{3-\delta}$, the structural stability of the material was improved while the oxygen permeability was also modified. The optimum Ba substituting content is within the range of x=0.3-0.5. The introduction of Ba also stabilised the lower oxidation states of B site metal ions. For example, Co and Fe ions prefer to exist in the form of Co^{3+} and Fe^{3+} instead of Co^{4+} and Fe^{4+}. The increased amount of B site cations with low valence state is expected to enlarge the tolerance factor (t) which explains why $Ba_xSr_{1-x}Co_{0.8}Fe_{0.2}O_{3-\delta}$ has stable cubic structure up to room temperature. Accordingly, increasing concentration of B site cations with low valence state also enhances the oxygen vacancy concentration, leading to the enhanced oxygen ionic conductivity. McIntosh et al. [97] compared the stability and oxygen permeability of $Ba_{0.5}Sr_{0.5}Co_{0.8}Fe_{0.2}O_{3-\delta}$ and $SrCo_{0.8}Fe_{0.2}O_{3-\delta}$ oxide. In contrast with $SrCo_{0.8}Fe_{0.2}O_{3-\delta}$, no oxygen vacancy ordered distribution was

observed in $Ba_{0.5}Sr_{0.5}Co_{0.8}Fe_{0.2}O_{3-\delta}$ oxide. Moreover, the oxygen content of $Ba_{0.5}Sr_{0.5}Co_{0.8}Fe_{0.2}O_{3-\delta}$ oxide is much higher than that of $SrCo_{0.8}Fe_{0.2}O_{3-\delta}$ oxide and even higher than that of ordered orthorhombic brownmillerite structure. In addition, Zeng et al. [133] reported that the oxygen permeation through $Ba_{0.5}Sr_{0.5}Co_{0.8}Fe_{0.2}O_{3-\delta}$ (BSCF) membrane is controlled by surface reaction even at the large membrane thickness of 1 mm. To this end, slow surface exchange kinetics on membrane surface together with high oxygen ionic conductivity on the bulk material results in the large discrepancy between oxygen partial pressure in the gaseous phase and membrane surface e.g. higher oxygen partial pressure on the membrane surface with respect to oxygen partial pressure in the atmosphere. However, the structural stability of the BSCF is questioned at intermediate temperature. It was reported that the oxygen permeability of BSCF membrane decreased by 50% after 240 hours of operation at 750°C due to the growth of hexagonal phase [134]. The structural instability for BSCF is ascribed to the oxidation of B-site cations which leads to its reduced ionic radius and increased Goldschmidt tolerance factor at intermediate temperature [135]. It was further confirmed by electron energy loss spectroscopy that the change in the valence state of cobalt which account for 80 mole% of B-site cation on BSCF at above 500°C [136]. This issue can be alleviated by partial substitution of Ba in $BaCoO_{3-\delta}$ by other cations with smaller ionic radius such as La and Sr. Through such substitution, the ionic radius discrepancy between A-site and B-site cations can be reduced so that lower tolerance factor can be obtained to stabilise the cubic structure [135].

Introducing metal ions with fixed valence state into B site can also be resorted to improve the structural stability of membrane. This method is more favorable to preserve high oxygen vacancy concentration in cobalt-containing perovskites and therefore ensuring higher ionic conductivity. Tong et al. [137] prepared $BaCo_{0.4}Fe_{0.6-x}Zr_xO_{3-\delta}$ whereby Fe in B site is partial substituted by Zr. Using this series of materials,

2200-hour stable operation in the membrane reactor was achieved; highlighting the excellent structural stability of $BaCo_{0.4}Fe_{0.6-x}Zr_xO_{3-\delta}$. Zeng et al. [138] reported that Sc^{3+} doping into B site of $SrCoO_{3-\delta}$ can stabilise the cubic structure; making it a promising membrane material for oxygen separation. Nagai et al. [125] conducted a systematic research on the B site cation doping onto $SrCoO_{3-\delta}$ based mixed conducting oxides. They found that $SrCo_{0.9}Nb_{0.1}O_{3-\delta}$ exhibited the best cubic structural stability and the highest oxygen permeation flux of 4.24 $cm^{-3}\cdot min\cdot cm^{-2}$ at 900 ^oC.

2.3.2 Cobalt-free perovskites

On current status, the practical application of cobalt-containing perovskite membranes is very limited due to their two main drawbacks. Firstly, they have very low structure stability. It has been reported that their structure could start to collapse at an oxygen partial pressure as low as only 10^{-5} kPa albeit substantial stabilization effect from dopants. Cobalt ion is redox reactive and therefore very unstable under such a reduced atmosphere; at which the reduction of cobalt ions to metal takes place resulting in the cubic to non-cubic structure transition which deteriorates the oxygen permeability. Secondly, they normally have a high thermal expansion coefficient, thus potentially introducing large stress across the membrane setup and sealing under asymmetric atmospheres and thermal cycling. Cracks might be easily formed, especially under a large oxygen gradient which would result in the membrane failure during operation. Recently, a large number of cobalt-free compounds have been developed; most of which are perovskite-type oxides [118,119,139-143]. Ishihara et al. [139] incorporated transition metals (e.g. Fe or Ni) into $LaGaO_{3-\delta}$ based oxide with a high oxygen ionic conductivity and low thermal expansion coefficient. The permeation results showed that $La_{0.8}Sr_{0.2}Ga_{0.6}Fe_{0.4}O_{3-\delta}$ membrane has higher oxygen fluxes than $La_{0.6}Sr_{0.4}Co_{0.2}Fe_{0.8}O_{3-\delta}$ under similar operating conditions. Yaremchenko et al. [140]

hypothesised that B-site doping of $LaGaO_{3-\delta}$ based oxides with bivalent cations (e.g. Mg, Ni or Cu) may improve ionic conductivity and more preferable than doping alkaline earth (e.g. Ca, Sr and Ba) into A-site. They found that partial filling of B-site cation by Mg leads to an increase in both electronic and oxygen ionic conductivity due to an increase in the average valence state of transition metal ions and the oxygen vacancies concentration, respectively. Zhu et al. [119] developed cobalt-free membrane based on $BaCe_xFe_{1-x}O_{3-\delta}$, which contains two phases, a Ce-rich phase and an Fe-rich phase; with only the latter phase favorable for the oxygen transport. Wang et al. [118] synthesized cobalt-free membrane material of $Ba_{0.5}Sr_{0.5}Zn_{0.2}Fe_{0.8}O_{3-\delta}$ based on that fact that the substituted $SrFeO_{3-\delta}$ has mixed oxygen ionic and electronic conductivity. This material exhibits high oxygen-permeation fluxes and good stability at high temperature. Efimov et al. [141] developed $Ba_{0.5}Sr_{0.5}Fe_{0.8}Cu_{0.2}O_{3-\delta}$ membrane with cubic structure. This material demonstrates good phase stability at high and intermediate temperatures and higher oxygen permeability in comparison to other Fe-based perovskite membranes. The oxygen fluxes of $Ba_{0.5}Sr_{0.5}Fe_{0.8}Cu_{0.2}O_{3-\delta}$ membrane were maintained at stable value for 200 hours at 1023 K. However, the main limitation of cobalt-free perovskite oxides lays on their substantially lower oxygen permeation fluxes (with respect to cobalt-containing perovskites). The condensed list of oxygen fluxes values through cobalt-containing and cobalt-free perovskite MIEC membranes as reported in literatures are listed in **Table 2-1**.

Table 2-1 Oxygen permeation fluxes of mixed conducting membrane materials

Materials	Temperatures (^oC)	$J_{O2} \times 10^6$ ($mol \cdot cm^{-2} \cdot s^{-1}$)	Thickness (mm)	Ref.
Cobalt-containing				
$SrCo_{0.8}Fe_{0.2}O_{3-\delta}$	850	0.1738	1	**[129]**
$La_{0.6}Sr_{0.4}CoO_{3-\delta}$	860	0.7649	1.5	**[127]**
$La_{0.6}Sr_{0.4}Co_{0.2}Fe_{0.8}O_{3-\delta}$	1000	0.0253	1	**[2]**

$La_{0.6}Sr_{0.4}Co_{0.8}Fe_{0.2}O_{3-\delta}$	860	0.4591	1.5	**[127]**
$La_{0.6}Sr_{0.4}Co_{0.8}Mn_{0.8}O_{3-\delta}$	860	0.372	1.5	**[127]**
$La_{0.6}Sr_{0.4}Co_{0.8}Ni_{0.2}O_{3-\delta}$	860	1.076	1.5	**[127]**
$La_{0.8}Sr_{0.2}Co_{0.3}Ga_{0.7}O_{3-\delta}$	700	0.233	0.5	**[130]**
$Ba_{0.5}Sr_{0.5}Co_{0.8}Fe_{0.2}O_{3-\delta}$	900	1.563	1.8	**[13]**
$Ba_{0.5}Sr_{0.5}Co_{0.8}Fe_{0.2}O_{3-\delta}$	950	3.266	0.22	**[9]**
$BaBi_{0.4}Co_{0.2}Fe_{0.4}O_{3-\delta}$	925	0.599	1.5	**[12]**
$SrCo_{0.9}Nb_{0.1}O_{3-\delta}$	900	3.155	1	**[125]**
$SrCo_{0.8}Sc_{0.2}O_{3-\delta}$	900	2.306	1	**[123]**
$SrCo_{0.9}Ti_{0.1}O_{3-\delta}$	900	1.36	0.65	**[122]**
Cobalt-free				
$La_{0.8}Sr_{0.2}Fe_{0.3}Ga_{0.7}O_{3-\delta}$	700	0.438	0.5	**[139]**
$La_{0.8}Sr_{0.2}Ni_{0.3}Ga_{0.7}O_{3-\delta}$	700	0.261	0.5	**[139]**
$LaGa_{0.5}Ni_{0.5}O_{3-\delta}$	950	0.066	1	**[140]**
$BaCe_{0.15}Fe_{0.85}O_{3-\delta}$	900	0.311	1	**[119]**
$Ba_{0.5}Sr_{0.5}Zn_{0.2}Fe_{0.8}O_{3-\delta}$	950	0.260	1.45	**[118]**
$Ba_{0.5}Sr_{0.5}Cu_{0.8}Fe_{0.2}O_{3-\delta}$	850	0.393	1	**[141]**

2.3.3 Selection of perovskite for oxygen permeation membrane

Although many perovskite MIEC membrane materials have been investigated and reported; only very few materials meet the requirements for practical application. First thing to be considered is the oxygen permeability. Current target for economic feasibility is 10 $cm^3 \cdot cm^{-2} \cdot min^{-1}$ **[144]**. Secondly, phase and structural stability is also crucial. Particularly when the membrane is utilized for partial oxidation or coupling reaction, it is subjected to large oxygen partial pressure gradient attributed to the exposure of one membrane surface to very low oxygen partial pressure environment ($\sim 10^{-19}$ atm) e.g. when hydrogen, carbon monoxide or methane is introduced.

In this case, developing and selecting the materials with high permeability, stable structure in long term practical operation, cheap cost and sufficient mechanical strength are of interest. Unfortunately, there is no straightforward theory for this.

Empirical rules and analogies have been largely used to guide research. Additionally, a particular material exerts MIEC property only at specific temperatures and oxygen partial pressures regime. Thus, a good material at one set of conditions might not be a good material at different set of conditions.

Several available empirical relationships between oxygen ionic transport and perovskite oxide crystal structure include the average metal-oxygen bond energy, the lattice opening degree, the saddle point formed by two A and one B site; all of which were reported as promising methods to predict potential perovskite materials having high ionic conductivity and low activation energy for oxygen transport [145-147]. Additionally, several studies on the stability of perovskites under reducing atmospheres showed that the properties of long-range disordered oxygen vacancies in lattice is largely affected by the binding energy of oxygen-metal ion.

2.3.3.1. Contributing aspects to the selection of membrane materials

2.3.3.1.1 Oxygen migration

As an oxygen ion conductor, two basic conditions should be met: firstly, a certain amount of mobile ions; secondly, passage for the transport of oxygen ions. It is known that oxygen permeability of the membrane is closely related to its electrical conductivity. In perovskite MIEC materials, the electronic conductivity is usually much higher than the oxygen ionic conductivity. Therefore, ionic conductivity is the primary variable to enhance the oxygen permeation fluxes expressed as [145]:

$$\sigma_i T = A \cdot \exp(-Ea/kT) \quad (5)$$

Where T is absolute temperature (K), Ea is the sum of activation energy of oxygen mobility and defect formation energy ($J \cdot mol^{-1}$), A is an exponential factor. To a certain temperature, increasing A value or decreasing Ea value improves the oxygen

ionic conductivity substantially. Neglecting the change of carrier concentration at various temperatures, the exponential factor A can be written as:

$$A=C\gamma(Z^2e^2/k)a_o^2\nu_o\exp(\Delta S_m/k) \quad (6)$$

Where C is the concentration of charge carriers, γ is geometric factor. Ze stands for the charge carrier number, a_o is the jump distance, ν_o is the jump odds. Generally, *E*a is equal to Δ*H*m (Δ*H*m for migration enthalpy). C can be determined from the concentration of oxygen vacancies which is exchanged with oxygen ions, namely,

$$C = N_o[V_o^{\cdot\cdot}](1-[V_o^{\cdot\cdot}]) \quad (7)$$

N_o is the number of the oxygen ions per unit volume, $[V_o^{\cdot\cdot}]$ is the oxygen vacancy concentration. When $[V_o^{\cdot\cdot}]$ is small, it is reasonable to assume C≈ $N_o[V_o^{\cdot\cdot}]$. The increase in oxygen vacancies concentration results in the increase of the exponential factor A. Consequently, the oxygen ionic conductivity is enhanced. This theory is based on the assumption that the oxygen vacancies act as the free carrier, without any association between them. However, in most cases, especially at low temperatures, the relationship between oxygen vacancies concentration and charge carriers concentration is not proportional. Moreover, the association will lead to the increase of oxygen migration energy, which causes the decline of oxygen ionic conductivity. Equation (5) implies that the oxygen permeability improvement can be achieved by lowering the activation energy. The oxygen migration activation energy (*E*a) has a very close relationship with cavity size (r_c), lattice free volume (Fv) and metal-oxygen average bond energy (ABE) [146,147].

During oxygen ion migration, oxygen ions needs to go through the narrowest space called saddle point, which consists of one B cation and two A cations with definition as:

$$r_c = \frac{r_A^2 + \frac{3}{4}a_o^2 - \sqrt{2}a_o r_B + r_B^2}{2(r_A - r_B) + \sqrt{2}a_o} \quad (8)$$

Where r_c is the critical radius, r_A and r_B are the A and B cation radius, respectively. a_o is the crystal parameter. r_c is usually less than 1.10 Å, which is smaller than the size of oxygen ion (1.40 Å). Therefore, the relaxation effect happens when oxygen ions go through the cavity. A substantial amount of energy is consumed in this migration which greatly contributes to the enhanced oxygen ion migration.

The lattice free volume is the difference between the lattice volume and the total volume of ions that constitute the crystal; which is defined as:

$$V_F = a_o^3 - 4/3\,\pi[r_A^3 + r_B^3 + (3-\delta)r_o^2] \quad (9)$$

r_o is oxygen ionic radius (1.40Å). Equation (9) shows that the lattice free volume increases with increasing average radius of A site and B site cations. Larger lattice free volume provides lower oxygen ion migration energy. Since r_c is normally less than the size of oxygen ions, it is expected that increasing the crystal free volume is more beneficial to enhance oxygen ionic transport.

In perovskite oxides, the formation of oxygen vacancies is closely related with A-O and B-O bond strength. To obtain high oxygen ionic conductivity, elemental composition with low average binding energy (ABE) should be selected. ABE affects both oxygen surface exchange kinetic and the oxygen ionic bulk diffusion. ABE value can be calculated as follows:

$$ABE=\{[\Delta_f H^o(A_mO_n)-m\Delta H^o A-D(O_2)/n]/12m\}+$$

$$\{[\Delta_f H^o(B_{m'}O_{n'})-m'\,\Delta H^o B-D(O_2)/n']/6m'\} \quad (10)$$

Where $\Delta_f H^o(A_mO_n)$ and $\Delta_f H^o(B_{m'}O_{n'})$ are standard formation enthalpy of oxides and $\Delta H^o A$ and ΔH^o B are sublimation energy of elementary substance, $D(O_2)$ is the decomposition energy of oxygen.

2.3.3.1.2 Stability

Stable structure at a wide range of temperature and oxygen partial pressure is required for practical use. Structure transformation usually leads to dramatic change in the oxygen permeability and lattice volume; causing substantial internal stress with subsequent crack of membrane. The structure stability is closely related with the properties of its element components such as ion radius, ion valence and the reactivity of related-metal.

Perovskite oxides require different cations to be incorporated into their A and B sites to form stable cubic structure. Study on the influence of A site cations shows that the structural stability of $LnCoO_{3-\delta}$ under reducing atmosphere increases with the increasing of ionic radius of lanthanides because of the 12-coordinated structure of the large size Ln ions [148]. Furthermore, the valence state of metal ions doped into A site of perovskite affects not only the defects formation but also the structural stability. For example, increasing amount of Sr doping in $LaCoO_{3-\delta}$ brought about increasing oxygen vacancies and Co^{4+} concentrations and the respective enhanced oxygen bulk diffusion with negative effect on the structural stability. On the other hand, when a cation with high valence state is introduced into A site of $LaCoO_{3-\delta}$, the structure stability will be improved due to the increased amount of Co^{2+} content. The properties of B site cations also have significant impact on the structural stability. The valence of B site cation, in particular dominantly determines the structural stability. Generally, the cubic to non-cubic structure transition is caused by the valence state transition of B site cations from high to low valence. To this end, suppressing the valence change of B site cations would suppress the structure transition. For example, several perovskite oxides with stable valence B site cations such as Ti^{4+}, Cr^{3+}, Sc^{3+} and Nb^{5+} possess stable cubic structures [122,125,126,138,140]. Nevertheless, the oxygen permeability is compromised due to the high oxygen migration energy in these perovskite oxides.

From the ionic radius point of view, large ionic radius for B-site cation is beneficial to preserve the cubic structure. This can be rationalised in terms of the stress reduction inside the lattice structure attributable to the mismatch between the size of A site and B site cations. Thus, tolerance factor (t) has been largely used as a guideline to correlate the structure formation with the size of A and B cations. Several studies are available that explains the stabilisation of cubic perovskite using the tolerance factor adjustment by doping with different cations [13,142]. However, it is generally difficult to pinpoint the exact effect of cation combination incorporated in the perovskite by calculating the tolerance factor since the calculated tolerance factor differs substantially depending on the assumed ionic radius of B-site cation which in turn, is governed by the particular valence and spin state adopted by B-site cation.

Beside cation radius, the valence state of cations also plays an important role on the stability of perovskite oxides, especially for B site cations. The distance between B site cations with relatively high valence state is shorter in hexagonal 2H-type structure than in cubic structure since the hexagonal structure has face-shared oxygen while the cubic structure has corner-shared one. The large electrostatic repulsion between B site cations from increasing average valence state of B site cation can make the hexagonal structure more unstable than the cubic structure. It has been observed that Zr^{4+}, Ti^{4+}, Nb^{5+} doped perovskite oxides demonstrate excellent stability [122,125,126]. Thus, B site cations with high valence state are preferred for cubic structure stability.

2.3.3.1.3 Guidelines

Previous sub-sections discuss several important parameters and approximate rules for the development of perovskite MIEC membrane materials. Important guidelines are summarised below, namely:

1. To maintain the perovskite structure, the tolerance factor of the selected metal

cations should be arranged between 0.75-1.0, particularly around 1.0 for the high electronic conductivity, ionic conductivity and structural stability at the practical conditions.

2. The ionic radius of A and B site cations should ideally be as large as possible. This is to maximise the lattice free volume for facilitating mobile oxygen transport. Moreover, at elevated temperature, the thermal reduction of B site multi-valence cation and the appearance of oxygen vacancies generally induce the expansion of structure and lattice volume, which may result in the distortion of crystal structure. Large lattice volume resulted from the large size of A and B site cations would suppress the structure transition because large lattice volume gained from large size of A and B site cations lead to larger tolerance factor (compared with smaller lattice volume) and larger resistance to structure transition due to lattice volume change. Also, in the presence of oxygen vacancies, the electrostatic repulsion between cations in the lattice needs to be considered which tends to be unfavourable towards structure stability. With increasing lattice volume, this repulsion is reduced as a result of low mutual exposure and long distance between cations. Moreover, the elements selected in the perovskite oxides should be with the low ABE to decrease the migration activation energy of the oxygen ions for the high ionic conductivity.
3. The valence state of A site cations should be low, e.g. divalent (+2) to enhance the oxygen ionic conductivity by increasing the oxygen vacancy concentration and the exponential factor A. On the other hand, it should be noticed that the ionic conductivity would be decreased because of the oxygen vacancy association and ordering when the oxygen vacancy concentration increases to some extent. Therefore, A site cations should be selected carefully.
4. Two type of cations should ideally be incorporated in B site cation; one which is

redox reactive (transition metal ion) and another one which has a fixed and high valence stable to counteract the redox effect from the first cation. It is preferred that the amount of second cation is low to avoid substantial degradation in electronic conductivity. While the valence change of B site cation is important for the oxygen vacancies creation at elevated temperature as well as the electronic conductivity, the valence change might be detrimental towards structural stability since the ionic radius change promoted by the valence state change bring might lead to structure distortion.

5. Considering the positive effects of A-site cation ordering on the improvement of oxygen transport, the development of new perovskite membranes with improved morphology, where the individual crystals can be oriented in one direction parallel to the membrane thickness direction to avoid the problem of the detoured and elongated transport path usually encountered in conventional randomly orientated polycrystalline ceramic membranes, will also be an interesting area. The successful fabrication of such membranes may greatly improve the oxygen permeation flux as compared to the similar membranes prepared from A-site cation ordered duoble perovskite oxides with randomly oriented crystalines. The available physical deposition method may be a nice technique to fabricate such thin membranes with special crystalline orientation

2.4 Application of mixed conducting membranes for clean energy delivery

Intense research and development on ceramic MIEC membranes has brought renewed interest and increasing attention especially to realise their great potential for clean energy applications [54,149-151]. Today, CO_2 emission due to the global coal-fire power plant is over 2 billion tons per year. Severe global climate change is challenging the traditional power generation system [152]. CO_2 capture technology is highly required

and can be achieved by retrofitting the existing energy infrastructure to sustain the fossil fuel usage without contributing emission. Among the three strategies suggested (oxyfuel, pre or post combustion capture), oxyfuel combustion is more competitive because of the relative less technological requirement to achieve almost zero emission and the high flexibility of retrofitting to the existing power stations. However, current tonnage O_2 production by cryogenic process is expensive and energy intensive. Coupling a cryogenic air separation unit at the front end of a coal gasifier or oxy-fuel power plant will reduce the overall efficiency of a power plant from around 40% to 30% [153,154], which can only be used in demonstration phase. For a long term profitable operation, new cost-effective oxygen production method must be adopted to replace the cryogenic method because of its lower energy efficiency. MIEC properties in these membranes at high temperature particularly, allow for their use in high temperature conditions in fossil fuel combustion on power plants, fossil fuel gasification or liquefaction. For oxy-fuel technology, an O_2-CO_2 recycle combustion process is applied in which highly pure oxygen (95% or higher) is fed to the combustion chamber and a major part of the CO_2 (~80%) rich exhaust gas is recycled back to maintain the combustion temperature at permissible level. Instead of using air as oxidant gas; O_2-CO_2 mixture is used which make flue gas contains mainly CO_2 and small amounts of acid such as SO_x and NO_x. By integrating MIEC membranes into air separation unit, the stream of recycled CO_2 (from the combustion process) can be utilized as a sweep gas to carry the permeated oxygen from the membrane back to combustion chamber. Compared with the conventional cryogenic distillation to separate O_2, this advanced technology has been predicted to reduce O_2 production cost by 35% or more [155]. When integrated in oxyfuel power plant, this cost-effective method to supply O_2 will significantly cut the energy penalty by 50% for CO_2 capture

reflected by the simplicity in process design and lower operation cost and heat integration opportunities [156].

For fossil fuel gasification or liquefaction such as coal gasification and natural gas conversion (syngas or C_2 hydrocarbons), perovskite membrane reactors also offer a promising future, since by coupling MIEC membranes as membrane and reactor; air can be directly used as the oxidant allowing oxygen separation and catalytic oxidation in one process. Furthermore, the heat generated from reforming reaction can sustain the elevated temperature required for oxygen permeation. Such coupling thus simplifies the process and reduced production cost can be projected. Another significant driving factor comes from environmental perspective with the large interest to convert natural fossil fuel to high-grade and high purity fuels using membrane reactors instead of firing the fossil fuel directly and venting or flaring the resultant natural gas which would contribute to global warming. Overall, MIEC membranes are ideal for clean energy delivery. Yet, the structural and mechanical instability of perovskite oxides in the presence of CO_2 or SO_2 still remains as the primary limiting factor for their wide scale application.

2.5 Summary and future development

Principles, advantages, progress and application problems of all kinds of dense ceramic membranes for air separation in the literature have been reviewed with emphasis on the discussion and exploration of perovskite material selection. The prospect of developing oxygen selective MIEC membrane materials with targeted transport properties to render this technology economically competitive seems promising. Still, performance improvement and cost reduction are required to meet the practical operation condition and commercialisation purpose. The approaches of

current research works have been focused on manufacturing asymmetric membrane with a porous thick substrate and a dense thin film layer, developing dual-phase membrane or membrane surface modification. Although major improvements have been obvious, the exploration on new perovskite materials or new kind of membranes are still on way due to the very limited number of perovskite oxide compositions showing both good structure stability and oxygen permeability. Below are our recommendations for future works in this area.

i) Molecular dynamic simulation

Most past and current research works have been heavily based on the empirical rules and analogy on which random introduction of different metal cations into A and B site of perovskite oxides was performed. To this end, molecular dynamic simulation might be a potentially good alternative to explain the oxygen transport properties of perovskite MIEC membranes [157,158]. To accurately describe the atomic interaction and bond breakage/formation associated with oxygen diffusion and surface reactions, first principle calculations are highly beneficial. In recent years, density functional theory (DFT) has been widely employed to study the mobility and permeation of oxygen in various oxides, like CeO_2 [159], $BiFeO_3$ [160], $La_2NiO_{4+\delta}$ [161], $SrMO_{2.5}$ (M=Fe, Co) [162], $CeMxO_{2-x}$ (M=La, Lu, Y) [163], $BaCo_{0.7}Fe_{0.3-x}Nb_xO_{3-\delta}$ [164], etc. A primary function of such computations is to clarify the electronic structures of complex oxides, particularly the electronic states close to the Fermi level, which play the dominant role in oxygen adsorption and dissociation. In addition, computational calculation is employed to understand the effect of defects on oxygen mobility and surface permeation. One of the central topics is oxygen vacancy, which has been widely found in complex oxides and may play a critical role for surface reactions involved in O_2 production. However, pure DFT has its limitation in the description of oxygen vacancies in those oxides, and thus advanced theoretical treatments, like DFT+U [165]

and hybrid DFT [166], are essential, which bring significant computational cost and are very expensive for complex oxides. Consequently one of the challenges for theoretical calculation and modeling is the description of oxygen vacancy and its role. In addition, it may provide some clues and even guidelines towards quantitative selection of A-site and B-site cations in perovskite oxides.

ii) New perovskite membrane materials with improved structural phase stability

Several perovskite materials are available which have been reported to retain their cubic structure during hundreds hour of oxygen permeation [144,167,168]. Yet, this performance lifetime is inferior to membrane used in oxygen ionic conductor configuration which can be operated continuously without observed degradation in months and even years. At this time, another limitation is the relatively low poisoning resistance of perovskite oxides to acidic gas such as sulfur dioxide and carbon dioxide. The understanding onto the interactions of acidic gas and perovskite oxides (primarily surface) is very limited and warrants further research. An innovative concept is currently being pursued intensively by European researchers in developing a very thin dense perovskite layer on top of thick porous substrate [169]. This concept is very promising as a very stable perovskite composition is chosen to ensure long lifetime operation whilst very thin film is engineered to obtain very high flux. Additionally, the mechanical support is provided by the porous substrate. The successful development of this strategy is still in process and requires more intense investigation on the proper coating and advanced fabrication techniques such as physical or chemical vapor deposition techniques to achieve defect-free thin film layer. The thermo-mechanical aspects of these asymmetric membranes cannot be overlooked as well as it forms the crucial part of their practical operation. Therefore, the development of perovskite membrane materials featuring excellent structure stability

whilst maintaining high ionic and electronic conductivity still serves as an important future challenge.

iii) Ion conducting ceramic membranes with external short circuit for oxygen separation

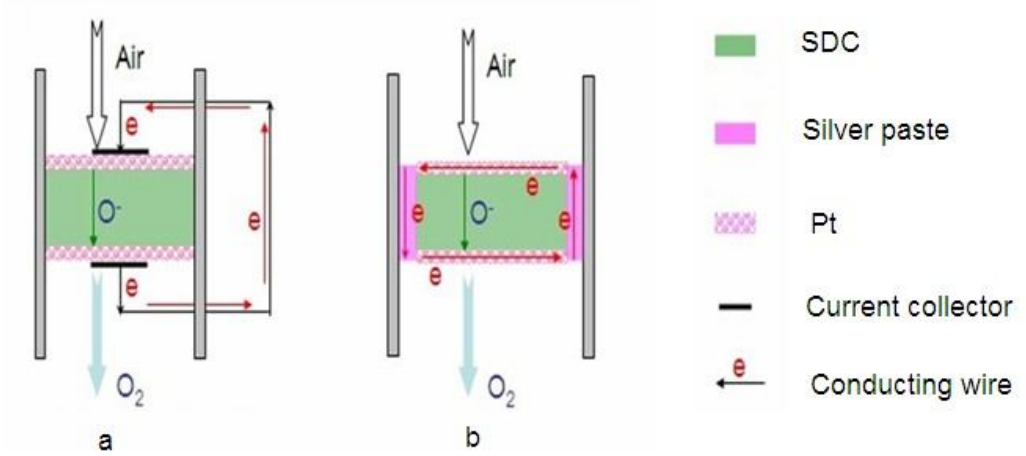

Fig.2-4 The schematic of the new membrane concept

Summarising all the results of currently developed MIEC ceramic membranes for O_2 separation, we can see that well qualified ceramic membrane addressing all the application criteria is rarely encountered. There is always a balance between the chemical stability and oxygen flux with improvement in one property but lowering down the other one. In order to get out from this dilemma, very recently, Zhang et al [170] have put forward a new membrane concept consisting of robust oxygen ion conducting ceramic membrane (i.e., fluorite-based SDC) with two surface platinum coating layers together with external short circuit as schematically illustrated in Fig.4a. In this concept, the mixed conducting function can be realised via the oxygen ion diffusion inside the fluorite bulk and electronic conduction along the external metal wire avoiding the mutual obstruction often resulted from the conventional dual phase membrane synthesised by powder mixing. When silver paste is used to seal the

ceramic membranes between the two different gas chambers, the external wire is no longer required as the electronic conduction can be completed via the silver sealing as long as silver sealing connects with the coated porous metal layer as displayed in **Fig.2-4b**. This new membrane concept has been verified by the direct detection and measurement of electrical currents which agreed very well with the theoretical calculation based on the equation correlating Faraday constant and oxygen flux. Given that the high O_2 fluxes, the intermediate operating temperature and the well-known high stability of the fluorite membrane structure, this new membrane concept is possibly making a breakthrough in the field of oxygen production for clean energy delivery.

2.6 References

1. R.M. Thorogood, *Gas. Sep. Purif.*, 1991, **5**, 83-94.
2. Y. Teraoka, H.M. Zhang, S. Furukawa and N. Yamazoe, *Chem. Lett.*, 1985, **11**, 1743-1746.
3. Y.S. Lin, W.Wang and J. Han, *AIChE J.*, 1994, **40**, 786-798.
4. D.P. Fagg, I.P.Marozau, A.L. Shaula, V.V. Kharton and J.R. Frade, *J. Solid State Chem.*, 2006, **179**, 3347-3356.
5. D.P. Fagg, A.L. Shaula, V.V. Kharton and J.R. Frade, *J. Membr. Sci.*, 2007, **299**, 1-7.
6. H.J.M. Bouwmeester, H. Kruidhof, A.J. Burggraaf and P.J. Gellings, *Solid State Ionics*, 1992, **53**, 460-468.
7. Y. Zeng, and Y.S. Lin, *J. Catal.*, 2000, **193**, 58-64.
8. S. Liu, X. Tan, Z. Shao and J.C. Diniz da Costa, *AIChE J.*, 2006, **52**, 3452-3461.
9. S. Liu and G.R. Gavalas, *J. Membr. Sci.*, 2005, **246**, 103-108.

10. J.E. ten Elshof, H.J.M. Bouwmeester and H. Verweij, *Solid State Ionics*, 81 1995, **81**, 97-109.
11. J.E. ten Elshof, H.J.M. Bouwmeester and H. Verweij, Oxidative coupling of methane in a mixed-conducting perovskite membrane reactor, *Appl. Catal. A*, 1995, **130**, 195-212.
12. Z.P. Shao, G. Xiong, Y. Cong and W. Yang, *J. Membr.Sci.*, 2000, **164**, 167-176.
13. Z.P. Shao, G.X. Xiong, J.H. Tong, H. Dong and W.S. Yang, *Sep. Purif. Technol.*, 2001, **25**, 419-429.
14. V.V. Kharton, A.P. Viskup, E.N. Naumovich and N.M. Lapchuk, *Solid State Ionics*, 1997, **104**, 67-78.
15. V.V. Kharton, A.V. Kovalevsky, V.N. Tikhonovich, E.N. Naumovich and A.P. Viskup, *Solid State Ionics*, 1998, **110**, 53-60.
16. J.W. Stevenson, , T.R. Armstrong, R.D. Carmeim, L.R. Pederson and L.R. Weber,, *J. Electrochem. Soc.*, 1996, **143**, 2722-2729.
17. J.F. Vente, W.G. Haije and Z.S. Rak, *J. Membr. Sci.*, 2006, **276**, 178-184.
18. S.P.S. Badwal and F.T. Ciacchi, *Adv. Mater.*, 2001, **13**, 993-996.
19. U. Balachandran and B. Ma, *J. Solid State Electrochem.*, 2006, **10**, 617-624.
20. D. Bayraktar, S. Diethelm, T. Graule, J. V. Herle and P. Holtappels, *J. Electroceram.*, 2009, **22**, 55-60.
21. X. Chen, H. Liu, Y.Wei, J. Caro and H. Wang, *J. Alloys Compd.*, 2009, **484**, 386-389.
22. J. Sunarso, J. Motuzas, S. Liu and J.C. Diniz da Costa, *J. Membr. Sci.*, 2010, **361**, 120-125.
23. C.S. Chen, S. Ran, W. Liu, P.H. Yang, D.K. Peng and H.J. M. Bouwmeester, *Angew. Chem. Int. Ed.*, 2001, **40**, 784-786.
24. Y. Cheng, H. Zhao, D. Teng, F. Li, X. Lu and W. Ding, *J. Membr. Sci.*, 2008, **322**,

484-490.

25. Q. Li, X. Zhu, Y. Hea and W. Yang, *Sep. Purif. Technol.*, 2010, **73**, 38-43.
26. X. Dong, G. Zhang, Z. Liu, Z. Zhong, W. Jin and N. Xu, *J. Membr. Sci.*, 2009, **340**, 140-144.
27. X. Zhu, S. Sun, Y. Cong and W. Yang, *J. Membr. Sci.*, 2009, **345**, 47-52.
28. J. Kniep and Y. S. Lin, *Ind. Eng. Chem. Res.*, 2010, **49**, 2768-2774.
29. K. Watenabe, M. Yuasa, T. Kida, Y. Teraoka, N. Yamazoe and K. Shimanoe, *Adv. Mater.*, 2010, **22**, 2367-2370.
30. M.A. Peña and J.L.G. Fierro, *Chem. Rev.*, 2001, **101**, 1981-2017.
31. S.M. Hashim, A.R. Mohamed and S. Bhatia, *Adv. Colloid Interface Sci.*, 2010, **160**, 88-100.
32. H.J.M. Bouwmeester and A.J. Burggraaf, Membr. Sci. Tech., 1996, **4**, 435-528.
33. A.F. Sammells and M.V. Mundschau*, Nonporous inorganic membranes for chemical processing,* Weinheim, Willey-VCH, c2006.
34. J. Sunarso, S. Baumann, J.M. Serra, W.A. Meulenberg, S. Liu, Y.S. Lin and J.C. Diniz da Costa, *J. Membr. Sci.*, **2008**, 320, 13-41.
35. W. Yang, H. Wang, X. Zhu and L. Lin, *Topics Catal.*, 2005, **35**, 155-167.
36. Y. Liu, X. Tan and K. Li, *Catal. Rev.*, 2006, **48**, 145-19.
37. D. Eng and M. Stoukides, Catal. *Rev. - Sci. Eng.*, 1991, **33**, 375-412.
38. M. Stoukides, Catal. *Rev.-Sci. Eng.*, 2000, **42**, 1-70.
39. V.V. Kharton, A.A. Yaremchenko, A.V. Kovalevsky, A.P. Viskup, E.N. Naumovich and P.F. Kerko, *J. Membr. Sci.*, 1999, **163**, 307-317.
40. Y. Zeng and Y.S. Lin, *J. Membr. Sci.*, 1998, **150**, 87-98.
41. B.C.H. Steele, *Current Opinion in Solid State & Mater. Sci.*, 1996, **1**, 684-691.
42. S.J. Xu and W.J. Thomson, *AIChE J.*, 1997, **43**, 2731-2740.
43. W. Wang and Y.S. Lin, *J. Membr. Sci.*, 1995, **103**, 219-234.

44. T. Nozaki and K. Fujimoto, *AIChE J.*, 1994, **40**, 870-877.

45. F.T. Akin and Y.S. Lin, *J. Membr. Sci.*, 2002, **209**, 457-467.

46. J.E. ten Elshof, H.J.M. Bouwmeester and H. Verweij, *Appl. Catal. A.*, 1995, **130**, 195-212.

47. J.E. ten Elshof, B.A. van Hassel and H.J.M. Bouwmeester, *Catal. Today*, 1995, **25**, 397-402.

48. Z.P. Shao, H. Dong, G. Xiong, Y. Cong and W. Yang, *J. Membr. Sci.*, 2001, **183**, 181-192.

49. U. Balachandran, J.T. Dusek, P.S. Maiya, B. Ma, R.L. Mieville, M.S. Kleefisch and C.A. Udovich, *Catal. Today.*, 1997, **36**, 265-272.

50. H. Luo, Y. Wei, H. Jiang, W. Yuan, Y. Lv, J. Caro and H. Wang, *J. Membr. Sci.*, 2010, **350**, 154-160.

51. H.J.M. Bouwmeester, *Catal. Today*, 2003, **82**, 141-150.

52. W. Zhu, W. Han, G. Xiong and W. Yang, *AIChE J.*, 2008, **54**, 242-248.

53. H. Wang, A. Feldhoff, J. Caro, T. Schiestel and S. Werth, *AIChE J.* 2009, **55**, 2657-2664.

54. X. Tan, K. Li, A. Thursfield and I.S. Metcalfe, Oxyfuel combustion using a catalytic ceramic membrane reactor, *Catalysis Today*, 2008, **131**, 292-304.

55. H. Jiang, Z. Cao, S. Schirrmeister, T. Schiestel and J. Caro, *Angew. Chem. Int. Ed.*, 2010, **49**, 5656-5660.

56. D.M. Smyth, *Ann. Rev. Mater. Sci.*, 1985, **15**, 329-357.

57. C. Zerner, *Phys. Rev.*, 1952, **82**, 403-405.

58. L. Qiu, T. H. Lee, L.-M. Lie, Y.L. Yang and A.J. Jacobson, *Solid State Ionics*, 1995, **76**, 321-329.

59. C.S. Chen, Z.P. Zhang and G.S. Jiang, *Chem. Mater.*, 2001, **13**, 2797-2800.

60. S.J. Xu and W.J. Thomson, *Chem. Eng. Sci.*, 1999, **54**, 3839-3850.

61. Ge, L., Z.P. Shao, K. Zhang, R. Ran, J. C. Diniz da Costa and S. Liu, *AIChE J.*, 2009, **55**, 2603-2613.

62. X. Tan and K. Li, *AIChE J.*, 2002, **48**, 1469-1477.

63. R. Bredesen, F. Mertins and T. Norby, *Catal. Today*, 2000, **56**, 315-324.

64. R.J. Chater, S. Carter, J.A. Kilner and B.C.H. Steele, *Solid State Ionics*, 1992, **53**, 597-605.

65. J.E. ten Elshof, M.H.R. Lankhorst and H.J.M. Boumeester, *J. Electrochem. Soc.*, 1997, **144**, 1060-1067.

66. J.E. ten Elshof, M.H.R. Lankhorst and J.J.M. Bouwmeester, *Solid State Ionics*, 1997, **99**, 15-22.

67. T.H. Lee, Y.L. Yang, A.J. Jacobson, B. Abeles and M. Zhou, *Solid State Ionics*, 1997, **100**, 77-85.

68. S. Kim, S. Wang, X. Chen, Y.L. Yang, N. Wu, A. Ignatiev, A.J. Jacobson and B. Abeles, *J. Electrochem. Soc.*, 2000, **147**, 2398-2406.

69. C. Wagner, *Prog. Solid State Chem.*, 1975, **10**, 3-16.

70. H.J.M. Bouwmeester, H. Kruidhof and A.J. Burggraaf, *Solid State Ionics*, 1994, **72**, 185-194.

71. J. A. Kilner, *in 2nd Int. Symp. On Ionics and Mixed Conducting Ceramics (eds. Warrell W. L., Tuller H. L.),* Electrochem. Soc., New Jersey, 1994, 174.

72. D. Gao, J. Zhao, W. Zhou, R. Ran and Z.P. Shao, *J. Membr. Sci.*, 2011, **366**, 203-211.

73. Z. Wang, , H. Liu, X. Tan, Y. Jin and S. Liu, *J. Membr. Sci.*, 2009, **345**, 65-73.

74. T.H. Lee, Y.L. Yang, A.J. Jacobson, B. Abeles and S. Milner, *Solid State Ionics*, 1997, **100**, 87-94.

75. V.V. Kharton, A.V. Kovalevsky, A.A. Yaremchenko, F.M. Figueiredo, E.N. Naumovich, A.L. Shaulo and F.M.B. Marques, *J. Membr. Sci.*, 2002, **195**, 277-

287.

76. X. Tan, Z. Wang, H. Liu and S. Liu, *J. Membr. Sci.*, 2008, **324**, 128-135.

77. X. Tan, Y. Lui and K. Li, *Ind. Eng. Chem. Res.*, 2005, **44**, 61-66.

78. T. Schiestel, M. Kilgus, S. Peter, K.J. Caspary, H. Wang and J. Caro, *J. Membr. Sci.*, 2005**, 258,** 1-4.

79. K. Li, X. Tan and Y. Lui, *J. Membr. Sci.*, 2006, **272**, 1-5.

80. X. Tan, Z. Wang, B. Meng, X. Meng and K. Li, *J. Membr. Sci.*, 2010, **352**, 189–196.

81. A. Leo, S. Smart, S. Liu and J.C. Diniz da Costa, *J. Membr. Sci.*, 2011, **368**, 64-68.

82. J. Sunarso, S. Liu, Y.S. Lin and J.C. Diniz da Costa, *Energy Environ. Sci.*, 2011, **4**, 2516-2519.

83. N. Liu, X. Tan, B.Meng and S. Liu, *Sep. Purif. Technol.*, 2011, **80**, 396-401.

84. H. Arashi and H. Naito, *Solid State Ionics*, 1992, **53**, 431-435.

85. C.S. Chen, B.A. Boukamp, H.J.M. Bouwmeester, G.Z. Cao, H. Kruidhof, A.J.A. Winnubst and A.J. Burggraaf, *Solid State Ionics*, 1995, **76**, 23-28.

86. A.A. Yaremchenko, V.V. Kharton, M.V. Patrakeev and J.R. Frade, *J. Mater. Chem.*, 2003, **13**, 1136-1144.

87. M.A. Daroukh, V.V. Vashook, H. Ullmann, F. Tietz and I.A. Raj, *Solid State Ionics*, 2003, **158**, 141-150.

88. V.V. Kharton, A.A. Yaremchenko and E.N. Naumovich, *J. Solid State Electrochem.*, 1999, **3**, 303-326.

89. B.C.H. Steele, *Mater. Sci. Eng. B*, 1992, **13**, 79-87.

90. T.H. Etsell and S.N. Flengas, *Chem. Rev.*, 1970, **70**, 339-352.

91. Y. Nigara, J. Mizusaki and M. Ishigame, *Solid State Ionics*, 1995, **79**, 208-211.

92. Y. Nigara, Y. Kosaka, K. Kawamura, J. Mizusaki and M. Ishigame, *Solid State Ionics*, 1996, **86**, 739-744.

93. J. Han, Y. Zeng and Y.S. Lin, *J. Membr. Sci.*, 1997, **132**, 235-243.

94. *W.T.A. Harrison*, *T.H. Lee*, *Y.L.* Yang, D.P. Scarfe, L.M. Liu and A.J. Jacobson, *Mater. Res. Bull.*, 1995, **30**, 621-630.

95. Z.Q. Deng, W.S. Yang, W. Liu and C.S. Chen, *J. Solid State Chem.*, 2006, **179**, 362–369.

96. H. Kruidhof, H.J.M. Bouwmeester, R.H.E. v. Doorn and A.J. Burggraaf, *Solid State Ionics*, 1993, **63**, 816-822.

97. S. McIntosh, J.F. Vente, W.G. Haije, D.H.A. Blank and J.M. Bouwmeester, *Solid State Ionics* 2006, **177**, 1737-1742.

98. A.F. Sammells, M. Schwartz, R.A. Mackay, T. F. Barton and D.R. Peterson, *Catal. Today*, 2000, **56**, 325-328.

99. A.F. Sammells, R.L. Cook, J.H. White, J.J. Osborne and R.C. MacDuff, *Solid State Ionics*, 1992, **52**, 111-123.

100. M. Schwartz, B.F. Link and A.F. Sammells, *J. Electrochem. Soc.*, 1993, **140**, L62-63.

101. A.A. Taskin, A.N. Lavrov and Y. Ando, Prog. *Solid State Chem.*, 2007, **35**, 481-490.

102. A. Tarancon, S.J. Skinner, R.J. Chater, F.H. Ramirez and J.A. Kilner, *J. Mater. Chem.*, 2007, **17**, 3175–3181.

103. A. Chang, S.J. Skinner and J.A. Kilner, *Solid State Ionics*, 2006, **177**, 2099-2011.

104. K. Zhang, L. Ge, R. Ran, Z. Shao and S. Liu, *Acta materialia.*, 2008, **56**, 4876-4889.

105. H. Gu, H. Chen, L. Gao and L. Guo, *Electrochim. Acta.*, 2009, **54**, 7094-7098.

106. Y. Lin, R. Ran, C. Zhang, R. Cai and Z. Shao, *J. Phy. Chem. A*, 2010, 114, 3764-3772.

107. T.J. Mazanec, T.L. Cable and J.G. Frye, *Solid State Ionics*, 1992, **53**, 111-118.

108. J. Kim and Y.S. Lin, *AIChE J.*, 2000, **46**, 1521-1529.

109. T.H. Lee, Y.L. Yang and A.J. Jacobson, *Solid State Ionics*, 2000, **134**, 331-339.

110. C.S. Chen, H. Kruidhof, H.J.M. Bouwmeester, H. Verweij and A.J. Burggraaf, *Solid State Ionics*, 1996, **86**, 569-572.

111. V.V. Kharton, A.V. Kovalevsky, A.P. Viskup, F.M. Figueiredo, A.A. Yaremchenko, E.N. Naumovich and F.M.B. Marques, *J. Electrochem. Soc.*, 2000, **147**, 2814-2821.

112. H. Luo, K. Efimov, H. Jiang, A. Feldhoff, H. Wang and J. Caro, *Angew. Chem. Int. Ed.*, 2011, **50**, 759-763.

113. L.G. Tejuca, J.L.Fierro and J.M.D Tascon, *Adv. Cata.*, 1989, **36**, 237-328.

114. V.M. Goldschmidt, *Math. Naturv. KI.*, 1926, **8**, 7-156.

115. N. Ramadass, *Mater. Sci. Eng.*, 1978, **36**, 231-239.

116. A.V. Kovalevsky, V.V. Kharton, V.N. Tikhonovich, E.N. Naumovich, A.A. Tonoyan, O.P. Reut and L.S. Boginsky, *Mater. Sci. Eng. B*, 1998, **52**, 105-116.

117. V.V. Kharton, , E.N. Naumovich, P.P. Shuk, A.K. Demin and A.V. Nikolaev, *Electrochemistry*, 1992, **28**, 1693-1702.

118. H. Wang, C. Tablet, A. Feldhoff and J. Caro, *Adv. Mater.*, 2005, **17**, 1785-1793.

119. X. Zhu, H. Wang and W. Yang, *Chem. Commun.*, 2004, **8**, 1130-1131.

120. J.F. Vente, S. McIntosh, W.G. Haije and H.J.M. Bouwmeester, *J. Solid State Electrochem.*, 2006, **10**, 581-588.

121. S. Diethelm and J.V. Herle, *J. Eur. Ceram. Soc.*, 2004, **24**, 1319-1323.

122. X. Chen, L. Huang, Y. Wei and H. Wang, *J. Membr. Sci.*, 2011, **368**, 159-164.

123. P.Y. Zeng, Z.P. Shao, S. Liu and Z. Xu, *Sep. Purif. Technol.*, 2009, **67**, 304-

311.

124. J.M. Kim, G.J. Hwang, S.H. Lee, C.S. Park, J.W. Kim and Y.H. Kim, *J. Membr. Sci.*, 2005, **250**, 11-16.

125. T. Nagai, W. Ito and T. Sakon, *Solid State Ionics*, 2007, **177**, 3433-3444.

126. H. Lu, J.P. Kim, S.H. Son and J.H. Park, *Mater. Sci. Eng. B*, 2010, **166**, 135-140.

127. Y. Teraoka, T. Nobunaga and N. Yamazoe, *Chem. Lett.*, 1988, **3**, 503-508.

128. Y. Teraoka, H.M. Zhang, K. Okamoto and N. Yamazoe, *Mater. Res. Bull.*, 1988, **23**, 51-62.

129. L. Tan, L. Yang, X. Gu, W. Jin, L. Zhang and N. Xu, *J. Membr. Sci.*, 2004, **230**, 21-27.

130. A.A. Yaremchenko, E.V. Tsipis, A.V. Kovalevsky, J.C. Waerenborgh and V.V. Kharton, *Solid State Ionics*, 2011, **192**, 259-268.

131. S. McIntosh, J.F. Vente, W.G. Haije, D.H.A. Blank and H.J.M. Bouwmeester, *Solid State Ionics*, 2006, **177**, 833-842.

132. F. Prado, N. Grunbaum, A. Caneiro and A. Manthiram, *Solid State Ionics*, 2004, **167**, 147-154.

133. P.Y. Zeng, , Z.H. Chen, W. Zhou, H.X. Gu Z.P. Shao and S.M. Liu, *J. Membr. Sci.*, 2007, **291**, 148-156.

134. K. Efimov, Q. Xu and A.Feldhoff, *Chem. Mater.*, 2010, **22**, 5866-5875.

135. S. Švarcová, K. Wiik, J. Tolchard, H. Bouwmeester and T. Grande, *Solid State Ionics*, 2008, **178**, 1787-1791.

136. M. Arnold, H. Wang and A. Feldhoff, *J. Membr. Sci.*, 2007, **293**, 44-52.

137. J. Tong, W. Yang, B. Zhu and R. Cai, *J. Membr. Sci.*, 2002, **203**,175-189.

138. P.Y. Zeng, R. Ran, Z.H. Chen, W. Zhou, H.X. Gu, Z.P. Shao and S. Liu, *J. Alloy. Compd.*, 2008, **455**, 465-470.

139. T. Ishihara, T. Yamada, H. Arikawa, H. Nishiguchi and Y. Takita, *Solid State Ionics*, 2000, **135**, 631-636.

140. A.A. Yaremchenko, V.V. Kharton, A.P. Viskup, E.N. Naumovich, V.N. Tikhonovich and N.M. Lapchuk, *Solid State Ionics*, 1999, **120**, 65-74.

141. K. Efimov, T. Halfer, A. Kuhn, P. Heitjans, J. Caro and A. Feldhoff, *Chem. Mater.*, 2010, **22**, 1540-1544.

142. K. Watanabe, D. Takauchi, M. Yuasa, T. Kida, K. Shimanoe, Y. Teraoka and N. Yamazoe, *J. Electrochem. Soc.*, 2009, **156**, E81-E85.

143. Y. Tsuruta, T. Todaka, H. Nisiguchi, T. Ishihara and Y. Takita, *Electrochem. Solid-State Lett.*, 2001, **4**, E13-E15.

144. P.V. Hendriksen, P. H. Larsen, M. Mogensen, F.W. Poulsen and K. Wiik, *Catal. Today*, 2000, **56**, 283-295.

145. K.A. Kilner and J. Brook, *Solid State Ionics*, 1982, **6**, 237-252.

146. R.L. Cook and A.F. Sammells, *Solid State Ionics*, 1991, **45**, 311-321.

147. R.L. Cook, R.C. Macduff and A.F. Sammells, *J. Electrochem. Soc.*, 1990, **137**, 3309-3310.

148. T. Arakawa, N. Ohara and J. Shiokawa, *J. Mater. Sci.*, 1986, **21**, 1824-1827.

149. T. Shimura, M. Itoh and H. Iwahara, *J. Appl. Electrochem.*, 1998, **28**, 683-688.

150. A. Leo, S. Liu, and J. C. Diniz da Costa, Int. *J. Greenhouse Gas Control*, 2009, **3**, 357-365.

151. S. Smart, C. X. C. Lin, L. Ding, K. Thambimuthu and J. C. Diniz da Costa, *Energy Environ. Sci.*, 2010, **3**, 268-278.

152. K. Brands, D. Uhlmann, S. Smart, M. Bram and J.C. Diniz da Costa, *J. Membr. Sci.*, 2010, **359**, 110-114.

153. K. Andersson and F. Johnsson, *Energy Conv. Manage.* 2006, **47**, 3487-3498.

154. M. Pehnt and J. Henkel, *Int. J. Greenhouse Gas Control*, 2009, **3**, 49-66.

155. G.J. Stiegel, *Separations Technology VI: New perspectives on very large scale operations, Fraser Island, Australia*, 2004.

156. H. Stadler, F.Beggel, M.Habermehl, B. Persigehl, R. Kneer, M. Modigellaan and P. Jeschke, *Int. J. Greenhouse Gas Control*, 2011, **5**, 7-15.

157. C.A.J. Fisher, M. Yoshiya, Y. Iwamoto, J. Ishii, M. Asanuma and K. Yabuta, *Solid State Ionics*, 2007, **177**, 3425-3431.

158. C. Wessel, M.W. Lumey and R, Dronskowski, *J. Membr. Sci.*, 2011, **366**, 92-96.

159. C. Frayret, A. Villesuzanne, M. Pouchard, F. Mauvy, J. Bassat and J.Grenier, *J. Phys. Chem. C*, 2010, **114**, 19062-19070.

160. S. Sæterli, Selbach, P. Ravindran, T. Grande and R. Holmestad, *Phys. Rev. B*, 2010, **82**, 064102-064110.

161. C. Frayret, A. Villesuzanne and M. Pouchard, *Chem. Mater.*, 2005, **17**, 6538-6544.

162. W. Paulus, H. Schober, S. Eibl, M. Johnson, T. Berthier, O. Hernandez, M. Ceretti, M. Plazanet, K. Conder and C. Lamberti, *J. Am. Chem. Soc., 2008, **130***, 16080-16085.

163. C. Frayret, A. Villesuzanne, M. Pouchard, F. Mauvy, J. Bassat and J. Grenier, *J. Phys. Chem. C*, 2010, **114**, 19062-19076.

164. P. Shen, X. Liu, H. Wang and W. Ding, *J. Phys. Chem. C, 2010, **114***, 22338-22345.

165. V. Anisimov, J. Zaanen and O. Andersen, *Phys. Rev. B*, 1991, **44**, 943-954.

166. B. Janesko, T. Henderson and G. Scuseria, *Phys. Chem. Chem. Phys.*, 2009, **11**, 443-454.

167. Z.P. Shao, W.S. Yang, Y. Cong, H. Dong, J.H. Tong and G.X. Xiong, *J. Membr. Sci.*, 2000, **172**, 177-188.

168. W. Ito, T. Nagai andT. Sakon, *Solid State Ionics*, 2007, **178**, 809-816.

169. M. Czyperek, P. Zapp, H.J.M. Bouwmeester, M. Modigell, K. Ebert, I. Voigt, W.A. Meulenberg, L. Singheiser and D. Stöver, *J. Membr. Sci.*, 2010, **359**, 149-159.

170. K. Zhang, Z. Shao, C. Li and S. Liu, *Energy Environ. Sci.*, 2012, **5**, 5257-5264.

Chapter 3: Novel CO_2-tolerant ion-transporting ceramic membranes with external short circuit for oxygen separation at intermediate temperatures

3.1 Introduction

Global climate change is challenging the existing power generation system and newclean energy delivery technologies with reduced CO_2 emission are urgently required. Among the promising options to integrate the existing coal-fired power stations with the CO_2 capture to produce low emission electricity, oxyfuel combustion seems to be more feasible than other options and several big projects have been initiated in the world such as CS Callide (Australia), Vattenfal (Germany), Inabensa (Spain), OXY-CFB-300 (Spain), TotalLacq (France) and FutureGen2 (USA) program with investment in billion dollars for each of these projects. Under the oxyfuel concept, coal will be fired with pure O_2 or O_2/CO_2 mixture instead of air; the major constituent of the waste gas produced during the new combustion process is highly concentrated CO_2 enabling its capture more economically feasible [1-3]. However, all these oxyfuel combustion projects are still in demonstration stage and cannot compete commercially with the conventional air-fired coal power plants because of the significantly high investment and operation costs. Among the basic operational units of the oxyfuel combustion, the complex air separation unit (ASU) via the cryogenic method to provide pure oxygen is the most expensive section accounting for 50% of the overall CO_2 capture cost. Addressing this concern to reduce the cost, oxygen ionic

conducting ceramic membranes have received increasing attention because they are envisaged to replace the cryogenics and reduce O_2 production cost by 35% or more offering the potential to tackle these energy penalties and improve the viability of zero emission technology [4-8]. However, these membranes must possess sufficiently high oxygen permeability and stable structural stability to withstand the real process conditions with the presence of highly concentrated CO_2.

The two main categories of ionic transport ceramic membranes for oxygen separation attracting intense attention are pure oxygen ion conducting membranes [9,10] and mixed ionic–electronic conducting (MIEC) membranes [11-17]. For the pure ion conducting membranes with concept schematically shown in **Fig.3-1a**, the external power source and electrodes are required to provide the electric current. Driven by the electrical potential gradient, the oxygen transport can be precisely controlled in quantity by applying the electric current with which the oxygen can be pumped in either direction regardless of the oxygen partial pressure gradient. Because of the structural complexity with external electric loadings, pure oxygen ion conducting membranes are seldom used for gas separation in contrast to the broad application in the fields of solid oxide fuel cells (SOFC) [18-20]. The MIEC membranes, driven by oxygen pressure gradient without the requirement of electrodes and external power source to operate, can be consisted of one single phase capable for both ionic and electronic conduction (**Fig.3-1b**) or dual phases i.e. with one metal (or perovskite) phase for electronic conduction and the other phase from fluorite structure for ionic conduction (**Fig.3-1c**). In MIEC membranes, as oxygen is transported in the ionic form only from high concentration side to low concentration side and therefore there must be a simultaneous flux of electrons in the opposite direction to charge compensate the oxygen flux to ensure the overall electric neutrality criteria. Currently, the intense studies of these single phase MIEC membranes are focused on perovskite

oxides with a general formula of $A_y A'_{(1-y)} B_x B'_{(1-x)} O_{(3-\alpha)}$ (x, y = 0-1) where the A and A' elements belong to the group consisting of La, Sr, Ba, Ca or Zr; the B and B' elements are taken from the group consisting of Mg, Al, Ti, Cr, Mn, Fe, Co, Ni, Cu, Ga, Zr, or Zn [21-27]. These perovskite membranes are characterized by the super-high oxygen fluxes, but they are suffering the poor chemical stability in real applying conditions with gases like CO_2, H_2S, H_2O, CH_4 and so on due to the reactions between the oxides and the gases which in turn destroy the perovskite structure and induce new phase formation and gradually lead to membrane failure. By contrast, the dual phase membrane is a promising alternative as these fluorite oxides possess inherently high chemical stability against these acid or reducing gases. Previously, the dual phase membranes were prepared by combining one of the metal phases usually chosen from Ag, Pd, Au, or Pt and the other one from the ion conducting phases with examples like yttria-stabilized zirconia (YSZ), Sm-doped ceria (SDC) or Gd-doped ceria (GDC) etc [28-30]. Each of the conducting properties requires a continuous material pathway which poses challenges on the preparation protocol regarding the mixture portions, mixing method, the particle size of the chosen membrane materials; and the high material cost cannot be avoided due to the usage of large amount of precious metals to form a continuous electronic conducting phase. The mismatch of these factors usually leads to the very low oxygen permeation fluxes sometimes several orders of magnitude lower than the single phase perovskite membranes. Reviewing all the results of currently developed ionic transport ceramic membranes for O_2 separation, we can see that a good ceramic membrane addressing all the application criteria is rarely encountered. There is always a balance between the chemical stability and oxygen flux with improvement in one property but sacrifice of the other.

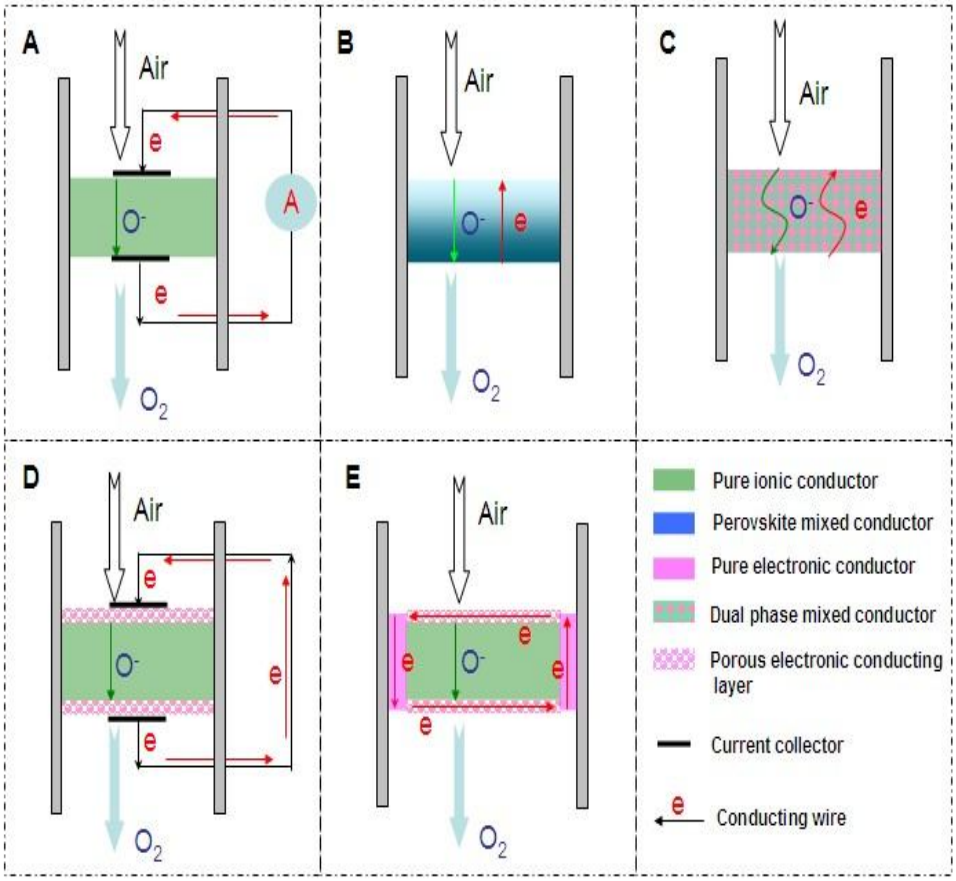

Figure 3-1 Diagrams of various oxygen ionic transport membranes for oxygen separation. (***A****: pure oxygen ion conducting membranes with external power source;* ***B****: Single phase mixed conducting membranes;* ***C****: Dual phase mixed conducting membranes prepared by mixing two phases together;* ***D****: Novel ion conducting ceramic membranes with metal coating layer and metal wire;* ***E****: Novel ion conducting ceramic membranes with metal coating layer and silver paste*.)

In order to get out from this dilemma, in this report, based on the progress of solid oxide fuel cells and mixed conducting membranes, we devised a new kind of ion conducting ceramic membrane with external short circuit for oxygen separation. As shown in **Fig.3-1d**, similar to the traditional dual phase membrane, the new concept membrane is also consisted of fluorite phase and metal phase. However, the novelty here is that the porous metal phase is being coated on the surface of the dense or gas tight fluorite phase membrane, but not being mixed inside the bulk fluorite with large amount of precious metal as what previously did. It should be mentioned that precious

metal coating is one of the strategies often applied by the single phase MIEC membranes to improve the oxygen fluxes by enhancing surface reaction kinetics [31]. In order to provide the continuous metal phase for electron conduction, the two sides of the coated metal layers, which also can be called cathode and anode adapted from the configurations of solid oxide fuel cells, are connected by one or two external wires. In this way, the mixed conducting function can be realised via the oxygen ion diffusion inside the fluorite bulk and electronic conduction along the external metal wires avoiding the mutual obstruction often resulted from the powder mixing of the two phases. Coincidently, the silver paste is usually used to seal the ceramic membranes between the two different gas chambers. In this case, the external wire is no longer required and the electronic conduction can be realised via the silver sealing as long as silver sealing touches the coated porous metal layer. This results in a very simplified membrane configuration as displayed in **Fig.3-1e**. In this report, this new membrane concept for oxygen separation has been experimentally verified by measuring the oxygen permeation flux and electrical current. Hopefully, this work will open a new research area in the field because the high chemical stability of these fluorite-based ceramics can resist the harsh practical conditions and the high oxygen fluxes of the membranes at relative lower temperatures.

3.2 Experimental Section

$Sm_{0.2}Ce_{0.8}O_{1.9}$ (SDC) composites oxides were synthesized by a combined EDTA-citrate complexing sol-gel process. $Ce(NO_3)_2.xH_2O$ and $Sm(NO_3)_3.xH_2O$ (A.R. grade) were applied as the raw materials for the metal-ion sources. For the precise controlling of the doping concentration, the individual metal nitrates were dissolved into aqueous solutions to determine their precise compositions by standard EDTA titration technique. For the fabrication of ceramic membrane, the as-obtained oxide powders were pressed into disk-shape membranes in a stainless steel module (15.0

mm in diameter) under a hydraulic pressure of approximately 1.5×10^8 Pa. These green membranes were further sintered in an electrical furnace at 1500 ^oC in air for 5 h at a heating/cooling rate of 1-2 ^oC min^{-1}. The thickness and diameter of the sintered electrolyte disks were ~0.4-1.5 and ~12 mm, respectively. Dual phase Ag/SDC membrane was synthesized by mixing 35 wt% Ag and 65 wt% SDC powder, and then sintering at 950 ^oC for 5 h. $Ba_{0.5}Sr_{0.5}Co_{0.8}Fe_{0.2}O_{3-\delta}$ (BSCF) perovskite membrane for oxygen permeation comparison purpose was also prepared as above mentioned EDTA-citrate method. The green BSCF membranes were then sintered at 1000^oC in air for 5 h with the similar condition as that for SDC membrane. Silver or Platinum slurry was applied to each side of the SDC membrane substrate as symmetrically as possible by paint-brushing method and then calcined at 600 ^oC in air for 2 h. A silver wire was used as the conductive wire to connect the two sides of membranes. Scanning Electron Microscopy (SEM) images were obtained using a Zeiss EVO 40XVP at an accelerating voltage of 15 kV. The XRD analysis was carried out on a Bruker D8 Advance X-ray diffractometer using Cu Ka radiation generated at 40 kV and 30 mA. The electrical current was measured with a HY H-15 Volt-Ohm-Milliammeter. Permeation properties of the membranes were investigated by the gas chromatography (GC) method. A silver paste or non-conductive ceramic paste was used as the sealant to fix the membrane disk onto a dense quartz tube and exposed an effective area of 0.45 cm^2 at the sweep side for permeation study. Helium was applied as the sweep gas to create an oxygen partial pressure gradient across the membrane, which also acted as the carrier gas to bring the permeated oxygen to a Shimadzu 2014A equipped with a 5Å capillary molecule column and thermal conductivity detector for quantitative oxygen concentration analysis.

The oxygen permeation flux was calculated by:

$$Jo_2\ (ml\ cm^{-2}\ \min^{-1}) = [C_{O_2} - C_{N_2} \times \frac{0.21}{0.79} \times \left(\frac{28}{32}\right)^{\frac{1}{2}}] \times \frac{F}{S}$$

Where C_O and C_N are the measured concentrations of oxygen and nitrogen in the gas on the sweep side, respectively (mol ml^{-1}), F is the flow rate of the exit gas on the sweep side (ml s^{-1}), and S is the membrane geometric surface area of the sweep side (cm^2).

3.3 Results and discussion

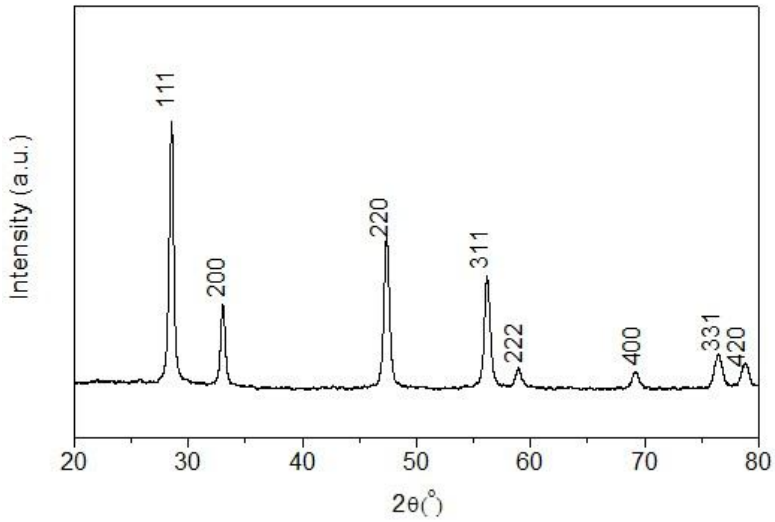

Figure 3-2. XRD pattern of the SDC powder prepared by the EDTA-citrate method after heat treatment at 700°C in air for 5 hours

Sm-doped ceria (SDC) and yttria-stabilized zirconia (YSZ) are commonly used as oxygen ion conducting solid electrolytes in solid oxide fuel cell (SOFC) system with the former can be applied in the intermediate temperature because of its higher ionic conductivity than YSZ at this temperature range [32]. Here, SDC, Ag or Pt coating, Ag wire, Ag paste and normal non-conductive ceramic paste have been used to demonstrate this concept step by step. SDC was synthesized by a combined EDTA-citrate complexing sol-gel process where $Ce(NO_3)_2.xH_2O$ and $Sm(NO_3)_3.xH_2O$ were applied as the metal-ion sources. To compare the phase stability properties of SDC

and perovskite membranes, the typical perovskite composition example of $Ba_{0.5}Sr_{0.5}Co_{0.8}Fe_{0.2}O_{3-\delta}$ (BSCF) powder was also prepared by this method. **Fig.3-2a** shows the typical XRD pattern. The characteristic peak locations at the respective 2θ angles of 28° (111), 33° (200), 47° (220), 52° (311), 58° (222) and 76° (331) are closely matching the reported fluorite structure [33]. To synthesize the SDC membrane, the as-obtained oxide powder was hydraulically pressed into disk-shape membranes and subsequently sintered at 1500°C to achieve the densification with good mechanical strength and gas-tightness. The sintered SDC membranes have the diameter of 12 mm and thickness arranged from 0.4 to 1.0 mm. **Fig.3-3a** show the dense structure after sintering with well-defined grains having grain sizes in the order of 0.5 to 1μm. The SDC membranes were tested at room temperature for gas-tightness. The surface composition of the SDC was verified by EDX results. Porous platinum or silver layer with a thickness of 5-10 μm was coated on both sides of the SDC membrane by brushing the platinum or silver paste. **Fig.3b** depicts the surface morphology change after Pt deposition. Different SDC membranes showing in Figure 1 were tested for the oxygen permeation under the sweep gas mode. **Table 3-1** shows the seven typical SDC membranes being tested with Samples I-V to verify the concept, Samples V-VII to show the effects of thickness on membrane performance and Samples VII-VIII to compare the stability. Sealed by normal nonconductive ceramic paste, Sample-I was plain SDC disk without any Pt/Ag coating. As expected, the pure ion conducting SDC membrane without the second metal phase or Pt/Ag coating layer for electronic conduction does not possess any O_2 permeation in the investigated temperature range from 500 to 800°C due to the lack of electronic conducting property. Actually, this is the reason for SDC to be widely applied as an excellent pure ion-conductor in SOFC area. Sample-II is the conventional dual phase membrane made by sintering the mixture of Ag and SDC powders. As can be seen,

when the operating temperature was from 500 to 700°C, almost no oxygen permeation flux could be detected; only after 700°C, the oxygen flux values up to 0.03 ml cm^{-2} min^{-1} was observed at 800°C. In case of Sample-III with working principles showing in **Fig.3-1d**, both sides of pure SDC membrane were coated with porous Ag layer and connected by Ag wire, but the coated SDC membrane was sealed to the quartz tube with ceramic paste. The O_2 permeation through Sample-III was clearly observed with flux values presented in **Fig.3-4**. The flux at 600°C was 0.027 ml cm^{-2} min^{-1}, but improved to 0.52 ml cm^{-2} cm^{-1} at higher temperature of 800°C in sharp contrast with lower flux value of 0.03 ml cm^{-2} min^{-1} from Sample-II and zero flux of sample-I at similar temperature. This is the direct experimental evidence for the oxygen permeation through this new membrane concept via the SDC phase for ionic diffusion and the external Ag coating plus Ag wire for electronic conduction together with the two surface reactions:

$\frac{1}{2}O_2 + 2e + V_o^{\cdot\cdot} \rightarrow O_o^x$ (O_2 high pressure side);

$O_o^x + 2h \rightarrow \frac{1}{2}O_2 + V_o^{\cdot\cdot}$ (O_2 low pressure side).

The electrical current through Ag wire in Sample-III was measured by a multimeter with values showing in **Fig.3-5** together the measured the oxygen fluxes at the same operating conditions. As can be seen, the electrical current was very low at lower temperatures, but it was increased sharply with the temperature improvement, which is due to the facilitated oxygen reduction and oxidation processes at the membrane surface by the higher temperature activation. In other words, more electrons were produced and consumed during these more active processes, which inspires a higher electrical currency. For instance, the electrical current value of 11 mA at 600°C was improved to 140 mA at 800°C. In theory, the electrical current value through the external wire should be equivalent to the current by ionic conduction through the SDC

bulk membrane for pure ionic conductor. In this case, the relationship between the oxygen flux and the measured current can be described by the equation as below [34]:

$$I(Current:mA) = 4F(Faraday's\ cons\tan t:96\,485\ \text{s A mol}^{-1}) \times \frac{J_{O2}(Oxygen\ \ flux:ml\ \text{min}^{-1}\ cm^{-2}) \times 22.4}{1000 \times 60} \times 1000$$

From this correlation, we can use the measured oxygen permeation fluxes to calculate the electrical currents or vice visa. Further inspection of **Fig.3-5** displays that the measured electrical current values are matching very well with the calculated values from the measured oxygen fluxes, particularly in the lower temperature range. However, in the higher temperature range from 700 to 800°C, the calculated current values are bit higher than the measured. This can be explained by the reason that at high temperatures for example above 700°C, the SDC is not a pure ionic conductor but displays a certain mixed conduction together with electronic conduction. Therefore the difference between the calculated electrical current values and the measured one is due to the direct electrical conduction through the SDC bul

Table 3-1 SDC membrane structure, coating material, sealing agent and membrane thickness

Sample No.	Structure type* in Fig.1	Coating material	Sealing agent	Membrane thickness
I	Pure SDC	Without coating	Ceramic paste**	1 mm
II	C (dual phase	Without coating	Ceramic Paste	1 mm
III (with Ag wire)	D	Ag	Ceramic paste	1 mm
IV	E	Ag	Ag paste	1 mm
V	E	Pt	Ag paste	1 mm
VI	E	Pt	Ag paste	1.5 mm
VII	E	Pt	Ag paste	0.4 mm
VIII	B (perovskite)	Without coating	Ag paste	1 mm

*The working principles are schematically shown in Figure 1.

**The ceramic paste is not electronic-conductive.

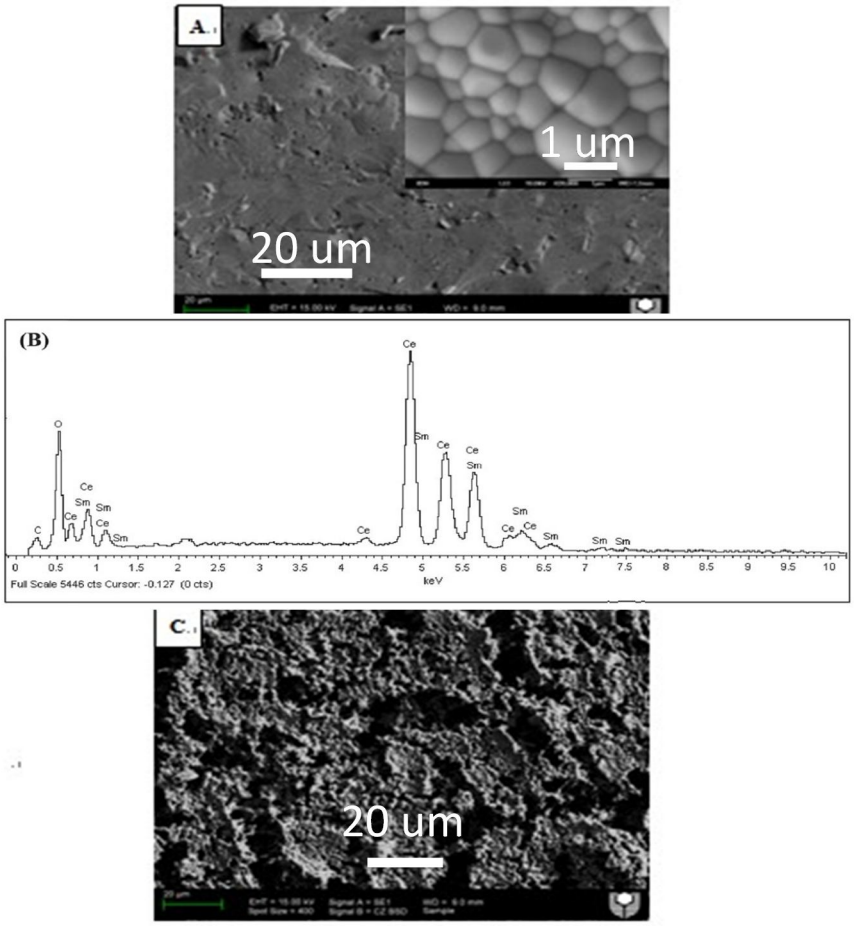

Figure 3-3. SEM image (A) of SDC membrane surface and its energy-dispersive X-ray spectra (EDXs) (B) before Pt coating, and SEM image after Pt coating (C).

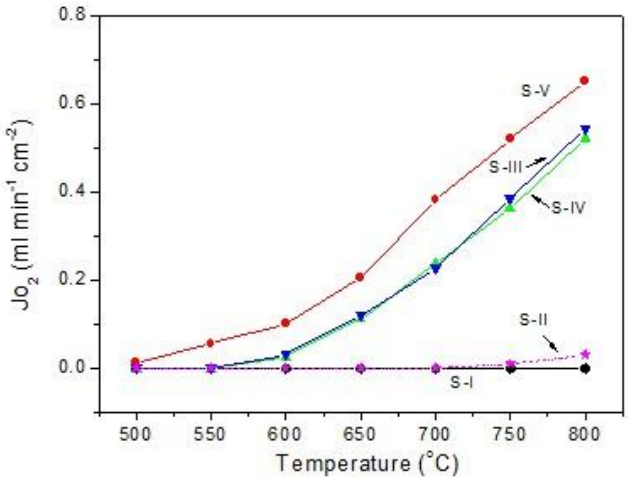

Figure 3-4. Oxygen permeation fluxes through various SDC membranes with 1-mm-thickness at different temperatures

*(**S-I**: pure SDC without any coating; **S-II**: SDC (65wt%)+Ag (35wt%) dual phase membrane prepared by powder mixing and sintering at 950°C; **S-III**: SDC+Ag coating+Ag wire; **S-IV**: SDC+Ag coating+Ag sealing; **S-V**: SDC+Pt coating+Ag sealing.)*

S-IV displayed the concept (**Fig.3-1e**) of using Ag seal to replace the Ag wire for oxygen permeation with electronic conduction through the continuous Ag phase from coating and sealing. As can be seen from **Fig.3-4**, the flux value of S-IV is almost similar to that of S-III indicating the feasibility of simplifying membrane configuration by avoiding the attachment of electrode and wire connection. Under this concept, S-V (**Fig.3-4**) depicts the permeation results of Pt coating other than Ag. Actually, the coated precious metal layer on the membrane surface would not only work as electronic conducting phase but also work as the catalyst to speed up the surface reactions. It is well known that Pt is a better catalyst than Ag for oxygen to be reduced to lattice oxygen. In agreement with this, oxygen fluxes of S-V (in Fig.4) could be observed with appreciable values at much lower temperatures than that from S-IV due to the better catalytic efficiency of Pt. **Fig.3-4** also shows that the O_2 fluxes through the ceramic membranes with external short circuit increased significantly with operating temperature. This phenomenon was normally observed for many other mixed conducting membranes, which can be explained by the improvements on ionic transport rates in the membrane bulk and two surface exchange reaction rates with the temperature increase. For instance, O_2 flux through S-V at 550^{o}C has been increased by a factor of 11 at 800^{o}C. Applying the Arrhenius equation, the calculated activation energies for oxygen permeation through the coated SDC membranes are 190.6 kJ/mol (600~650^{o}C) and 68.51 kJ/mol (700~800^{o}C) for Ag coated samples, and 109.1 kJ/mol (500~650^{o}C) and 65.60 kJ/mol (650~800^{o}C) for Pt-coated samples, respectively. The activation energy results clearly imply that Pt coating and high temperature operation facilitate the oxygen permeation process.

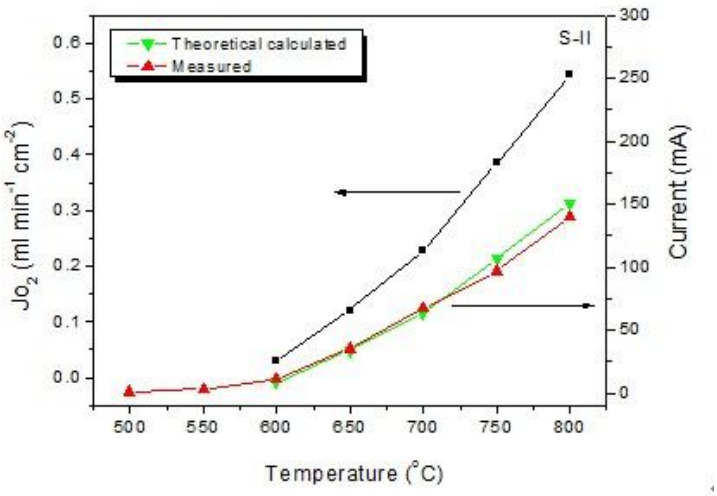

Figure 3-5. Effects of operating temperature on oxygen flux through Sample-III SDC membrane (SDC+ Ag coating + Ag wire) and the electrical current through the external wire with values measured and theoretically calculated

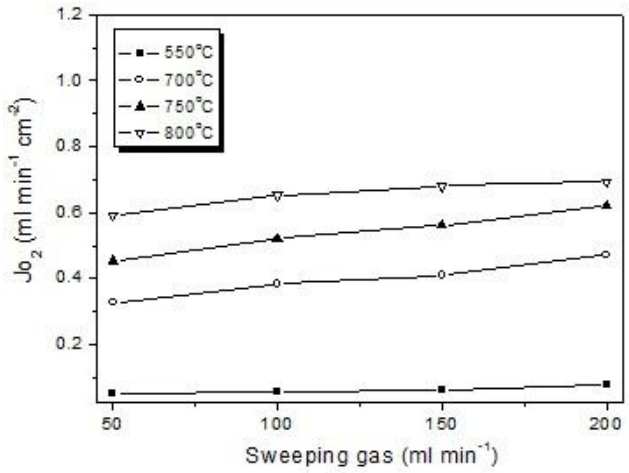

Figure 3-6. Effects of helium sweep rate on the oxygen flux through SDC membrane of sample-V with 1mm thickness (SDC +Pt coating+ Ag sealing)

Fig.3-6 displays that the oxygen flux increased with increasing helium sweep rate. At 700°C, for example, increasing the helium flow rate from 50 to 200 ml min^{-1} raised the oxygen flux from 0.32 to 0.47 ml cm^{-2} min^{-1}. The effect of the sweep flow rate on the oxygen flux has been noted on other membranes [35]. The flux increase is obviously due to the decrease of the oxygen partial pressure at the permeate side. **Fig.3-7** illustrates the effects of SDC membrane thickness on the permeation fluxes. As can be seen, decrease in SDC thickness resulted in higher oxygen fluxes. For

instance, reduction the membrane thickness by a factor of 3.7 from 1.5 to 0.4 mm increased the oxygen fluxes by approximately the same factor of 3.0 from 0.21 to 0.61 ml min^{-1} at 700 ^{o}C. The inverse linear relationship between the oxygen fluxes and the membrane thickness indicates the ionic diffusion in the SDC bulk is the controlling step consistent with Wagner theory. With this finding, the higher oxygen fluxes can be easily achieved by reducing the SDC thickness via coating or hollow fibre technology. Compared to dual phase membranes via the conventional concept by mixing two phases together, the novel SDC membranes exhibited fluxes at least two orders of magnitude higher than that from YSZ based membranes at similar membrane thickness and operating conditions [30]. More striking is that the novel membrane can deliver appreciably higher fluxes at relative lower temperatures starting at 500^{o}C comparing very differently with the developed single phase perovskite membranes which usually requires high temperatures than 800^{o}C. In addition, compared to the high material cost of the dual phase membranes, the novel SDC membrane developed in this work has a big saving in membrane construction cost due to the less usage of expensive precious metals like Ag or Pt. All these factors will be considered in the future for cheaper and simpler integration of the membranes into oxygen consuming industrial processes such as oxy-fuel coal power plants.

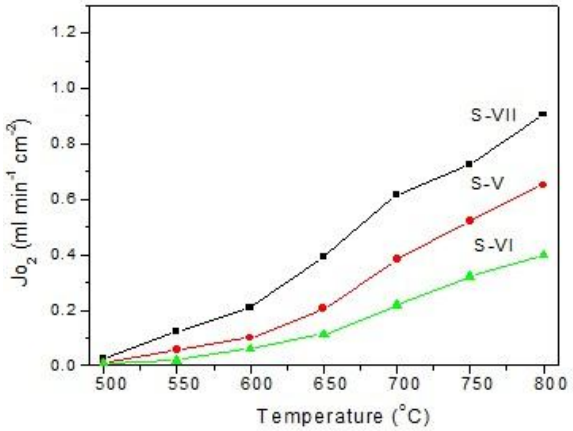

Figure 3-7. Thickness dependence of oxygen permeation flux through SDC membrane (samples (V to VII) with different thickness (S-V: 1 mm, S-VI: 1.5 mm, S-VII: 0.4 mm).

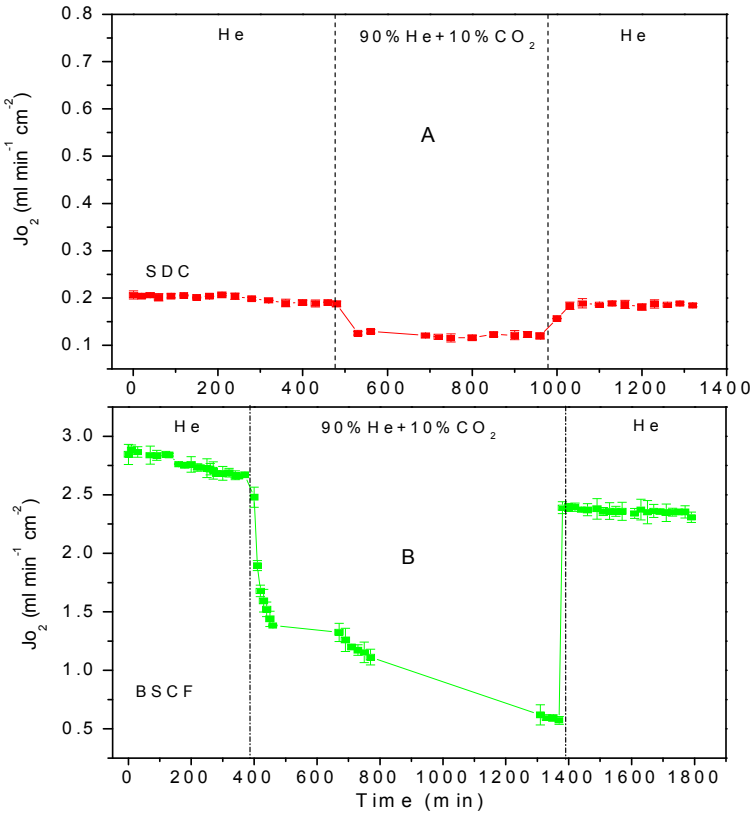

Figure 3-8. The long term oxygen permeation fluxes through sample-VII (SDC) membrane (0.4 mm) at 600 °C (A) and sample-VIII (BSCF) membrane (1-mm-thickness) at 850°C (B) under He or He+CO_2 mixture (total sweep gas flow: 100 ml min^{-1})

Fig.3-8 shows the oxygen flux stability of the new SDC membrane (Sample-VII) and makes a comparison with the typical perovskite BSCF membrane under the gas

mixture with 10 % CO_2 plus 90% He. The coated SDC membranes with 0.4-mm-thickness displays very stable oxygen fluxes in not only He but also in CO_2 containing mixtures. After switching the sweep gas from pure He to the CO_2 containing mixture gas, the fluxes turned to lower but stable values; and when the sweep gas was changed back to He, the oxygen flux was fully recovered to the original values. The lower flux value in the mixture gas is due to the stronger CO_2 adsorption to the membrane surface, but not due to the reaction between CO_2 and SDC. It is well known that SDC can withstand the presence of CO_2. However, in the case of perovskite BSCF membrane (sample-VIII), just as evidenced by **Fig.3-8b**, the oxygen permeation flux experienced a continuing decline even in pure He as sweep gas. Perovskite BSCF is very sensitive to CO_2 and H_2O even with low concentrations in air atmosphere. Furthermore, after the sweep gas was switched to the 10% CO_2 containing gas, the oxygen flux dropped very sharply, bottoming out at only 0.57 ml cm^{-2} min^{-1} at ~1400 min with 80% loss of the initial oxygen flux at 2.87 ml cm^{-2} min^{-1}. Even operated for more than 1000 minutes, the flux still kept the trend of downgrading. When the sweep gas was changed back to pure helium, the oxygen permeation flux of pervoskite BSCF could not be recovered to its original value any more due to the carbonate formation from the reactions between the alkaline earth metals like Ba/Sr and CO_2 at high temperatures [36,37]. Although the stability of these two membranes were tested for less than 30 hours, this striking comparison strongly proves that this new concept membrane has an excellent tolerance for CO_2 gas satisfying the most important stability requirement for their application in clean energy technologies.

3.4 Conclusions

Conventional dual phase membranes made by mixing two phases together to form two distinct and continuous material networks for electronic and ionic conduction are usually characterised by very low O_2 permeation fluxes and high material cost. Single phase mixed conducting perovskite membranes are suffering the poor chemical stability under the real applying conditions. Combining the recent progress in solid oxide fuel cells and mixed conducting membranes, a new ion conducting ceramic membrane concept with external short circuit has been put forward and experimentally verified step by step based on SDC disk, Pt/Ag coating, Ag wire and Ag sealing with the measurement of oxygen permeation flux and electrical current. Higher O_2 permeation fluxes through the new concept membranes have been observed at relative lower temperatures. Strong correlation between the membrane thickness and the O_2 flux values implies the membrane performance can be further improved by reducing the membrane thickness. More inspiringly, the SDC membrane exhibits excellent oxygen permeation stability under CO_2 atmosphere. Considering the high O_2 fluxes, the intermediate operating temperature and the well-known high stability of the fluorite membrane structure, this work is possibly making a breakthrough in the field of oxygen production for clean energy delivery.

3.5 References

1 C. Descamps, C. Bouallou and M. Kanniche, *Energy*, 2008, **33**, 874-881

2 J. M. Beér, *Prog. Energy Combust. Sci.*, 2007, **33**, 107-134.

3 M. Pérez-fortes, A. D. Bojarski, E. Velo, J. M. Nougués and L. Puigjaner, *Energy*, 2009, **34**,1721-1732.

4 K. Jordal, M. Anheden, J. Yan, L. Str€omberg, E. S. Rubin, D. W. Keith, C. F.

Gilboy, M. Wilson, T. Morris, J. Gale and K. Thambimuthu, *in Greenhouse Gas Control Technologies 7*, Elsevier Science Ltd, Oxford, 2005, pp. 201–209.

5 D. Bücker, D. Holmberg and T. Griffin, *in Carbon Dioxide Capture for Storage in Deep Geologic Formations*, Elsevier Science, Amsterdam, 2005, pp. 537–559.

6 G. J. Stiegel, A. Bose and P. Armstrong, *Development of ion transport membrane (ITM) oxygen technology for integration in IGCC and other advanced power generation systems*, US Dept. of Energy, 2006.

7 E. Kakaras, A. Doukelis, D. Glannakopoulos and A. Koumanakos, *6th European Meeting on Coal Research and Its Applications, Canterbury, England*, 2006.

8 S. Smart, C. X. C. Lin, L. Ding, K. Thambimuthu and J. C. Diniz da Costa, *Energy Environ. Sci.*, 2010, **3**, 268-278.

9 P.N. Dyer, R. E. Richards, S. L. Russek and D. M. Taylor, *Solid State Ionics*, 2000, **134**, 21-33.

10 J. Han, G. Xomeritakis and Y.S Lin, *Solid State Ionics*, 1997, **93**, 263-272.

11 H. Jiang, H. Wang, F. Liang, S. Werth, T. Schiestel, and J_rgen Caro, *Angew. Chem. Int. Ed.* 2009, **48**, 2983 –2986.

12 X. Zhu, H. Wang and W. Yang, *Chem. Commun.*, 2004, **8**, 1130-1131.

13 H.J.M. Bouwmeester, H. Kruidhof and A.J. Burggraaf, *Solid State Ionics*, 1994, **72**,185-194.

14 Y.S. Lin, W. Wang and J. Han, *AIChE J.*, 1994, **40**, 786-798.

15 M. Anderson and Y.S. Lin, *J. Membr. Sci.*, 2010, **357**, 122-129.

16 B. Zydorczak, K. Li and X. Tan, *AIChE J.*, 2010, 56, 3084-3090.

17 X. Tan, Z. Wang, B. Meng, X. Meng and K. Li, *J. Membr. Sci.*, 2010, **352**, 189-196.

18 Z.L. Zhan and S.A. Barnett, *Science*, 2005, **308**, 844-847.

19 Z. Shao and S. M. Haile, *Nature*, 2004, **431**, 170-173.

20 Y. H. Huang, R. I. Dass, Z. L. Xing and J. B. Goodenough, *Science*, 2006, **312**, 254-257.

21 Y. Teraoka, H.M. Zhang, S. Furukawa and N. Yamazoe, *Chem. Lett.*, 1985, **11**, 1743-1746.

22 H. Wang, C. Tablet, A. Feldhoff and J. Caro, *Adv. Mater.*, 2005, **17**, 1785-1793.

23 H. Luo, K. Efimov, H. Jiang, A. Feldhoff, H. Wang and J. Caro, *Angew. Chem. Int. Ed.*, 2011, **50**, 759-763.

24 V.V. Kharton, A.V. Kovalevsky, A.P. Viskup, F.M. Figueiredo, A.A. Yaremchenko, E.N. Naumovich and F.M.B. Marques, *J. Electrochem. Soc.*, 2000, **147**, 2814-2821.

25 P.Y. Zeng, Z.P. Shao, S. Liu and Z. Xu, *Sep. Purif. Technol.*, 2009, **67**, 304-311.

26 K. Efimov, T. Halfer, A. Kuhn, P. Heitjans, J. Caro and A. Feldhoff, *Chem. Mater.*, 2010, **22**, 1540-1544.

27 W. Ito, T. Nagai andT. Sakon, *Solid State Ionics*, 2007, **178**, 809-816.

28 J. Kim and Y.S. Lin, *J. Membr. Sci.*, 2000, **167**, 123-133.

29 C.S. Chen, B.A. Boukamp, H.J.M. Bouwmeester, G.Z. Cao, H. Kruidhof, A.J.A. Winnubst, A.J. Burggraaf, *Solid State Ionics* 1995, **76**, 23-28.

30 T.J. Mazanec, T.L. Cable, J.G. Frye Jr., Electrocatalytic cells for chemical reaction, *Solid State Ionics*, 1992, **53**, 111-118.

31 C. Yacou, J. Sunarso, C.X.C. Lin, S. Smart, S. Liu and J. C. Diniz da Costa, *J. Membr. Sci.*, 2011, **380**, 223-231.

32 J.B. Goodenough, *Annu. Rev. Mater. Res.*, 2003, **33**, 91-128.

33 S. Li, S.Wang, Y.Wang, H.Nie, and T. L.Wen, *Fuel Cell*, 2006, **6**, 451-454.

34 T. Tomohiko, K.K. Moe, M. Ito and S. Goto, *Chem. Eng. Sci.*, 1999, **54**, 1553-1557

35 J. Sunarso, S. Liu, Y. S. Lin and J. C. Diniz da Costa, *Energy Environ. Sci.*, 2011,**4**, 2516-2519.

36 M. Arnold, H.H. Wang and A. Feldhoff, *J. Membr. Sci.*, 2007, **293**, 44-52.

37 A.Waindich, A. Mobius and M. Müller, *J. Membr. Sci.*, 2009, **337**, 182–187.

Chapter 4: Enhanced oxygen permeation performance of CO_2 tolerant ion conducting membrane with easily sintered bismuth-based oxide

4.1 Introduction

Our human civilization is facing the severe climate challenge in 21st century due to the large quantity of anthropogenic greenhouse gas emissions since the beginning of the industrial revolution. Emissions from electricity generation contribute the largest portion of the world overall emissions. How to meet an ever increasing energy demand without causing climate change or altering the delicate balance of our ocean system is a great challenge facing all industrialized countries. To mitigate the climate change, the greenhouse gas emission from these fossil fuel burning power plants needs to be significantly reduced; for this purpose, CO_2 capture and storage (CCS) is one of the most important technologies that many countries are currently looking at [1-5]. The deployment of CCS technology is depending on the success of several major technological sections include CO_2 capture, liquefaction, transport, geological sequestration and so on. However, it is very difficult to find an economically feasible technology to capture CO_2 from these flue gas streams with very low CO_2 concentration. Normally, this capture process represents over 80% of the total costs of CCS. In order to get highly CO_2-concentrated flue gas, a new combustion method-oxyfuel has been proposed. Under the oxyfuel concept, coal or gas will be fired with pure O_2 or an O_2/CO_2 mixture instead of air and the major constituent of the flue gas produced during the new combustion process is highly concentrated CO_2 enabling its

capture more economically feasible. However, to get the pure O_2 via conventional cryogenic air separation method is very energy intensive and expensive, which is a big impediment to the commercial application of this oxyfuel technology. Dense ceramic membrane technology is regarded as the best candidate to replace the cryogenics in the oxy-fuel power plant for CO_2 capture with the potentials to cut the O_2 production cost up to 50% [6-8].

Many studies on oxygen permeable membranes have focused on perovskite mixed ionic and electronic oxides (ABO_3) due to their high O_2 fluxes resulted from their inherently high electronic and ionic conductivities [9-20]. Unfortunately, the low material stability of these perovskites greatly restricts their practical application or scale up. When applied in the oxy-fuel combustion process or as membrane reactors for high temperature oxidations, the membranes will be exposed to the acidic gas atmosphere containing CO_2, H_2S or SO_2 and water vapor. These perovskite oxides normally with alkaline-earth elements on A or B sites will be easily eroded by the reaction with these acidic gases. This in the long run will ultimately fail the membranes. As an alternative, ion-conducting fluorite–type materials have attracted much interest because of their high stability to resist these acidic gases at high temperatures. These fluorite-type oxides such as yttria-stabilized zirconia (YSZ) or doped-ceria (SDC/GDC) are widely used as electrolytes for solid oxide fuel cells [21-23]. However, these robust ion conductors do not possess sufficient electronic conductivity for oxygen permeation under mixed conducting concept like the perovskite ones unless the incorporation of another electronic conducting phase via dual phase membrane concept or the addition of external power source and electrodes via the oxygen pump concept [24-30]. The dual phase membranes are characterized by their super-low oxygen permeation fluxes due to the mismatching factors between the two phases, making them far away to be of commercial interest. The pure ion

conducting membranes operated by oxygen pump are also rarely considered because of their structural complexity with external electric loadings. In our previous work with the example of fluorite-type $Sm_{0.2}Ce_{0.8}O_{1.9}$ (SDC), a breakthrough has been made via a new membrane concept-pure ion conducting membrane with external short circuit to use these robust ion conductors for oxygen separation [31]. The measured values of electrical current agree very well with the theoretical calculation using the equation correlating Faraday constant and oxygen fluxes.

For continuing this new membrane concept, in this work, we are looking at a new oxygen ion conductor (yttria stabilized bismuth oxide (YSB)) with external short circuit to examine the oxygen permeation flux and its stability to resist the typical acid gas of CO_2. Compared to SDC membrane being investigated previously, YSB has better ion conductivity at much lower temperatures and therefore it has the potentials to give a higher oxygen flux at a reduced temperature environment.

4.2 Experimental Section

$Y_{0.25}Bi_{0.75}O_{1.5}$ (YSB) composites oxides were synthesized by a combined EDTA-citrate complexing sol-gel process. $Y(NO_3)_3.xH_2O$ and $Bi(NO_3)_3.xH_2O$ (all in A.R. grade) were applied as the raw materials for the metal-ion sources. For the precise controlling of the doping concentration, the metal nitrate compositions were precisely verified and determined by standard EDTA titration technique. Necessary amounts of metal nitrates in the state of aqueous solution were then prepared into a mixed solution according to the target composition, followed by the introduction of EDTA and citric acid as the complexing agents with the mole ratio of total metal ions: EDTA: citric acid=1:1:2. The pH value of the system was controlled at ~ 6 with the help of $NH_3.H_2O$. A transparent purple gel was obtained by continuous heating at 90^oC to slowly evaporate the water. The gel was pre-fired at 250 ^oC followed by calcinations at various temperatures in air for 5 h to get the products with the final composition

and phase structure. For the fabrication of ceramic membrane, the as-obtained oxide powders were pressed into disk-shape membranes in a stainless steel mold (15.0 mm in diameter) under a hydraulic pressure of approximately 1.5×10^8 Pa. These green membranes (~1.0 mm in thickness) were further sintered in an electrical box furnace at 750, 800, 850 and 900 ^oC in air for 5 h at a heating/cooling rate of 1-2 $^oC\ min^{-1}$. The thickness and diameter of the sintered electrolyte disks were ~0.4-1.5 and ~12 mm, respectively. Platinum slurry was applied to each side of the YSB membrane by vacuum spraying deposition and then re-calcined at 600 ^oC in air for 2 h. Silver paste was used as the conductive phase to connect the two sides of membranes. For the details of this external short-circuited structure, it can be referred to **Fig.4-1**. Scanning Electron Microscopy (SEM) images were obtained using a Zesis EVO 40XVP at an accelerating voltage of 15kV. The XRD analysis was carried out on a Bruker D8 Advances X-ray diffractometer using Cu Ka radiation generated at 40 kv and 30 mA. Thermo-gravimetric analysis (TA) was carried out by TA instrument (TA Q600). 500 mg of the membrane sample was placed in sample holder and heated from 50^oC to 850^oC at a rate of 10$^oC\ min^{-1}$with the 100 ml min^{-1} flow rate of N_2, CO_2 or CO_2+H_2O. Permeation properties of the membranes were investigated by the gas chromatography (GC) method. Silver paste was used as the sealant to fix the membrane disk onto a dense quartz tube and exposed an effective area of ~ 0.45 cm^2 at the sweep side for permeation study. Helium and carbon dioxide were applied as the sweep gas to create an oxygen partial pressure gradient across the membrane. To the study the effect of H_2O on the oxygen permeability, the sweep gases were passed through a water vapor saturator at the temperature where the gases were saturated by H_2O (~3% H_2O at 28 ^oC). Helium was used as the carrier gas to carry the permeated oxygen to a Shimadzu 2014A equipped with a 5Å capillary molecule column and thermal conductivity

detector for quantitative oxygen concentration analysis. The oxygen permeation flux was calculated by:

$$Jo_2\ (ml\ cm^{-2}\ \min^{-1}) = [C_{O_2} - C_{N_2} \times \frac{0.21}{0.79} \times \left(\frac{28}{32}\right)^{\frac{1}{2}}] \times \frac{F}{S}$$

Where C_O and C_N are the measured concentrations of oxygen and nitrogen in the gas on the sweep side, respectively (mol ml^{-1}), F is the flow rate of the exit gas on the sweep side (ml min^{-1}), and S is the membrane geometric surface area of the sweep side (cm^2). In theory, only oxygen would be permeated though the membrane. Due to the possible gas leakage through the sealing area, nitrogen sometimes would be detected; in this case, the oxygen contribution by the leakage was subtracted using the above equation.

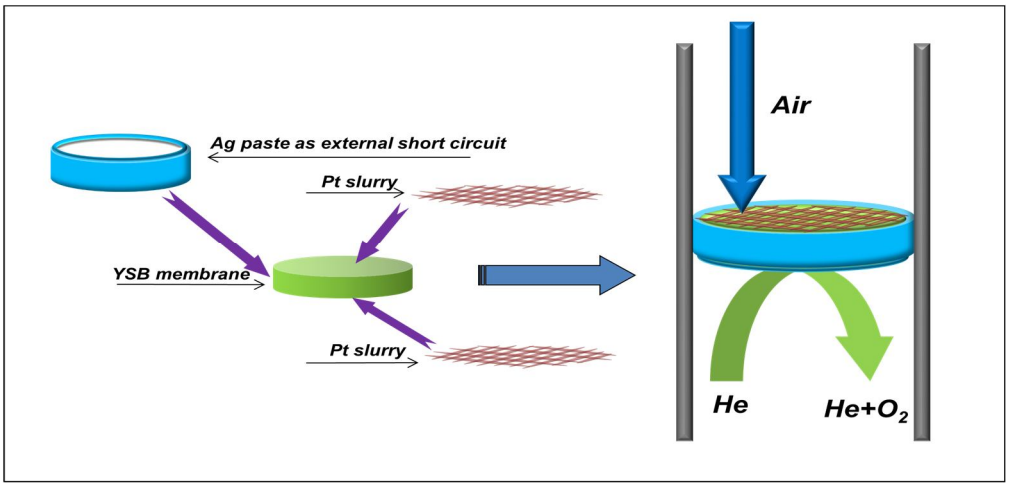

Fig.4-1 The configuration of YSB membrane with external short circuit

4.3 Results and discussion

$Y_{0.25}Bi_{0.75}O_{1.5}$ (YSB) oxide was prepared by the described sol-gel method with final calcination at 650°C for 5 hours under an air atmosphere. Its XRD pattern was displayed in **Fig.4-2**. The characteristic peaks were located at the respective 2θ angles of 28° (111), 33° (200), 47° (220), 52° (311), 58° (222) and 76° (331), in a good agreement with previous published results. The prepared YSB powder has been used

as the initial membrane material to fabricate the qualified dense membrane by sintering at high temperatures. Experimental results illustrate that the sintering temperature can be arranged from 750 to 850 ^{o}C to achieve the densified structure. **Fig. 4-3** shows the SEM morphologies of the YSB membrane sintered at 750, 800 and 850^{o}C for 5 hours in air, respectively.

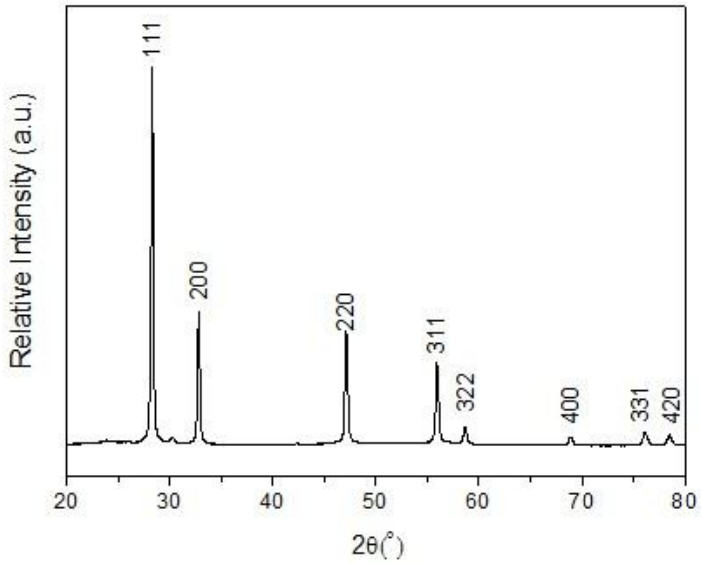

Fig.4-2 XRD pattern of the YSB powder calcinated at 650 ^{o}C for 5 hours

In addition, the SEM of the membrane (sintered at 800^{o}C) after the long term permeation test in the presence of CO_2 is also included, which will be discussed in the later section. All the three membranes are well densified with the relative density of 94, 96 and 97%, respectively, measured by Archimedes liquid displacement method. The YSB densification with the increase of sintering temperature by particle grain growth is clearly observed. For sintering at 750 ^{o}C, most of the grain size is less than 1 micron; however it quickly increases to 2.5 or 3 microns when the sintering was carried out at higher temperatures of 800 or 850^{o}C, respectively. Compared to other oxygen selective ceramic membranes, the sintering temperature of YSB membrane is significantly lower than SDC or perovskites whose sintering temperature normally is higher than 1000 ^{o}C. The relative easy sintering of YSB ceramic is closely related to

its lower melting point of bismuth-based oxide, because of which, it has been frequently used as the sintering aid to facilitate the densification of other ceramics with higher melting points. Sintering temperature could have significant effects on the oxygen permeability of the ceramic membranes, which will be discussed shortly.

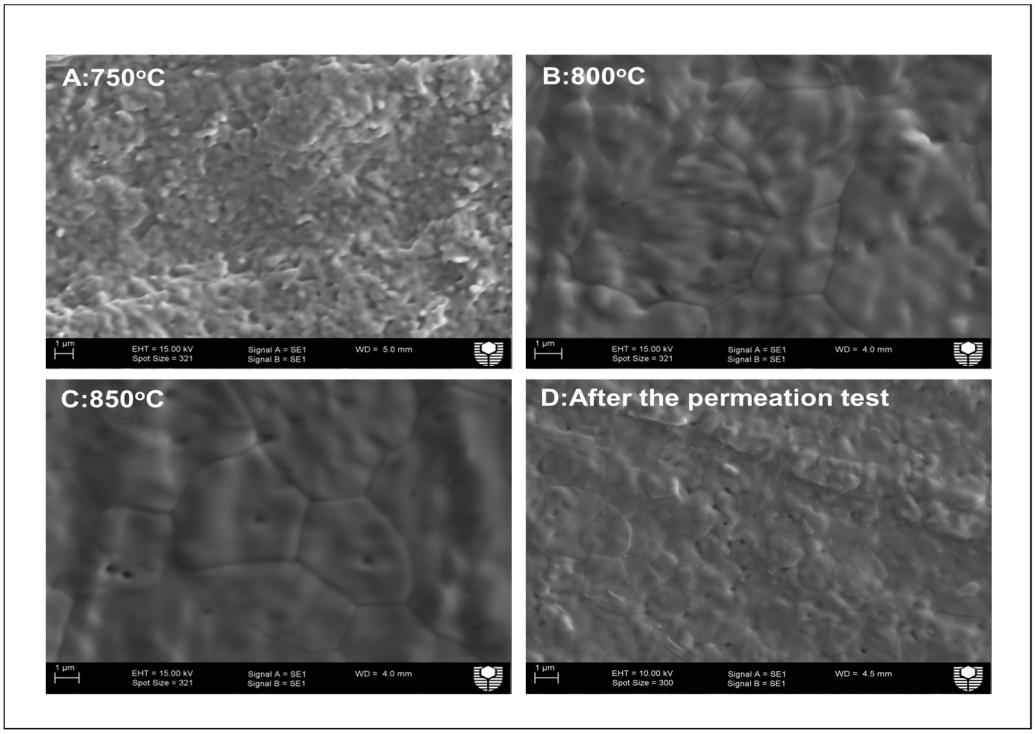

Fig. 4-3 SEM morphologies of the YSB membranes sintered from 750°C, 800°C, 850°C for 5 hours and after the oxygen permeation test.

The oxygen permeation flux through 1-mm-thick YSB membrane coated by Pt porous layer with external Ag circuit with the configuration showing in **Fig.4-1** is depicted by **Fig.4-4** as a function of operating temperature. For comparison purpose, the oxygen permeation fluxes through SDC and blank YSB membranes with the same thickness are also presented in **Fig.4-4**. As we can see, the blank YSB membrane did not exhibit any permeation value in the entire temperature range investigated from 600 to 850 °C as YSB is a pure ion conductor and cannot be used as an oxygen permeating membrane due to the lack of electronic phase. By contrast, short-circuited YSB (Sample-B) gave constantly increasing fluxes with temperature increment. At 600 °C,

the oxygen flux is only 0.07 ml cm^{-2} min^{-1}. When the temperature increases to 850 ^{o}C, the oxygen flux can reach as high as ~1.33 ml cm^{-2} min^{-1}. Membrane configuration of Sample-B is given in **Fig.4-1**. Here the porous Pt layer coated on the surface of YSB membrane was working as two functions. One is to fulfill the full electron transport route together with the external circuit of silver paste for electrons passing from oxygen poor side to oxygen rich side and another function is working as the catalyst for oxygen reduction and oxidation at the membrane surface. Sample-c shows the oxygen flux through SDC membrane with exactly similar configuration as YSB. At the high temperature zone from 700 to 800 ^{o}C, the oxygen flux of YSB membrane was steadily higher than SDC membrane. It is interesting to note that, at 800 ^{o}C, the oxygen flux of YSB membrane standing at 1.1 ml cm^{-2} min^{-1} is almost twice as that of SDC membrane (~0.6 ml cm^{-2} min^{-1}). This significant improvement is resulted from the high oxygen ionic conductivity of the YSB material. It was reported that the ionic conductivity of bismuth-based oxide is one or two orders of magnitude larger than that of the doped-ceria oxide (SDC). **Fig.4-4** also tells that the oxygen flux of YSB membrane dropped very quickly with the decrease of the temperature from 750 to 700 ^{o}C. At temperatures below 700^{o}C, the YSB flux is lower than SDC membrane. The reduced flux values with temperature decrease can be explained by the slow oxygen ion diffusion rate and slow surface reaction kinetics. To explain the phenomenon of YSB flux lower than SDC at reduced temperatures, YSB phase structure transition has to be considered. Bismuth-based oxide is known as a defect fluorite type structure (δ phase). The high oxygen vacancy concentration and its disorder distribution in δ phase leads to the excellent oxygen ionic transport capacity [32]. However, the δ phase is unstable at lower temperatures because of the phase transition to the oxygen vacancy order phase (α phase). As a result, this phase transition degrades the oxygen ionic conductivity. In order to make the bismuth-based oxide feasible to act as an

ionic conductor, some cations such as La, Ca, Gd and Y, have been introduced as dopants to stabilize the δ phase Bi_2O_3 system [33-35]. Yttria-stabilized bismuth oxide with high ionic conductivity exhibits δ phase over a wide temperature range in ambient oxygen atmosphere and therefore displays a higher oxygen flux. However, the stability of the YSB is questioned under a reducing atmosphere and the loss of stoichiometric oxygen in YSB oxide facing the permeate side may take place when it is exposed at low oxygen partial pressure, leading the destruction of the fluorite structure [36,37]. Meanwhile, a decay in ionic conductivity was observed on stabilized bismuth oxides below 650^{o}C due to the aging effect from the ordering of oxygen vacancies [38]. In this case, oxygen ion transportation through the YSB membrane became very difficult at lower temperature range. Therefore, phase transition is the reason for the observed lower YSB oxygen flux than SDC at the lower temperature range. Despite of this, compared to perovskite membrane like $Ba_{0.5}Sr_{0.5}Co_{0.8}Fe_{0.2}O_{3-\delta}$ (BSCF), the YSB membrane still showed better oxygen fluxes at lower temperatures like 650 ^{o}C. The good oxygen permeability from 700 to 850 ^{o}C is coincidently in the temperature range of gas partial oxidation to syn-gas and C_2 hydrocarbons, encouraging the potential use of the YSB membrane as a high temperature membrane reactor.

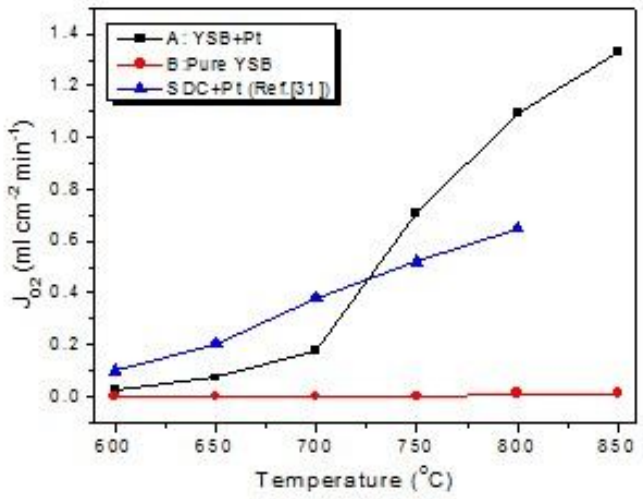

Fig.4-4 Temperature dependence of the oxygen permeation fluxes through various YSB membrane with 1mm thickness

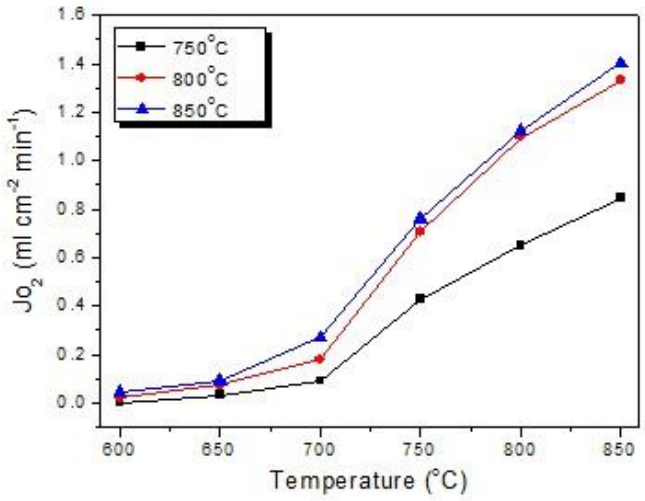

Fig.4-5 Oxygen permeation fluxes through the YSB membrane sintered at different temperatures.

As discussed above, the dense YSB membranes can be prepared at different sintering temperatures, which influence the grain size, morphologies and oxygen permeation behavior of the resultant membranes. **Fig.4-5** is investigating the effects of sintering temperatures on the oxygen fluxes through YSB membranes sintered at three different temperatures but with the same thickness. During the measurement, oxygen partial pressure at the oxygen rich side membrane surface was maintained at 0.21 atm while the helium sweep rate at the oxygen lean side was fixed at 100 ml min^{-1}. It can be

seen that the three fluxes increased obviously with the operation temperature attributing to the increase in oxygen diffusion rate and surface reaction kinetics. Meanwhile, at the same operating temperature, the membrane sintered at higher temperatures gave better oxygen fluxes. For example, YSB membranes sintered at 750 and 800 ^{o}C delivered the flux values of 0.85 and 1.33 ml cm^{-2} min^{-1} respectively when operated at 850 ^{o}C. However, when the membrane sintering was carried out at above 800 ^{o}C, the flux improvement is very marginal with only 8 % increment at sintering temperature of 850 ^{o}C compared to that sintered at 800^{o}C. All these phenomena can be explained by their specific membrane morphologies achieved at their particular sintering temperatures. The YSB membrane sintered at lower temperature like 750 ^{o}C is in a more porous structure with smaller grain size as observed in **Fig.4-3**. When oxygen was permeated through, oxygen was easily entrapped inside these isolated spaces; on the other hand, smaller grain size makes the ceramic bulk to have more grain boundary area. Both of these two factors cause larger oxygen transport resistance and therefore bring up a lower permeation flux. When the sintering temperature was higher or equal to 800 ^{o}C, the change of YSB morphology or particle grain size is very minimal and thus would not induce much difference in the flux value just like the case of YSB membranes sintered at 800 and 850 ^{o}C. Considering the balance between the manufacturing cost and the membrane performance, sintering at 800 ^{o}C seems a good option for the YSB membranes.

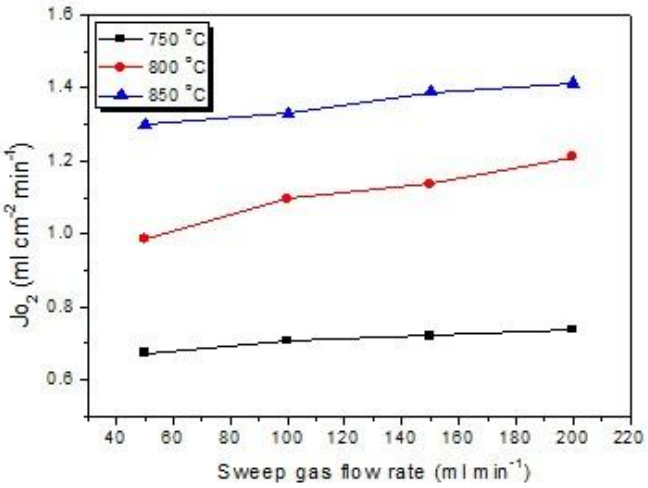

Fig.4-6 Oxygen permeation fluxes through the YSB membranes sintered at 800°C with different sweep gas flow rates

Fig.4-6 demonstrates the oxygen flux through the YSB membrane under different Helium sweeping flow rate. It can be observed that the oxygen flux increased with the increase of the helium flow rate. This improvement mainly resulted from the rise of the driving force by lowering the oxygen partial pressure at oxygen poor side. The effect of the sweep flow rate was also investigated on other membranes [39,40]. In the case of the slow surface exchange process as the permeation rate determination step, the improvement factor for the oxygen permeation flux can be achieved to several times just by increasing the sweep flow rate. However, in this study, the increase of the helium flow rate only resulted in a very slight increase of the oxygen permeation flux. For example, raising the sweep flow rate by a factor of 400% from 50 to 200 ml min^{-1} only caused the permeation flux increased by a factor of 11% from 1.1 to 1.21 ml cm^{-2} min^{-1} at 800 °C. This result implied that the relative slow oxygen ionic bulk transport in the YSB membrane controlled oxygen permeation process.

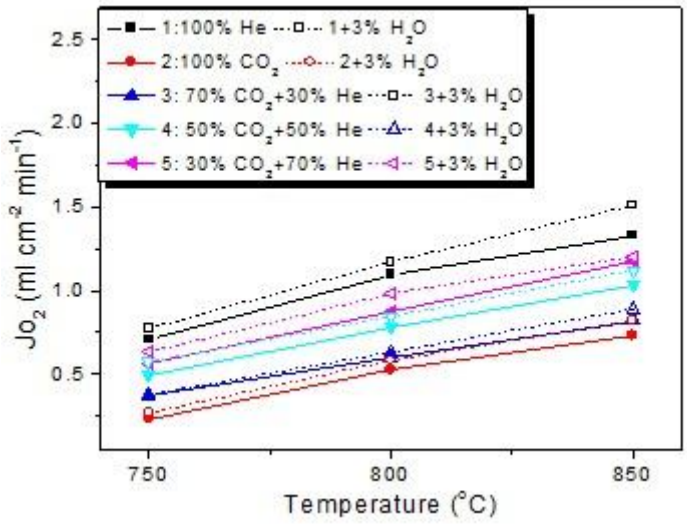

Fig.4-7 Oxygen permeation fluxes through the YSB membrane with different sweep gases (total flow rate is 100 ml min^{-1})

In practical application, the oxygen permeation membranes are usually exposed in the presence of acid gas containing atmospheres such as CO_2, SO_2 and water vapor. Therefore, it is important to investigate the influence of the acid gases on oxygen permeability of the YSB membranes. **Fig.4-7** shows the effects of CO_2 and water vapor on the oxygen permeation flux through one YSB membrane. The total flow rate of CO_2 and He sweep gases was maintained at 100 ml min^{-1}. Fig.6 shows that the oxygen permeation flux experienced an obvious decline when CO_2 was introduced into the sweep gas. Furthermore, the oxygen flux steadily decreased with the increase of the CO_2 concentration in the sweep gas, suggesting that the negative effect of CO_2 on the oxygen flux is correlated to CO_2 concentration. For instance, under the condition of pure helium as the sweep gas, the oxygen permeation flux can achieve as high as 1.33 ml cm^{-2} min^{-1} at 850°C, however lowered down by 60% to 0.73 ml cm^{-2} min^{-1} with using the pure CO_2 as the sweep gas. The similar result, regarding this falloff of the oxygen permeability based on the perovskite-type membranes, has been observed by many other researchers as well [41,42]. In these cases, the immediate drop of the oxygen permeation through perovskite-type membrane with the CO_2 containing

atmospheres at high temperatures was mainly ascribed to the carbonate formation on the membrane surface. Different from this, the fluorite-type oxides have the good chemical and structural stability, even at the highly reducing atmosphere. Besides, these very tough materials can withstand the erosion effect from the acid gases. Some of fluorite oxides can even maintain their stability under the direct exposure to strong acidic solutions such as HNO_3 or HCl [43]. Generally, oxygen exchange reaction on the membrane surface is a very important step for the oxygen permeation process. Previous studies indicated that, instead of the formation of carbonate layer on the membrane surface, CO_2 strong chemical adsorption on the membrane surface impedes the oxygen oxidation. As a result of this negative effect, the oxygen release from the membrane oxygen poor side has been slowed down [44,45]. Therefore, this is a general influence of CO_2 on all dense ceramic membranes for oxygen separation. Compared to the irreversible membrane damage caused by carbonate formation, the negative influence of CO_2 chemical adsorption is temporary and can be easily recovered if CO_2 is replaced by other gases, which will be further discussed shortly. Here, we continue to discuss the influence of other gas on the permeation behavior. The influence of water vapor, another common byproduct from most of petro-chemistry production or any combustion processes, was investigated. It can be clearly seen from Fig.6 that all the samples experienced a flux growth in the presence of ~3% H_2O in the sweep gases of the pure helium or the CO_2 containing atmospheres. For example, at 850^oC, the oxygen fluxes have been increased from 1.33 to 1.51 or from 0.73 to 0.82 ml cm^{-2} min^{-1} when 3% H_2O was added in the pure helium or pure CO_2 as the sweep gases, respectively. In case of perovskite oxides, the presence of H_2O can accelerate the carbonate formation on the membrane materials to deteriorate their oxygen permeability. For a more stable material like YSB, the carbonate formation mechanism cannot be employed to explain this oxygen flux enhancement

phenomenon in the presence of water vapor at high temperatures, which is contrary to that observed in perovskite oxide. The oxygen generated on the poor side comes from the desorption of the dissociated oxygen atom on the membrane surface. It is well known that the oxygen surface exchange process, especially for the oxygen desorption, is very difficult. In the traditional oxygen permeation process, the removal of oxygen from membrane surface to ambient gases is realized by the oxygen concentration gradient, i.e., oxygen itself. Besides, the desorption energy for the oxygen removal ($E_D(O)$) on metal oxides was found to be very high, which means a lot of energy will be consumed in the process of the oxygen desorption from the oxide surface[46,47]. The presence of water vapor can assist the oxygen desorption from the oxide surface by the combination of H_2O and O accompanying the formation of –O-H bond. Hydrogen induced –O-H bond can weaken the desorption energy of oxygen atom species which makes it easier to be removed from the surface of oxides. **Fig.4-8** depicts the schematic diagram of the oxygen permeation through the YSB membrane in the presence of H_2O. With the help of H_2O, -O-H bonds were developed on the membrane surface in both helium and CO_2 atmospheres. The surface oxygen atom may react with a H_2O molecule to form the two –O-H bonds. Subsequently, oxygen can be released from the membrane surface with desorption of –O-H bond which has much lower desorption energy than oxygen atom itself [46]. This explains that with the introduction of H_2O in the presence of CO_2, the oxygen flux steadily increased rather than decreased.

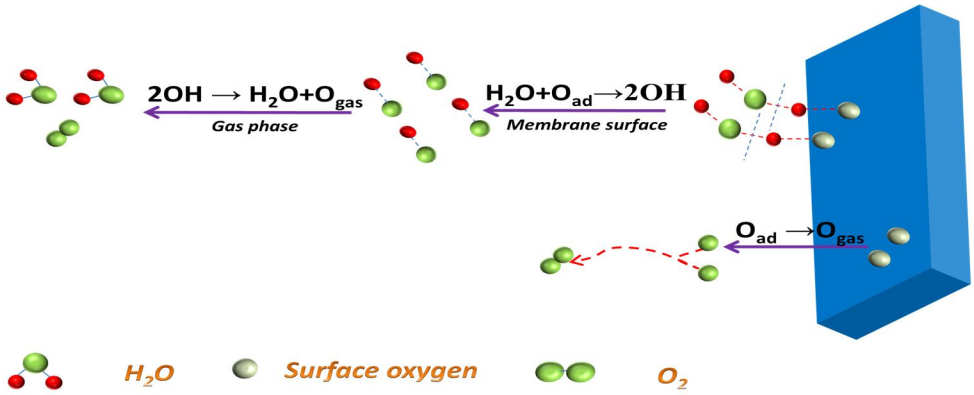

Fig.4-8 Diagram of oxygen permeation mechanism of the YSB membrane in the presence of H_2O

Fig.4-9 shows the oxygen permeation flux through the YSB membrane as a function of time at 800°C with different atmospheres up to 700 minutes. With pure He as the sweep gas, the oxygen flux was stabilized at 1.01 ml cm^{-2} min^{-1}. When the sweep gas was switched to 30% CO_2+70% He, the oxygen flux had an obvious decline but still kept a very stable value at 0.73 ml cm^{-2} min^{-1} during the 200 min permeation test. As discussed above, this flux decline was resulted from the CO_2 chemical absorption on the membrane surface. After that, 3% H_2O was introduced into the sweep gas mixture of CO_2 and He, resulting in a slight increase of the oxygen flux. When the sweep gas finally changed back to the pure helium, the oxygen flux was fully recovered to the original value indicating that the influence of CO_2 or H_2O to the YSB membrane is temporary and there is no permanent damage to the material phase or membrane morphology as shown in **Fig.4-3**. Strikingly, the similar exposure treatment to perovskite membrane would lead to the membrane failure due to the irreversible reactions between the membrane materials and these gases [48,49]. Sufficient chemical stability of the membrane material against these acid gases will be the first prerequisite to be considered for further application in oxyfuel combustion or high temperature gas partial oxidations. In this sense, YSB membrane with higher chemical stability has the promising potential to meet the application requirements.

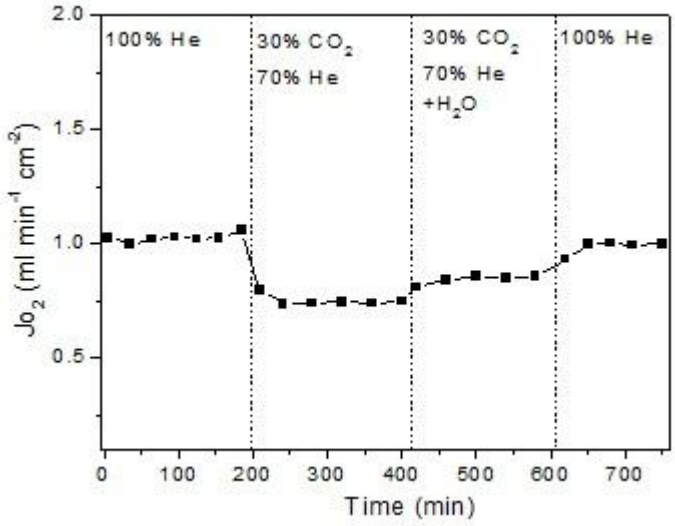

Fig.4-9 Long term oxygen permeation test of the YSB membranes under different gas atmospheres.

4.4 Conclusions

Under a new membrane concept-pure ion conducting membranes with external short circuit derived from the configuration of solid oxide fuel cells, yttria stabilized bismuth oxide (YSB) membrane has been synthesized and its performance for air separation has been tested in real application conditions containing acid gas of CO_2 and water vapor. Higher O_2 permeation fluxes through YSB have been observed at relative lower temperatures. YSB membrane also displayed high chemical and flux stability in the CO_2 and water vapour containing atmosphere. Compared to the fast and permanent membrane damage caused by CO_2 reaction in case of the mixed conducting perovskite oxides, there is no membrane damage observed for YSB membranes after the permeation test. On the contrary, the presence of water vapour is beneficial for oxygen permeation evidenced by the flux increment and a possible mechanism has been put forward to explain this phenomenon. Considering the much lower sintering temperature for preparation, high O_2 fluxes, the intermediate operating temperature and the well-known high stability of the fluorite membrane structure,

YSB membrane deserves further fundamental studies like maximising its oxygen fluxes via the combined thin film and surface modification technology and its scaling up in real applications like oxyfuel combustion for clean energy delivery.

4.5 References

1. C. Lastoskie, Caging carbon dioxide, *Science*, 2010,**330**, 595-596.
2. D.M. D'Alessandro, B. Smit, J.R. Long, *Angew. Chem. Int. Ed.,* 2010, **49**, 6058-6082.
3. C.A. Scholes, K.H. Smith, S.E. Kentish, G.W. Stevens, *Int. J. Greenhouse gas control*, 2010, **4**, 739-755.
4. J.D. Figueroa, T. Fout, S. Plasynski, H. Mcllvried, R.D. Srivastava, *Int. J. Greenhouse gas control*, 2008, **2**, 9-20.
5. N. MacDowell, N. Florin, A. Buchard, J. Hallett, A. Gallndo, G. Jackson, C.S. Adjiman, C.K. Williams, N. Shah, P. Fennell, *Energy Environ. Sci.*, 2010, **3**, 1645-1669.
6. H. Stadler, F. Beggel, M. Habermehl, B. Persigehl, R. Kneer, M. Modigell, P. Jeschke, *Int. J. Greenhouse Control*, 2011, **5**,7-15.
7. S. Smart, C.X.C. Lin, L. Ding, K. Thambimuthu, J.C.Diniz da Costa, *Energy Environ. Sci.*, 2010, **3**, 268-278.
8. G.J. Stiegel, A. Bose and P. Armstrong, *Development of ion transport membrane (ITM) oxygen technology for integration in IGCC and other advanced power generation systems*, U.S. Dept. of Energy, 2006.
9. H. Wang, S. Werth, T. Schiestel, J. Caro, *Angew. Chem. Int. Ed.*, 2005, **44**, 6905-6909.
10. H. Wang, C. Tablet, A. Feldhoff, J. Caro, *Adv. Mater.*, 2005, **17**, 1785-1788.
11. Z. Shao, W. Yang, Y. Cong, H. Dong, J. Tong, G. Xiong, *J. Membr. Sci.*, 2000, **172**, 177-188.
12. A. Leo, S. Smart, S. Liu, J.C. Diniz da Costa, *J. Membr. Sci.*, 2011, **368**, 64-68
13. X. Dong, W. Jin, N. Xu, K. Li, *Chem. Commun.,* 2011, **47**, 10886-10902.
14. K. Li, X. Tan, Y. Liu, *J. Membr. Sci.*, 2006, 272, 1-5.
15. Z.Q. Deng, W.S. Yang, W. Liu, C.S. Chen, *J. Solid State Chem.*, 2006, 179, 362-369.

16. X. Zhu, H. Wang, W. Yang, *Chem. Commun.*, 2004,1130-1131.

17. Y. He, X. Zhu, Q. Li, W. Yang, *AIChE J.*, 2009, **55**, 3125-3133.

18. J. Sunarso, S. Baumann, J.M. Serra, W.A. Meulenberg, S. Liu, Y.S. Lin, J.C. Diniz da Costa, *J. Membr. Sci.*, 2008, **320**, 13-41.

19. B. Zydorczak, K. Li, X. Tan, *AIChE J.*, 2010, **56**, 3084-3090.

20. P. Zeng, Z. Chen, W. Zhou, H. Gu, Z. Shao, S. Liu, *J. Membr. Sci.*, 2007, **291**, 148-156.

21. Z. Zhan, S.A. Barnett, *Science*, 2005, **308**, 844-847.

22. S. Park, J.M. Vohs, R.J. Gorte, *Nature*, 2000, **404**, 265-267.

23. Z. Shao, S.M. Haile, Nature, 2004, **431**, 170-173.

24. H. Jiang, A. Feldhoff, H. Wang, J. Caro, *Angew. Chem. Int. Ed.,* 2011, **50**, 759-763.

25. X. Zhu, H. Liu, Y. Cong, W. Yang, *Chem. Commun.*, 2012, **48**, 251-253.

26. C.S. Chen, H. Kruidhof, H.J.M. Bouwmeester, H. Verweij, A.J. Burggraaf, *Solid State Ionics*, 1996, **86**, 569-572.

27. C.S. Chen, H. Kruidhof, H.J.M. Bouwmeester, H. Verweij, A.J. Burggraaf, *Solid State Ionics*, 1997, **99**, 215-219.

28. T. Hibino, K. Ushiki, Y. Kuwahara, *Solid State Ionics*, 1997, **93**, 309-314.

29. D.L. Meixner, D.D. Brengel, B.T. Henderson, J.M. Abrardo, M.A. Wilson, D.M. Taylor, R.A. Cutler, *J. Electrochem. Soc.*, 2002, **149**, D132-D136.

30. W. Zhou, Z. Shao, R. Ran, Z. Chen, P. Zeng, H, Gu, W. Jin, N. Xu, *Electrochim. Acta*, 2007, **52**, 6297-6303.

31. K. Zhang, Z. Shao, C. Li, S. Liu, *Energy Environ. Sci.*, 2012, **5**, 5257-5264.

32. E. Capoen, M.C. Steil, G. Nowogrocki, M. Malys, C. Pirovano, A. Löfberg, E.B. Richard, J.C. Boivin, C. Mairesse, R.N. Vannier, *Solid State Ionics*, 2006, **177**, 483-488.

33. T. Takahashi, H. Iwahara, T. Arao, *J. Appl. Electrochem.*, 1975, **5**, 187-195.

34. T. Takahashi, T. Esaka, H. Iwahara, *J. Appl. Electrochem.*, 1975, **5**, 187-202.

35. J.C. Boivin, D.J. Thomas, *Solid State ionics*, 1981, **5**, 523-525.

36. Y. Zeng, F.T. Akin, Y.S. Lin, *Appl. Catal. A*, 2001, **213**, 33-45.

37. Y. Zeng, Y.S. Lin, *J. Catal.*, 1999, **182**, 30-36.

38. N. Jiang, R.M. Buchanan, F.E.G. Henn, A.F. Marshall, D.A. Stevenson, E.D. Wachsman, *Mater. Res. Bull.*, 1994, **29**, 247-254.

39. X. Tan, Z. Wang, H. Liu, S. Liu, *J. Membr. Sci.*, 2008, **324**, 128-135.

40. C. Yacou, J. Sunarso, C.X.C. Lin, S. Smart, S. Liu, J.C. Diniz da Costa, *J. Membr. Sci.*, 2011, **380**, 223-231.

41. M. Arnold, H. Wang, A. Feldhoff, *J. Membr. Sci.*, 2007, **293**, 44-52.

42. J. Yi, M. Schroeder, *J. Membr. Sci.*, 2011, **378**, 163–170.

43. Y. Lin, C. Su, C. Huang, J.S. Kim, C. Kwal, Z. Shao, *J. Power Sources*, 2012, **197**, 57-64.

44. X. Tan, N. Liu, B. Meng, J. Sunarso, K. Zhang, S. Liu, *J. Membr. Sci.*, 2012, **389**, 216-222.

45. J. Tang, Y. Wei, L. Zhou, Z. Li, H. Wang, *AIChE J.*, 2012, **58**, 2473-2478.

46. K. Hermann, M. Witko, R. Druzinic, R. Tokarz, Top. Catal., 2000, **11**, 67-75.

47. E.M. Stuve, R.J. Madix, B.A. Sexton, Surf. Sci., 1981, **111**, 11-25.

48. J. Yi, S. Feng, Y. Zhao, W. Liu, C. Chen, *Chem. Mater.*, 2003, **17**, 5856-5861.

49. A. Yan, B. Liu, Y. Dong, Z. Tian, D. Wang, M. Chen, *J. Membr. Sci.*, 2008, **80**, 24-31.

Chapter 5: CO_2-tolerant ceramic membrane driven by electrical current for oxygen production at intermediate temperatures

5.1 Introduction

Oxygen has been ranked among the most frequently used chemicals in many fields of our modern society, such as the petroleum and power industries, and medical applications. How to develop cost-effective and reliable oxygen production technologies for different application purposes is always of researchers' interest. Currently, for industrial oxygen tonnage production (i.e., more than 1000 tons per day), the viable technology is air separation by conventional cryogenic distillation method. However, high investment cost, high equipment replacement frequency, and safety hazards associated with the handling of these pressurized containers at low temperatures make this technology energy-intensive and expensive, which is prohibitive for novel applications like clean energy technologies where large quantity of pure oxygen is required as the feed gas. Another approach for intermediate scale production less than 500 tons per day is called Pressure Swing Absorption (PSA), a more flexible way to produce oxygen based on selective gas absorption. The drawback of PSA method is that these selective absorption materials, i.e., zeolite or carbon molecule sieves, can be easily contaminated by the pollutant in air and thus needs frequent cleaning. Furthermore, the oxygen purity from PSA is always less than 95% as these absorbents only remove nitrogen from air leaving other components unchanged.[1] In addition to these two conventional methods, a new technology using ion transporting ceramic membranes for oxygen production has the potential to cut

down the cost and provide oxygen with purity up to 100%.[2-25] Generally, the oxygen separation process through these ion conducting membranes is realized by either pressure driving force or electrically driving force, depending on the different membrane configurations. For pressure-gradient driving design, mixed ion and electron conducting (MIEC) membranes in one material phase or dual (or more than two) phases are applied to simplify the membrane design without the necessity of any external electrical circuit. The oxygen is permeated through the membrane driven by the oxygen partial pressure gradient between the two sides of the membrane. To create sufficiently high driving force for good oxygen fluxes, a very large pressure is employed on the air feed side, which requires additional gas compressors and high membrane mechanical strength. More complicated is that most of these MIEC membranes of interest are made from perovskite oxides, which are not stable at practical application conditions due to the reactions between the membrane materials and the acid gases like CO_2. Fortunately, robust ceramic ion conductors do exist and can be found from these doped fluorite oxides like Sm-doped ceria (SDC) or yttria-stabilized zirconia (YSZ). The applications of these pure ion conductors for oxygen production are based on electrically driving membrane designs (also called electrical oxygen pump (EOP)) with an external circuit to provide the electrical current/voltage. The main advantage of EOP membrane is that oxygen transport direction and flux value are completely dependent on the electrical current being applied, but independent of the oxygen partial pressure difference; thus pure oxygen can be generated from the air just at atmospheric pressure without using compressors or vacuum pump. These benefits open the potential for the development of miniaturized devices for portable and continuous oxygen supply with applications can be found in aquarium, hospitals, aeroplanes, vehicles or offices at plateau region, even as membrane reactors for separation and reactions.[26] The application of EOP membrane

is also possible for large scale oxygen production for clean coal energy delivery such as integrated gasification combined cycle (IGCC) or oxyfuel combustion in these countries rich in coal resource like Australia and China as they can possibly make the economic justification of the coal consumed for the electricity portioned for oxygen production section.[27]

Previous studies of the EOP ceramic membrane is based on yattria stabilized zirconia (YSZ) as an electrolyte and noble metals such as Pt as the electrodes.[28] Unfortunately, the high cost and low oxygen production efficiency make it unpractical for massively scalable use. Recently, efforts have been focused on developing new ion conducting oxides to lower the oxygen production temperature and using mixed conducting oxides as the electrodes to replace these expensive noble metals. Several studies investigated the oxygen permeation behavior based on cobalt-containing perovskite as the electrodes and fast ion conducting oxide of doped ceria as the electrolyte with improved performance.[29-31] Sufficient stability to resist the CO_2 containing atmosphere is very critical for prospective industrial applications since CO_2 is a natural constituent in the air as well as a by-product in oxidative hydrocarbon activation reactions. However, the stability against CO_2 containing atmospheres for these cobalt-containing perovskite electrodes is questioned due to their low structure stability and thermodynamically favorable formation of carbonates.[32-33]

In this paper, we present a high CO_2 tolerant EOP membrane based on $Sm_{0.2}Ce_{0.8}O_{1.9}$ (SDC) electrolyte and a cobalt-free $La_{0.6}Sr_{0.4}FeO_{3-\delta}$ (LSF) electrode. The oxygen permeation performance and CO_2 stability of the SDC/LSF electrochemical membrane were systemically investigated. Compared to YSZ, SDC has higher ionic conductivities at intermediate temperature range. LSF is a well-known more stable perovskite oxide than these cobalt-containing perovskite with excellent electrode kinetics for oxygen reduction and recombination. Hopefully, the combination of SDC

electrolyte and LSF electrode improves the stability and makes the electrical oxygen production at reduced temperatures.

5.2 Experimental Section

$Sm_{0.2}Ce_{0.8}O_{1.9}$ (SDC) and $La_{0.6}Sr_{0.4}FeO_{3-\delta}$ (LSF) composites oxides were synthesized by a combined EDTA-citrate complexing sol-gel process. $Ce(NO_3)_2.xH_2O$ and $Sm(NO_3)_3.xH_2O$ $La(NO_3)_3.xH_2O$, $Sr(NO_3)_2.xH_2O$ and $Fe(NO_3)_3.xH_2O$ were applied as the raw materials for the metal-ion sources. For the precise controlling of the doping level, the metal nitrates were first made into aqueous solutions (~1M) separately with their precise concentrations determined by standard EDTA titration technique. Necessary amounts of metal nitrates in the state of aqueous solution were then prepared into a mixed solution according to the aimed composition, followed by the introduction of EDTA and citric acid as the complexing agents at the mole ratio of total metal ions: EDTA: citric acid=1:1:2. The pH value of the system was controlled at ~ 6 adjusted by the addition of $NH_3.H_2O$. Continuous heating at 90 ^oC to evaporate water from the solution was carried out until a transparent purple gel was obtained, which was pre-fired at 250 ^oC followed by calcination at high temperatures (700 and 1000 ^oC for SDC and LSF, respectively) in air for 5 h to get the products with the ideal composition and phase structure.

For the fabrication of dense membranes, the as-synthesized SDC oxide powders were pressed into disk-shape membranes in a stainless steel mold (15.0 mm in diameter) under a hydraulic pressure of approximately 1.5×10^8 Pa. These green membranes were further sintered in an electrical box furnace at 1400 ^oC in air for 5 h at a heating /cooling rate of 1-2 ^oC min^{-1}. To perform as electrode layers, LSF, dispersed in an ink vehicle mixed solution, was applied to the surface of 1 mm thick dense SDC membrane by brush pasting and then calcined at 1300 ^oC in air for 2 h.

Scanning Electron Microscopy (SEM) images were obtained using a Zesis EVO 40XVP at an accelerating voltage of 15kV. The XRD analysis was carried out on a Bruker D8 Advances X-ray diffractometer using Cu Ka radiation generated at 40 kv and 30 mA. The electrical conductivity was measured by four-probe *dc* method based on sintered bars of approximately dimensions 2×5×12 mm^3. The measurements were performed in air upon cooling from 900 to 300 ^oC at 5 ^oC per step. A constant current was applied to the two current wires and the voltage response on the two voltage wires was monitored using a Keithley 2420 Sourcemeter. The area specific resistance (ASR) of the membranes was measured by impedance spectroscopy using a GAMRY Reference 3000 with the frequency of 0.1 to 10^6 Hz.

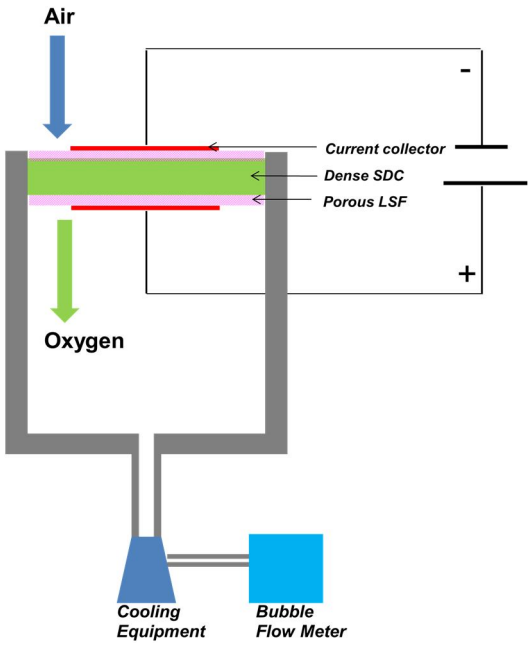

Fig.5-1 Schematic diagram of the oxygen pump based on SDC/LSF membrane

Permeation properties of the membranes were conducted by using different current density across the membrane using an oxygen pump membrane test apparatus as shown in **Fig.5-1**. A ceramic paste was used as the sealant to fix the membrane disk onto the top of a dense quartz tube. The membrane has an effective area of ~ 0.3 cm^2

for the permeation study. The feed side of the membrane was exposed to natural air atmosphere. The electrical current density was applied by GAMRY Reference 3000 with the range from 200mA·cm^{-2} to 3000mA·cm^{-2}. The oxygen permeation flux was measured by soap bubble meter. The values of the voltage and oxygen flux were recorded only after the steady state of the voltage was achieved.

For stability test in CO_2 atmosphere, pure CO_2 with a flow rate of 15 ml min^{-1} was fed into the permeate side of the oxygen pump membrane; then, the oxygen flux and ASR performance of the membrane were tested. After the oxygen permeation test under pure CO_2 gas, the used SDC/LSF membrane was further characterized by SEM and EDX. Meanwhile, fresh SDC and LSF oxide powder was treated similarly under the pure CO_2 gas with the flow rate of 20 ml min^{-1} at 800 ^{o}C for 10 h. After that, the phase structure information of treated powder sample was checked by XRD.

5. 3 Results and discussion

5.3.1 Preparation of SDC/LSF EOP membrane

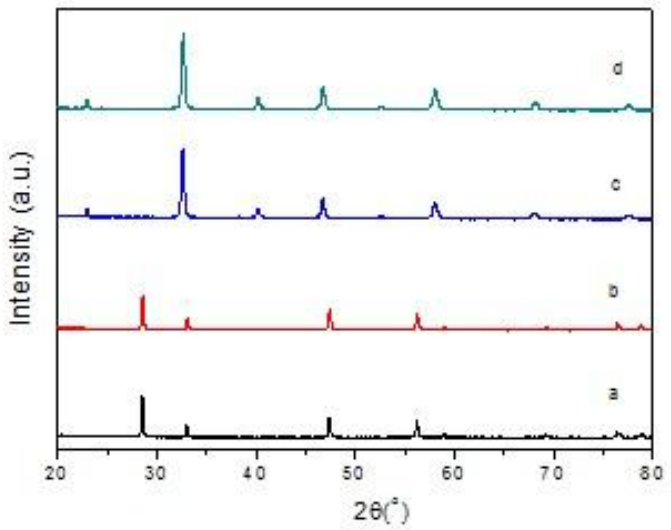

Fig.5-2 XRD pattern of SDC and LSF before and after the CO_2 treatment at 800^{o}C, a: fresh SDC; b: SDC after CO_2 treatment; c: fresh LSF; d: LSF after CO_2 treatment.

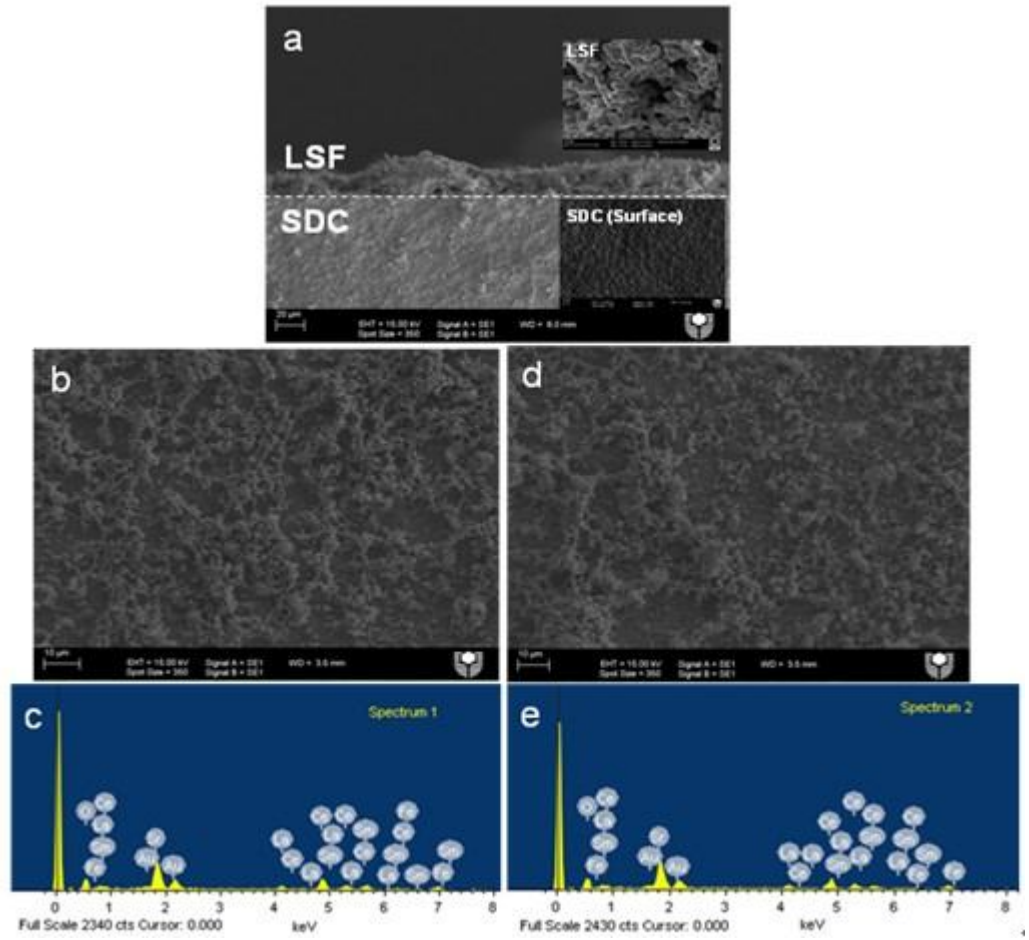

Fig.5-3 SEM images of SDC/LSF membrane cross section (a) and surface area before (b) and after (c) the CO_2 test at 800°C, and energy dispersive X-ray spectrum before (d) and after (e) the CO_2 test at 800°C.

Fig.5-2 shows the typical XRD patterns of the SDC and LSF powders which were synthesized by the combined EDTA-citrate sol-gel method. The characteristic peaks of SDC fluorite oxides are located in **Fig.5-2a** at the respective 2θ angles of 28° (111), 33° (200), 47° (220), 52° (311), 58° (222) and 76° (331), which is consistent with the previously reported.[31] The XRD pattern of LSF displays a clean single phase of cubic perovskite structure with typical characteristic peaks identified at the 2θ angles of 23° (012), 32° (110), 40° (202), 47° (024) and 58° (300), respectively. **Fig.5-3** presents the SEM images of the prepared EOP membrane with the top porous LSF electrode layer of a thickness around 15 μm and the bottom layer as the densified SDC electrolyte (1 mm thickness). As can be seen, the two layers of electrode and

electrolyte were integrated very well without obvious peeling-off phenomenon. From the inserted higher SEM magnification, the respective grain sizes of SDC and LSF are about 2 and 1 μm. An energy dispersive X-ray (EDX) (Spectrum-1) of top surface shows the presence of the elements Ce, Sm, La, Sr, Fe and O from the electrolyte and electrode. The detection of Au is due to the Au coating for a better SEM observation. SEM image of **Fig.5-3d** and EDX of Spectrum-2 is from the tested sample for comparison purpose, which will be discussed shortly.

5.3.2 Oxygen permeation behavior driven by electrical current

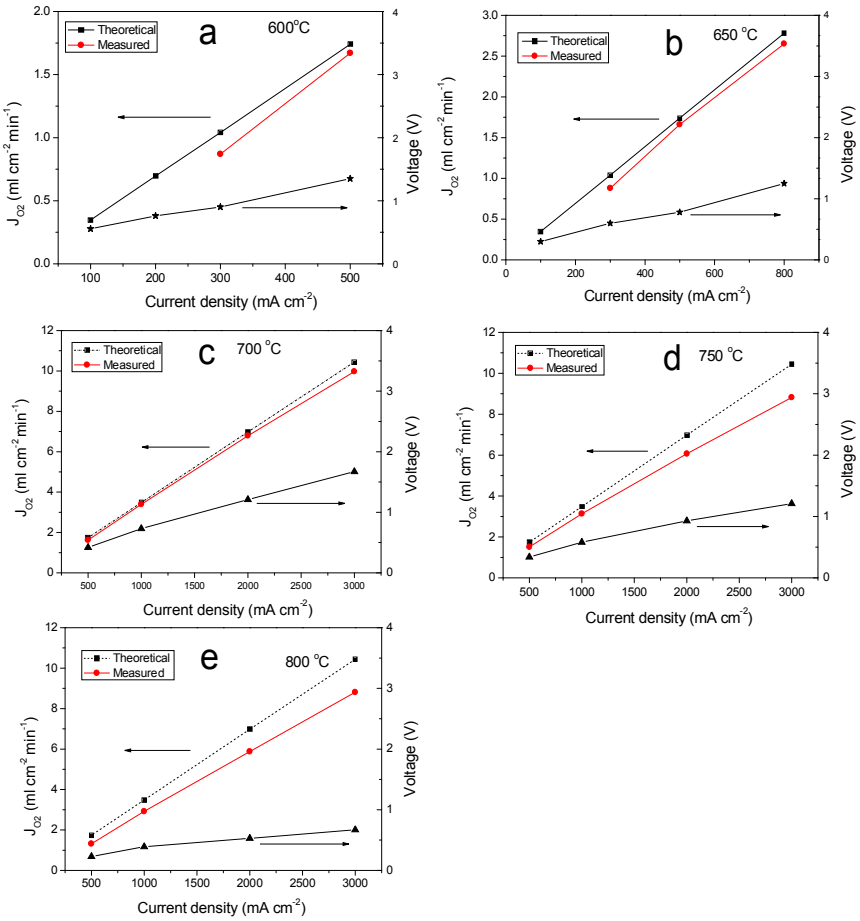

Fig.5-4 The oxygen flux and voltage with applied current density under various temperatures

The oxygen permeation performance for SDC/LSF EOP membrane was tested at different electrical current values and operation temperatures. As seen in **Fig.5-4**, the

oxygen flux constantly increased with the increase of the applied current density from 0 to 3000 mA·cm^{-2}, suggesting that the oxygen permeation was mainly controlled by the applied current. At 700^{o}C, the oxygen flux through SDC/LSF membrane with 3000mA·cm^{-2} current density could reach ~ 9.97 ml cm^{-2} min^{-1}. Here, the external electrical current provided not only the driving force for oxygen ion transport across the membrane bulk but also the electrons to facilitate oxygen reduction and oxidation at the membrane surface. In theory, the oxygen ionic current through the SDC/LSF membrane should be exactly equivalent to the external electrical current. Therefore, the theoretical oxygen flux can be calculated by the following equation:

$$J_{O_2}\,(oxygen\ flux: mol\ s^{-1}) = \frac{I\ (current: A)}{4F(Farady\ Constant)} \qquad (1)$$

By comparison of the calculated values of oxygen flux to the experimentally observed, it indicates that there is a discrepancy between them especially at high temperatures (>700^{o}C) and large current density (>1000 mA·cm^{-2}). The measured values were lower than the theoretical oxygen flux values from the Faraday equation. This result could be attributed that at high temperatures (above 700^{o}C), the SDC is not a pure oxygen ion conductor but displays a certain mixed conduction of oxygen ionic and electronic conduction. As the result, the difference between measured and calculated flux values was ascribed to the direct electronic conduction through SDC membrane as schematically shown in **Fig.5-5a&b**. Meanwhile, with large external current applied, the reduction effect from electrical current on the electrolyte membrane should not be ignored. Therefore, the reduction of Ce^{4+} to Ce^{3+} may take place at such reducing environments, leading to non-negligible leaked current under the influence of strong external electrical current. This internal electronic going through the SDC electrolyte could slow down the oxygen transport rate as an oxygen pump membrane. In the case of the existence of internal electric current by short circuit, the external applied current should be balanced with both oxygen ionic current and internal

electronic current, not only just with oxygen ionic current. The difference of the working principles of EOP membrane with pure ionic conductor and mixed conductor is shown in **Fig.5-5**. This explains that the observed discrepancy between flux values from experimental values and theoretical values based on the Faraday equation, especially at the high temperatures above 700°C. At the same operation temperature varying from 600°C to 800°C, the recorded voltages were not lineally consistent with the applied currents due to the gradual decline of the overall resistance of EOP membrane system with the improvement of electrical/ionic conductivity at high temperatures. Our results clearly support the hypothesis that high operation temperature and strong applied current may result in the partial electronic conduction in SDC membrane.

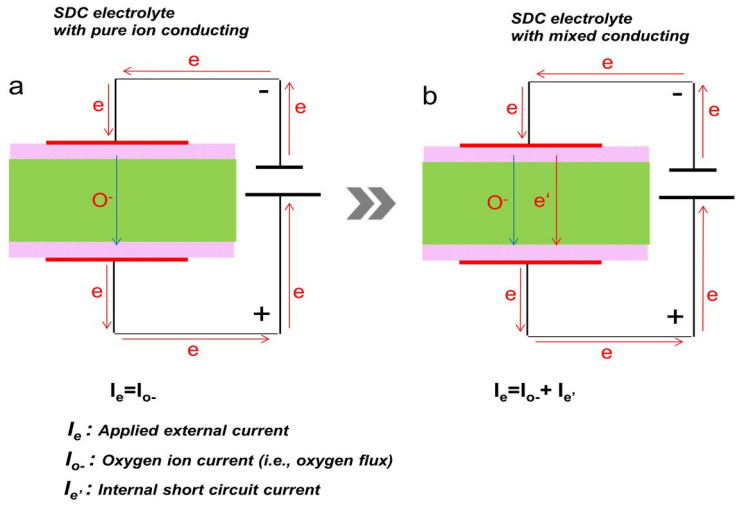

Fig.5-5 Schematic diagram of the SDC/LSF membrane working on the SDC electrolyte with a: pure ion conducting; b: mixed ion and electron conducting

To further investigate the oxygen permeation properties of the SDC/LSF membrane, electrochemical impedance spectroscopy (EIS) was used to analyze the electrochemical characteristic of the permeation model based on the SDC/LSF EOP membrane.

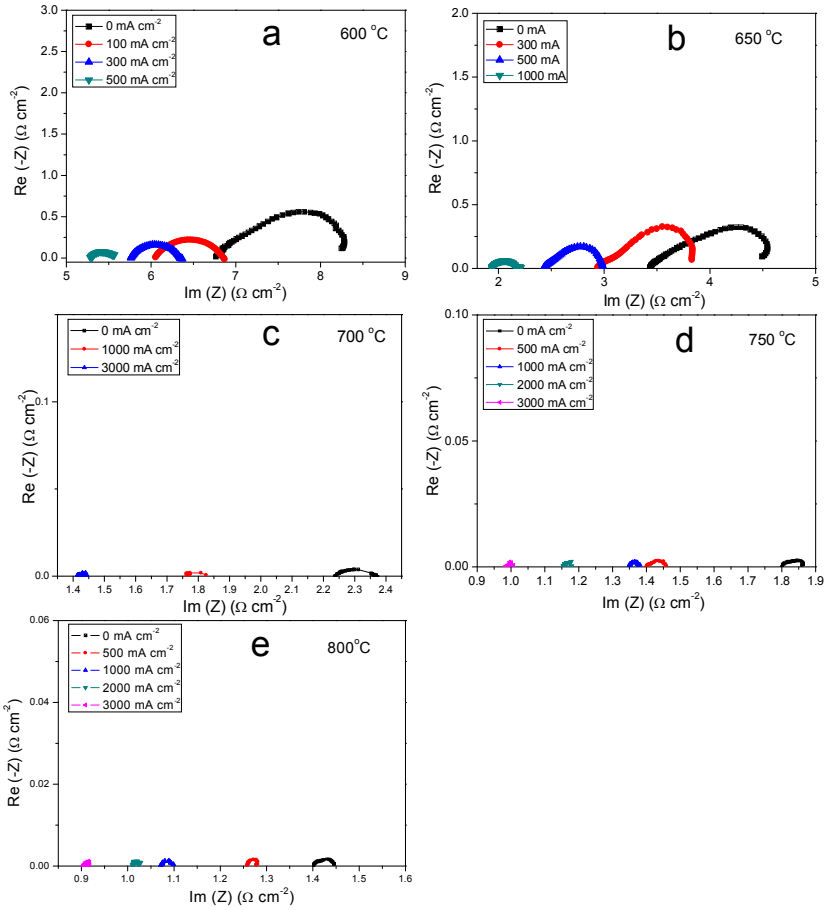

Fig.5-6 Impedance spectrum of SDC/LSF membrane under the current polarization.

Fig.5-6 exhibits the area specific resistance (ASR) of the SDC electrolyte membrane with LSF electrode under various polarization currents. The overall ASR of the membrane system consists of the bulk, grain boundary impedance and interfacial polarization resistance. The high frequency intercept of the impedance spectrum gives the ohmic resistance of the membrane sourced from the membrane bulk transport resistance, while the low frequency intercept reflects the total resistance (overall ASR) including the ohmic resistance and surface polarization resistance. As can be seen, both bulk resistance and surface resistance are very larger at lower temperatures, but they decrease sharply with the temperature increases, which are owning to the increased ionic conductivity of SDC membrane and facilitated oxygen exchange reaction kinetics at membrane surface by the higher temperature activation effect.

When no direct current was applied, the surface polarization resistance and the bulk resistance of SDC/LSF membrane at 600°C was ~1.5 and ~6.7 $\Omega \cdot cm^2$, respectively. The large surface polarization resistance suggested that LSF electrode was prone to be a pure electronic conductor and the oxygen surface exchange reaction was restricted only at the boundary area of three phases of SDC, LSF and oxygen from air. Similar electrode behavior was also observed in $La_{0.6}Sr_{0.4}MnO_3$ under open circuit condition.[34] However, polarization resistance decreased sharply, as shown in **Fig.5-6**, to only ~0.2 Ω cm^2 at 600°C when 500 mA cm^{-2} direct current density was applied to the LSF electrode. Such significant improvement in electrode performance was attributed to the generation of oxygen vacancies at the electrode/electrolyte interface region as a result of partial reduction of Fe^{4+} in LSF to Fe^{3+} or even to Fe^{2+} by the current polarization.[35] In this case, oxygen surface exchange reaction area could be extended to the whole surface of LSF electrode rather than the limited boundary area. On the other hand, the large bulk resistance was stemmed from the relative thick SDC membrane (1mm thickness) and smaller ionic conductivity at lower temperatures. Similar to the electrode resistance, the electrolyte resistance also experienced an obvious decline with the increase of the current. For example, the bulk resistance decreased from ~6.7 Ω cm^2 to ~5.3 Ω cm^2 after adjusting the current density from 0 mA cm^{-2} to 500 mA cm^{-2}. This bulk resistance reduction is consistent with the observed non-linear relationship between the applied current and the corresponding voltage across the SDC/LSF membrane, suggesting that large current polarization would cause the electrochemical reduction of SDC bulk membrane. On the contrary to the positive effect on the oxygen permeation performance from the LSF electrode polarization reduction, such reduction of SDC membrane may result in the degradation of permeation (Faradic) efficiency. However, absolutely pure oxygen ion conducting ceramics operated at high temperatures rarely exist. Fortunately, as shown

in **Fig.5-7**, the permeation efficiency could still reach above 95% at lower temperatures (≤700°C), implying the potentials of SDC/LSF EOP membranes to be applied around 600-700 °C. Compared to these traditional oxygen pump membranes based on YSZ electrolyte with noble metal electrode, e.g. Pt, this SDC/LSF membrane has less energy consumption to achieve the same oxygen flux due to its smaller ionic transport resistance at the lower temperatures.[27,36]

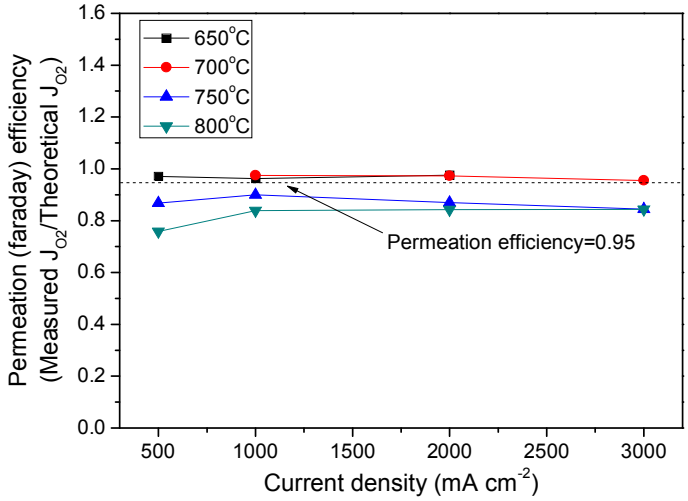

Fig.5-7 Oxygen permeation (faraday) efficiency of SDC/LSF membrane under different temperatures

5.3.3 SDC/LSF membrane stability in CO_2 atmosphere

In addition to high oxygen permeation performance, the EOP membrane must sustain sufficient stability at practical applications with the presence of CO_2. **Fig.5-8** shows the ASR spectrum of electrochemical SDC/LSF membrane operated at 800°C under pure CO_2 atmosphere. It could be clearly observed that the surface polarization resistance of SDC/LSF membrane increased dramatically by a factor of 4 from ~0.05 to 0.2 Ω·cm^2 under the open circuit after the introduction of 15 ml min^{-1} pure CO_2 into the permeate side of the membrane. By contrast, there was no obvious change for the bulk resistance of the membrane. This result indicates that CO_2 exerted a negative

impact more on the electrode performance rather than on the electrolyte. Noteworthy is that the degradation of the electrode performance suffering CO_2 poisoning can be alleviated by applying the current polarization. The electrode resistance constantly decreased with the increase of the current density. For example, under the polarization current of 1000 $mA \cdot cm^{-2}$, the electrode resistance could still be as low as 0.03 Ω cm^2 in CO_2 atmosphere, which almost reach the electrode performance without CO_2 presence under the same polarization current. Normally, the existence of more oxygen vacancies will aggravate the CO_2 poisoning effect on the perovskite oxide electrode. Previous studies confirmed that acidic CO_2 gas is easier to be absorbed by these perovskite oxides with high concentration of the oxygen vacancy, which would speed up the carbonate formation with these oxides.[37,38] Here, the decline of the electrode performance in the electrochemical SDC/LSF membrane is probably also related to that negative effect of chemical absorption by CO_2 on the oxide electrode. After ~2 hours CO_2 treatment with the SDC/LSF membrane, the permeate gas was switched over from CO_2 to atmospheric air. It is interesting to note that the electrode resistance of the membrane almost recovered back to its original state under various polarization currents (Fig.5-9a), echoing the analysis that the decline in the electrode performance of SDC/LSF membrane was due to the strong adsorption effect of CO_2 on the LSF oxide surface, but not the reaction between CO_2 and the membrane materials. In addition, the result of the oxygen pumping permeation performance of SDC/LSF membrane after the CO_2 treatment in **Fig.5-9b** is in good agreement after and before the CO_2 treatment further indicating that the electrochemical SDC/LSF membrane has a good stability in CO_2 containing atmospheres.

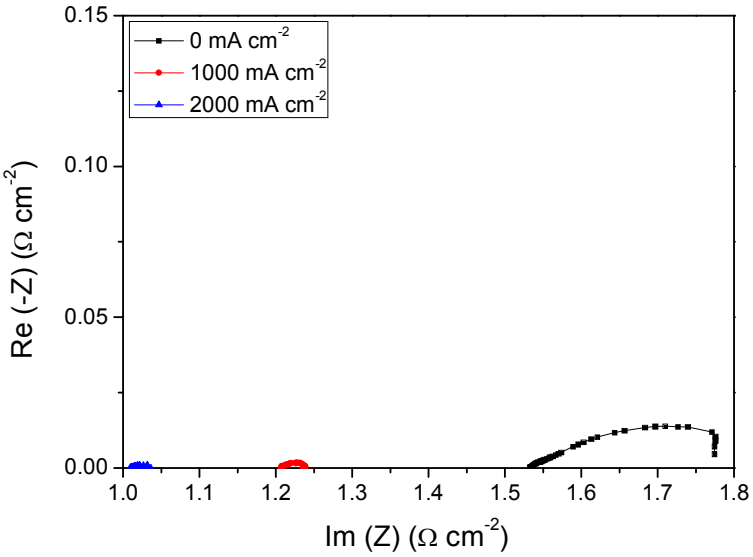

Fig.5-8 Impedance spectrum of SDC/LSF membrane under CO_2 atmosphere at 800°C

After the oxygen permeation test through electrochemical SDC/LSF membrane in CO_2-containing atmospheres, the membrane sample was further characterized by, SEM, EDS and XRD. **Fig.5-3d** presents SEM microstructure of the membrane after the oxygen permeation test in CO_2 containing atmosphere. After the oxygen permeation test with CO_2 gas, the membrane surface still keeps intact as compared with the fresh membrane. Furthermore, EDX result (spectrum-2) proved that there was no carbon detected on the membrane surface. According to the XRD results (**Fig.5-2**), there was no impure phase observed on the samples after the CO_2 treatment, which further confirmed that electrochemical SDC/LSF membrane could sustain its phase structure against the CO_2 erosive effect. All these above results indicates that electrochemical SDC/LSF membrane possesses good oxygen permeation performance and stability in CO_2 containing atmosphere, showing its highly promising applications in oxygen production, oxyfuel technologies and hydrocarbon partial oxidation.

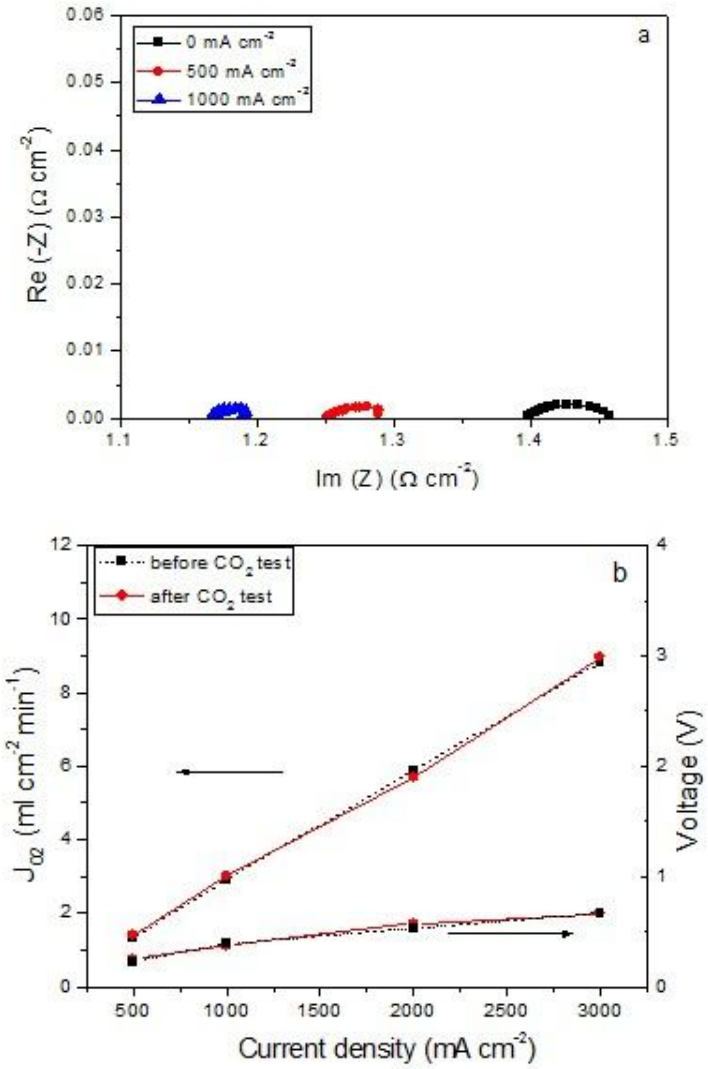

Fig.5-9 Impedance spectrum (a) and oxygen permeation test (b) of SDC/LSF membrane after the CO_2 test at 800°C

5.4 Conclusion

$Sm_{0.2}Ce_{0.8}O_{1.9}$ (SDC)/$La_{0.6}Sr_{0.4}FeO_{3-\delta}$ (LSF) electrochemical membrane was designed to produce pure oxygen at intermediate temperature range. This SDC/LSF membrane exhibits high Faraday efficiency for oxygen permeation, which could reach above 95% at temperatures of 600-700°C with the oxygen flux value at 9.97 ml cm^{-2} min^{-1} under 3000mA·cm^{-2} current density at 700°C. After exposing the SDC/LSF membrane in pure CO_2 atmosphere for 100 hours, the oxygen permeation performance of SDC/LSF membrane was re-examined together with the re-characterization by SEM, EDS and

XRD. No appreciable change in structure, morphology and permeation behavior was observed, reflecting the good operational stability of SDC/LSF electrochemical pump membrane in CO_2 containing atmosphere.

5.5 References

1. R.M. Thorogood, *Gas Sep. Purif.* , 1991, **5**, 83-94.

2. Y. Teraoka, H.M. Zhang, S. Furukawa and N. Yamazoe, *Chem. Lett.*, 1985, **7,** 1743-1746.

3. H. Jiang, Z. Cao, S. Schirrmeister, T. Schiestel and J. Caro, *Angew. Chem. Int. Ed.*, 2010, **49**, 5656-5660.

4. N. Zhu, X. Dong, Z. Liu, G. Zhang, W. Jin and N. Xu, *Chem. Commun.*, 2012, **48**, 7137-7139.

5. H. Wang, S. Werth, T. Schiestel and J. Caro, *Angew. Chem. Int. Ed.*, 2005, **44**,6906-6909.

6. H. Jiang, H. Wang, F. Liang, S. Werth, T. Schiestel and J. Caro, *Angew. Chem. Int. Ed.*, 2009, **48**, 2983-2986.

7. H. Luo, K. Efimov, H. Jiang, A. Feldhoff, H. Wang and J. Caro, *Angew. Chem. Int. Ed.*, 2011, **50**, 759-763.

8. J. Tang, Y. Wei, L. Zhou, Z. Li and H. Wang, *AIChE J.*, 2012, **58**, 2473-2478.

9. J. Sunarso, S. Baumann, J.M. Serra, W.A. Meulenberg, S. Liu, Y.S. Lin and J.C.D. da Costa, *J. Membr. Sci.*, 2008, **320**, 13-41.

10. J. Sunarso, S. Liu, Y.S. Lin and J.C.D. da Costa, *J. Membr. Sci.*, 2009, **344**, 281-287.

11. P. Haworth, S. Smart, J. Glasscock and J.C.D. da Costa, *Sep. Purif. Technol.*, 2011, **81**, 88-93.

12. H. Zhao, Y. Cheng, N. Xu, Y. Li, F. Li, W. Ding and X. Lu, *Solid State Ionics*, 2010, **181**, 354-358.

13. N. Xu, H. Zhao, Y. Shen, T. Chen, W. Ding, X. Lu and F. Li, *Sep. Purif. Technol.*, 2011, **89**, 16-21.

14. C. Yang, Q. Xu, C. Liu, J. Liu, C. Chen and W. Liu, *Mater. Lett.*, 2011, **65,** 3365-3367.

15. X. Tan and K. Li, *Curr. Opin. Chem. Eng.*, 2011, **1**, 69-76.

16. X. Tan, Z. Pang and K. Li, *J. Membr. Sci.*, 2008, **310**, 550-556.

17. B. Zydorczak, K. Li and X. Tan, *AIChE J.*, 2010, **56**, 3084-3090.

18. X. Qi, Y.S. Lin and S.L. Swartz, *Ind. Eng. Chem. Res.*, 2000, **39**, 646-653.

19. M. Anderson and Y.S. Lin, *J. Membr. Sci.*, 2010, **357**, 122-129.

20. Y. Zeng and Y.S. Lin, *J. Cata.*, 2000, **193**, 58-64.

21. X. Zhu, H. Liu, Y. Cong and W. Yang, *Chem. Commun.*, 2012, **48**, 251-253.

22. X. Zhu, H. Wang and W. Yang, *Chem. Commun.*, 2004, **1**, 1130-1131.

23. X. Dong, W. Jin, N. Xu and K. Li, *Chem, Commun.*, 2011, **47**, 10886-10902.

24. Z. Rui, Y. Li and Y.S. Lin, *Chem. Eng. Sci.*, 2009, **64**, 172-179.

25. Z. Shao, G. Xiong, Y. Cong and W. Yang, *J. Membr. Sci.*, 2000, **172**, 177-188.

26. S.P.S. Badwal and F.T. Ciacchi, *Adv. Mater.*, 2001, **13**, 993-996.

27. D. J. Clark, R. W. Losey, and J.W. Suitor, Sep. Purif., 1992, **6**, 201-205.

28. I.V. Yentekakis and C.G. Vayenas, *J. Catal.*, 1988, **111**,170-188.

29. M. Yadav, W. Gong and A.J. Jacobson, *J. Solid State Electrochem.*, 2011, **15**, 293-301.

30. D. L. Meixner, D.D. Brengel, B.T. Henderson, J.M. Abrardo, M.A. Wilson, D.M. Taylor and R.A. Cutler, *J. Electrochem. Soc.*,2002, **149**, D132-D136.

31. W. Zhou, Z. Shao, R. Ran, Z. Chen, P. Zeng, H. Gu, W. Jin and N. Xu, *Electrochim. Acta*, 2007, **52**, 6297-6303.

32. A. Yan, B. Liu, Y. Dong, Z. Tian, D. Wang and M. Cheng, *Appl. Catal. B, Environ.*, 2008, **80**, 24-31.

33. O. Czuprat, M. Arnold, S. Schirrmeister, T. Schiester and J. Caro, *J. Membr. Sci.*, 2010, **364**,132-137.

34. K. Yasumoto, N. Mori, J. Mizusaki, H. Tagawa and M. Dokiya, *J. Electrochem. Soc.*, 2011, **148**, A105-11.

35. F.J. Berry, J.F. Marco and X. Ren, *AIP Conf. Proc.*, 2006, **765**, pp. 200-205.

36. A. Q. Pham, R. S. Glass, *Electro. Acta*, 1998, 43, 2699-2707.

37. Z. Homonnay, K. Nomura, G. Juhasz, M. Gal, K. Solymos, S. Hamakawa, T. Hayakawa and A. Vertes, *Chem. Mater.*, 2002, **14**, 1127-1132.

38. K. Nomura, Y. Ujihira, T. Hayakawa and K. Tekehira, *Appl. Catal. A: Gen.*, 1996, **137**, 257-259.

Every reasonable effort has been made to acknowledge the owners of copyright material. I would be pleased to hear from any copyright owner who has been omitted or incorrectly acknowledged.

Chapter 6: Robust ion-transporting ceramic membrane with an internal short circuit for oxygen production

6.1 Introduction

Global greenhouse gas emission is one of the major challenges facing our contemporary society. These emissions are mainly anthropogenic derived from burning fossil fuels, particularly coal power plants. Hence, there is a drive to shift energy production towards clean energy generation where carbon emissions can be captured, transported and safely stored in geological formation. Current clean energy delivery processes of importance include integrated gasification combined cycle (IGCC) and oxyfuel coal combustion plants. These processes partially combust or totally combust coal with oxygen instead of air. Hence, these plants require an air separation unit at the front end which can be based on cryogenic process, pressure swing adsorption or dense ceramics.

Out of these oxygen production processes, ceramic based ion transporting membrane (ITM) can be cost effective to meet the commercialization requirements of these clean energy technologies. For instance, oxygen ITM has the potential to replace the cryogenics process by reducing oxygen production costs by 35% or more [1-5]. As such ITM is attracting significant research interests not only from research institutes and industries (i.e. Air Products) but also from governments exemplified by the significant investments from the Department of Energy in the USA of $148 million since 1999 to scale up the technology. The prerequisite for the successful application of these

ceramic membranes for oxygen production is the high oxygen flux values and sufficient material stability under high temperature operating conditions [6-20].

Most studies on ITM have been concentrated on the perovskite-type oxides because of their attractive oxygen flux values and their mixed ionic-electronic conducting property which simplifies the membrane design without the requirement of external electric loadings. Teraoka and coworkers pioneered this area by their first report of the permeation properties of $SrCoO_{3-\delta}$ perovskite membranes in the 1980s [21]. Today after more than 20 years' development, super-high oxygen flux values up to 14 ml cm^{-2} min^{-1} can be achieved under oxygen gradient created by air/inert sweep gas [22]. From the viewpoint of flux value, these perovskite membranes already reach the commercial target [22, 23]. However, the real application of these perovskite membranes is still limited by their intrinsic drawback of low structural phase stability under practical conditions in the presence of gases like CO_2, SO_2 and H_2O vapour. Membrane performance degradation is normally observed in long term operations as the reactions between the membrane materials and these gases/vapours cause the membranes to fail. Although the perovskite stability can be improved by compositional tailoring with robust elements, the problem of low material stability remains.

To address this problem, many attempts have been directed to the development of dual phase membranes, which can allow ionic and electronic conductions through two different phases [24-30]. However, they are characterized by very low O_2 fluxes due to the mismatch occurring between the two phases of the membrane prepared by traditional methods of powder mixing. Hence, a more robust solution is required if ITMs are to be deployed as the technology of choice in clean energy processes. One option is focusing on pure ion conducting materials, instead of MIEC materials. Pure ion conducting fluorite oxides such as yttria-stabilized zirconia (YSZ), samarium-

doped ceria (SDC) or gadolinium-doped ceria (GDC) do possess inherently sufficient chemical stability and are currently widely applied as electrolyte layers in solid oxide fuel cells (SOFC) with typical operating principles showing in **Fig.6-1a**. Many of the SOFC operations involve exposure of these pure ionic conductors to CO_2 and H_2O, and SOFC electrolytes are therefore desirable materials for oxygen separation from air. This setup is favorable as it enhances the driving force (i.e. oxygen partial pressure gradient) and consequently delivers high oxygen fluxes. Therefore, it is necessary to understand and adopt the SOFC technology to an oxygen production technology.

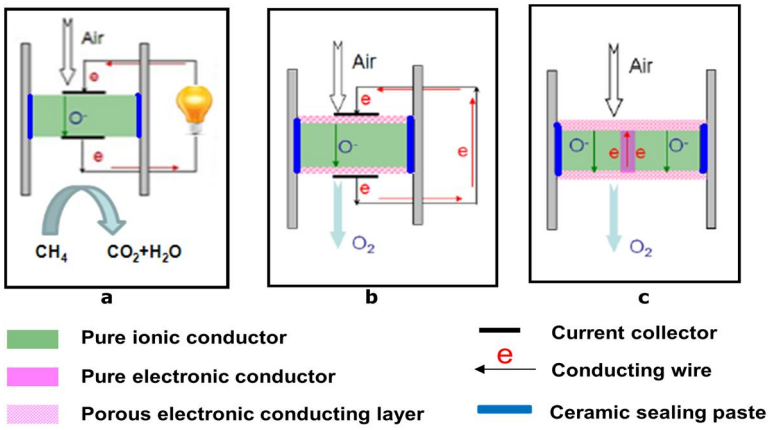

Fig.6-1. Working principles of oxygen ionic transporting membranes for solid oxide fuel cell(a), oxygen separation via external short circuit (b) or internal short circuit (c)

The SOFC cell consists of three main components namely: a dense electrolyte layer like SDC or YSZ sandwiched between a porous cathode and a porous anode [31-33]. The cathode with the electrocatalyst is exposed to an air feed, where molecular oxygen is reduced into oxygen ions. The oxygen ions are transported through the electrolyte layer and reach the anode where the fuel is electrochemically oxidized and releases electrons. Then, the electrons flow through an external circuit to the cathode to compensate for the electron consumed by air reduction and to complete the circuit with electric energy delivery. In SOFC, the driving force (or the open circuit voltage) is provided by the O_2 partial pressure difference between the cathode and anode. In

the case of a SOFC system, the major function of fuel is to lower the oxygen concentration by fuel oxidation.

The adoption of this design to oxygen separation in oxyfuel combustion requires switching the fuel gas to CO_2 to sweep the anode chamber or by pressurizing the air feed stream. This allows the O_2 partial pressure to be lowered further in the permeate stream, or to increase the driving by increasing O_2 partial pressure difference, respectively. In turn, these designs provide the driving force requirement for the oxygen ion to diffuse from the cathode to anode. However, the O_2 partial pressure in the permeate stream cannot be lowered as significantly as to levels afforded by fuel reaction, because the open circuit voltage will be too low to provide the practical electric energy for real application purpose. In this case, it is possible to sacrifice the cell by internal short-circuit and use it only for oxygen separation as showing in **Fig.6-1b**. This leads to a novel class of ceramic membranes for oxygen separation using these structurally robust fluorite-based ceramics that can withstand the attack of CO_2 or other acid gases at oxyfuel conditions. In our previous work, we verified the configuration with external short circuit [34, 35]. The measured values of electrical current agreed very well with the theoretical calculation using the equation correlating Faraday constant and oxygen fluxes.

This work investigates an important aspect of this novel membrane configuration. We propose that oxygen separation can be carried out by using membranes with internal short circuit instead of external short circuit as schematically shown in **Fig.6-1c.** Compared to the membrane configuration using external circuit (**Fig.6-1b**), the membrane design in **Fig.6-1c** further simplifies the system by obviating the need of an external circuit and can be more conveniently used in the planar stack like design. The performance of the membrane configurations are evaluated based on oxygen

production rates at several temperature regimes under air exposure and inert gas exposure.

6.2 Experimental Section

$Sm_{0.2}Ce_{0.8}O_{1.9}$ (SDC) electrolyte was synthesized by a combined EDTA-citrate complexing sol-gel process. $Ce(NO_3)_2.xH_2O$ and $Sm(NO_3)_3.xH_2O$ (all in A.R. grade) were applied as the raw materials for the metal ion sources. For the precise controlling of the doping concentration, the chemical compositions of the used metal nitrates were verified by standard EDTA titration technique. The required amount of metal nitrates in the state of aqueous solution was prepared into a mixed solution according to the targeted composition, followed by the addition of EDTA and citric acid as the complexing agents. Thehe mole ratios of total metal ions to EDTA and citric acid were set at 1:1:2. The solution was thickened by continuous heating at 90^{o}C to evaporate water until a gel was obtained, which was pre-fired at 250^{o}C and heated 700^{o}C in air for 5 h to get the oxide powder as the membrane material.

To fabricate the ceramic membrane, the as-obtained oxide powder was pressed into disk shaped membrane in a stainless steel mold (15.0 mm in diameter) under a hydraulic pressure of approximately 1.5×10^{8} Pa. The green membrane (~1.0 mm in thickness) was further sintered in an electrical furnace at 1500 ^{o}C in air for 5 h. Silver wire with silver paste was used as the conductive wire to connect the two sides of membrane. To prepare the internal short circuited SDC membrane, a channel (~0.5 mm in diameter) through the bulk of SDC membrane was firstly made by ultra-high speed driller; then a thin Ag wire (~0.3 mm in diameter and ~1.0 mm in length) was implanted inside the through channel and sealed with silver paste to ensure the material connectivity and gas-tightness. Silver slurry was applied to both sides of the

SDC membrane with similar thickness and further calcined at 600 ^{o}C in air for 2 h to increase the adhesion. The protocol for this membrane design is schematically shown in **Fig.6-2**.

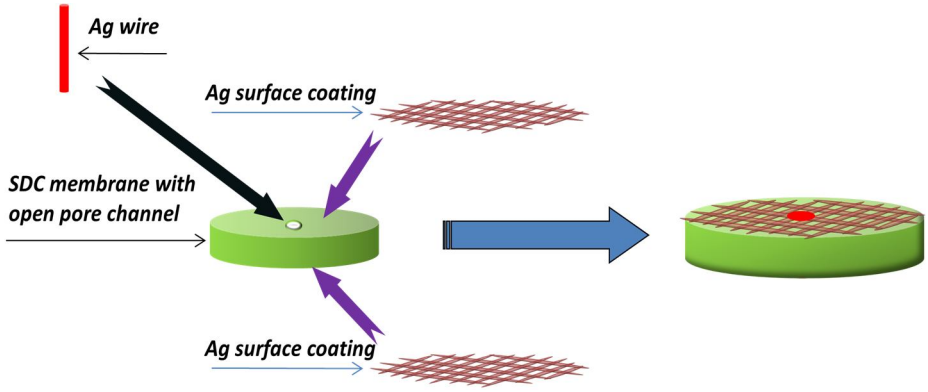

Fig.6-2 the schematic of the SDC membrane with the internal short structure

Permeation properties of the membranes were investigated by the gas chromatography (GC) method using a high-temperature apparatus. A silver paste or non-conductive ceramic paste was used as the sealant to fix the membrane disk onto a dense quartz tube and exposed an effective area of ~ 0.45 cm^2 at the sweep side for permeation study. Helium was applied as the sweep gas to create an oxygen partial pressure gradient across the membrane, which also acted as the carrier gas to bring the permeated oxygen to a Shimadzu 2014A equipped with a 5Å capillary molecule column and thermal conductivity detector for quantitative oxygen concentration analysis.

6.3 Results and discussion

6.3.1 Membrane Preparation and Characterization

Fig.6-3a displays the XRD pattern of the $Sm_{0.2}Ce_{0.8}O_{1.9}$ (SDC) powder sample with the characteristic peaks at the respective 2θ angles of 28^{o} (111), 33^{o} (200), 47^{o} (220), 52^{o} (311), 58^{o} (222) and 76^{o} (331) which are closely matching the reported fluorite

structure [36,37]. Sintering at higher temperature (1350°C) increased crystallization evidenced by the change on the diffraction pattern with more intense peaks but reduced width in comparison with the original powder (700°C). The crystal structure of the prepared SDC powder was also studied by HRTEM investigation. TEM image at low magnification (**Fig.6-4a**) shows the particle agglomerates, from which small crystal particles with a size around 35 nm are clearly observed. As the agglomerates consist of densely packed crystallites, it could not be easily dispersed during the sample preparation for TEM observation. TEM image at higher magnification (**Fig.6-4b**) clearly displays the fringe pattern with interplane distance as 2.60 ±0.1 Å which was assigned to (2 0 0) plane of $Sm_{0.2}Ce_{0.8}O_{1.9}$. Using these powders, SDC membranes were prepared by sintering at 1350 °C to achieve the gas-tightness and sufficient mechanical strength.

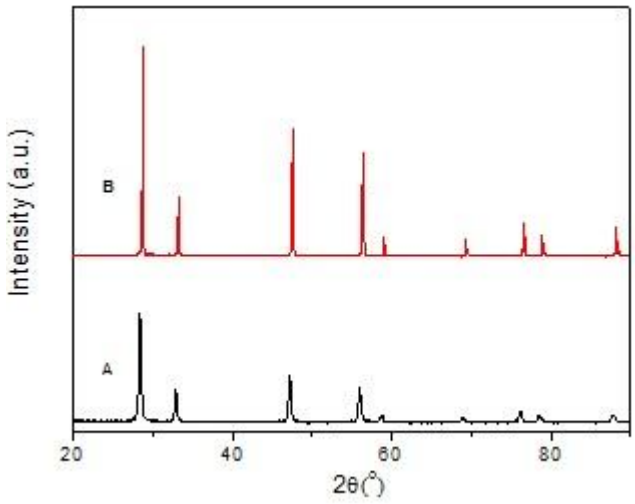

Fig.6-3 XRD pattern of SDC oxide, A: SDC powder prepared by EDTA-citrate method; B: SDC disk sintered at 1350 °C

Fig.6-5a&b show the SEM images of the cross sectional view of the densified SDC membrane. The grain size in the range of 0.5 to 1μm is clearly observed. The SDC membrane was not fully densified as there are many pores with sizes around 0.2 microns inside the SDC ceramic. The gas-tightness of the membrane was confirmed

by the gas leakage test, thus suggesting these pores are not interconnected to allow the direct passage of gas molecule from one side of the membrane to the other side. Noteworthy is that the presence of porous structure inside the ceramic is not favorable for ion diffusion; however, the porous structure through to the surface layer is favorable to the surface O_2 exchange reactions [38, 39]. **Fig.6-5c, d & e** show the photos of pure SDC, Ag paste coated SDC and the internally short-circuited SDC membranes, respectively. The thickness of SDC disk membranes was controlled from 0.5 to 2 mm. Only the gas-tight membranes were selected for O_2 permeation test.

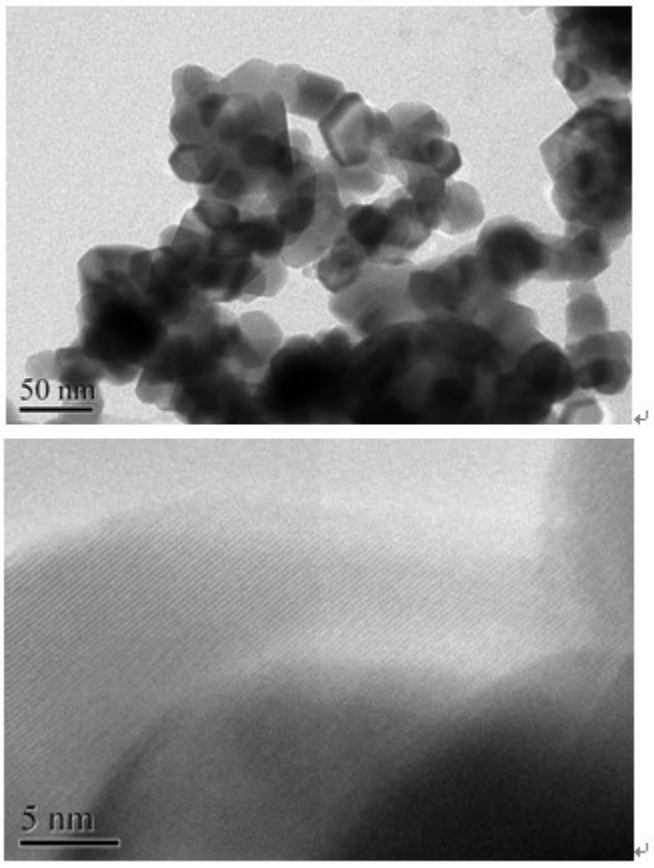

Fig.6-4 TEM image of SDC oxide powder prepared by EDTA-citrate method after treatment under 700°C in air for 5 hours

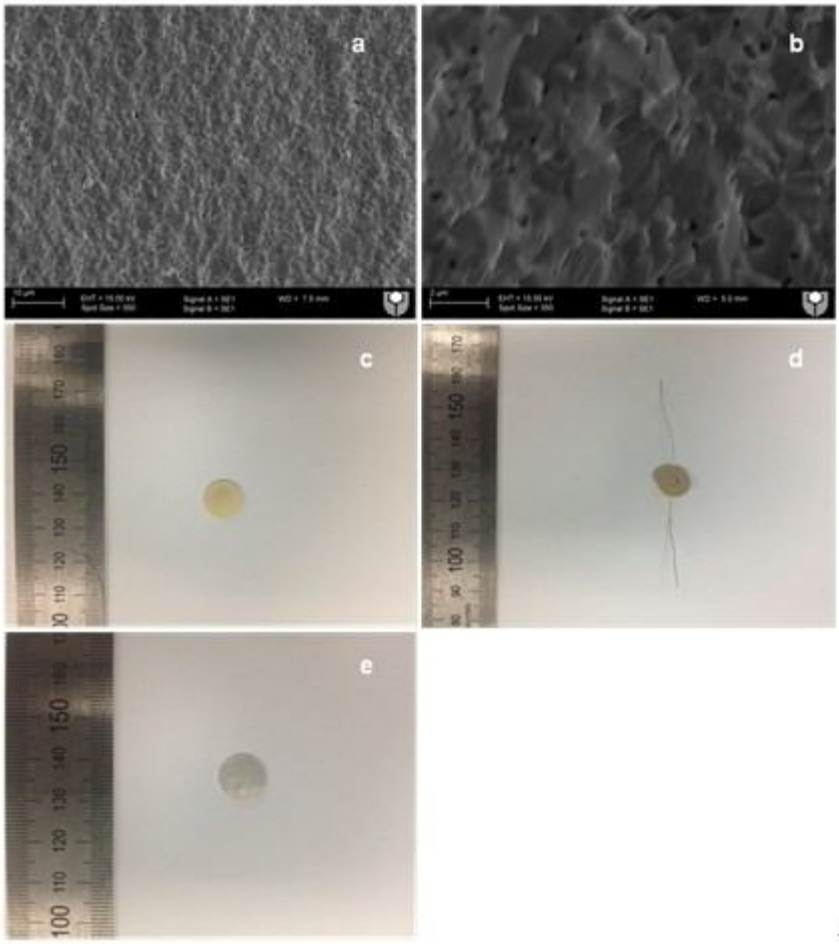

Fig.6-5 Images of SDC membrane, (a) and (b): SEM images for cross section, digital photo images for (c): pure SDC membrane, membrane (d): with internal short circuit and (e) Ag surface modification

6.3.2 Oxygen Permeation Test

In order to verify the feasibility of the internally short circuited membrane and the influence of different number of pathways of short circuits at different locations on the oxygen fluxes, six samples (**Table 6-1**) were designed and tested with results displayed in **Fig.6-6**. Sealed by normal nonconductive ceramic paste, Sample (S)-1 was a plain and pure ion conducting membrane. As expected, the pure SDC membrane would not display the oxygen permeating behavior from 500 to 800^{o}C as it is lack of electron conducting phase. By contrast, the oxygen permeation through S-2 with one internal circuit was clearly observed with flux values steadily increasing

from 0.028 ml cm^{-2} min^{-1} at 600°C to 0.67 ml cm^{-2} min^{-1} at 850 °C. Oxygen transport from air side to the permeate side is not consisted of 100% physical processes but involving a series of physical processes and surface reactions with three major steps in sequence as below:

1) Oxygen molecular reduction to oxygen ions via oxygen vacancies and electrons at the membrane surface (air side):

$$\frac{1}{2}O_2 + 2e + V_o^{\cdot\cdot} \rightarrow O_o^x$$

2) Oxygen ion bulk diffusion across the membrane;

3) Oxygen ion oxidation to molecular oxygen at the other membrane surface (permeate side):

$$O_o^x \rightarrow \frac{1}{2}O_2 + 2e + V_o^{\cdot\cdot}$$

In order to maintain the electrical neutrality of the oxygen ion bulk diffusion (step 2), the electrons released from the oxidation at the permeate side (step 3) travelled along the internal short circuit to the other membrane side to compensate for the consumed electron by the oxygen reduction (step 1). Therefore, as oxygen was transported in the ionic form and opposite to the electron transport direction, the material charge neutrality viewed from the overall cross section of the membrane was maintained. As can be seen, to enable the membrane function for the oxygen transportation, the ion conductor (SDC), electron collector/distributor (Ag or Pt coating layer) and internal circuit are three major components without each of which the function of oxygen separation from air cannot be fulfilled.

The internal short circuit design as proposed in this work was also tested for samples containing up to four pathways of short circuits as displayed in **Fig.6−6**. Very

interestingly, there was no much difference in oxygen flux values between all tested membranes. These results strongly suggest that the surfaces of the membranes have good electron collector and distributor properties, as a single and multi-internal short circuit deliver similar oxygen fluxes independently of the number of the pathways of short circuits. In addition, the O_2 fluxes of the SDC membrane with external short circuit (S-6) also gave similar O_2 flux thus mirroring the required electronic conduction for O_2 transportation, which can be fulfilled either as an internal or external short circuit configuration. As long as the metal wire used as the short circuit can withstand the weak electrical current at high temperatures and the porous metal coating layers are qualified for electron collection and distribution, one short circuit pathway in one location inside the membrane is sufficient to realise the desirable function of this novel design. **Fig.6-6** also displays the flux increment with the temperature increase, which is a normal observation for any type of ITM as the ionic diffusion rate and the surface exchange reaction rates can be significantly enhanced as a function of the temperature.

Table 6-1. Different SDC membranes being tested for oxygen permeation

Sample No	Short Circuit	Coating materials	Sealing agent	Membrane Thickness (mm)
I	No	No	Ceramic Paste	1.0
II	Yes, 1 internal	Ag	Ceramic Paste	1.0
III	Yes, 2 internal	Ag	Ceramic Paste	1.0
IV	Yes, 3 internal	Ag	Ceramic Paste	1.0
V	Yes, 4 internal	Ag	Ceramic Paste	1.0
VI	Yes, external	Ag	Ag Paste	1.0
VII	Yes, 1 internal	Ag	Ceramic Paste	1.5
VIII	Yes, 1 internal	Ag	Ceramic Paste	0.6
IX	No,	No	Ceramic Paste	1.0

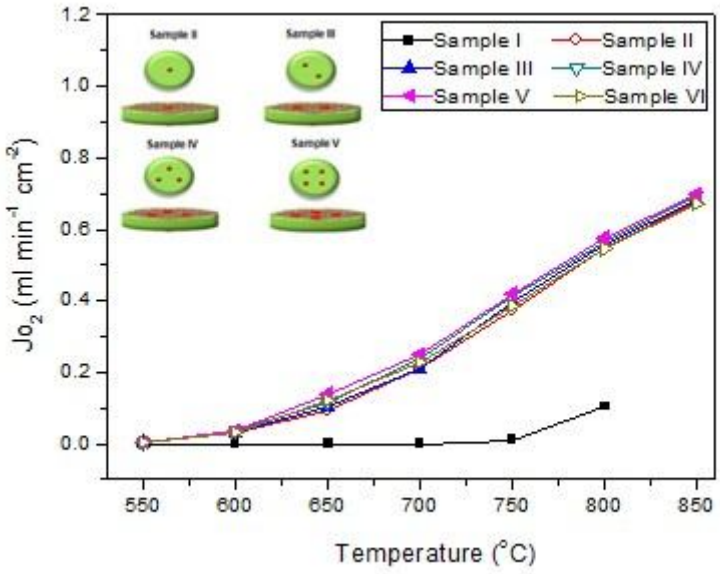

Fig.6-6 The oxygen permeation fluxes through the SDC membranes with various structures

Fig.6-7 depicts the dependence of SDC membrane thickness on the permeation fluxes. In these measurements, all the three samples were fixed at one short circuit located at the membrane centre with membrane thicknesses varying from 0.6 to 1.0 and 1.5 mm. A decrease in SDC thickness normally results in higher oxygen fluxes as it shortens the oxygen ion transport path. For instance, at 800 °C the O_2 fluxes successively increased from 0.48 to 0.57 and 0.65 ml cm^{-2} min^{-1} as the thickness reduced from 1.5 to 1.0 and 0.6 mm, respectively. As temperature lowers, the oxygen fluxes tend to converge and the effect of membrane thickness is no longer apparently applicable. This phenomenon can be explained by the relative limiting resistance from bulk diffusion and surface reactions [40]. The overall oxygen transport process is jointly controlled by the resistances from both processes and the relative limiting effects of these processes are very dependent on the membrane material, thickness, surface morphology and operating conditions like temperature, O_2 partial pressure and so on. From the point of view of membrane synthesis to improve the O_2 flux, efforts should be placed not only in membrane thickness reduction but also in membrane surface reaction kinetic improvement by deposition of catalyst or enlargement of the porous

surface area. For instance, in terms of process operation **Fig.6-8** shows the effect of sweep gas flow rate on oxygen fluxes. In addition to the temperature, oxygen partial pressure gradient is another important driving force for oxygen transport through the membrane. Increasing sweep gas rate lowers the oxygen partial pressure in the permeate side thus pushing the oxygen flux to a higher value.

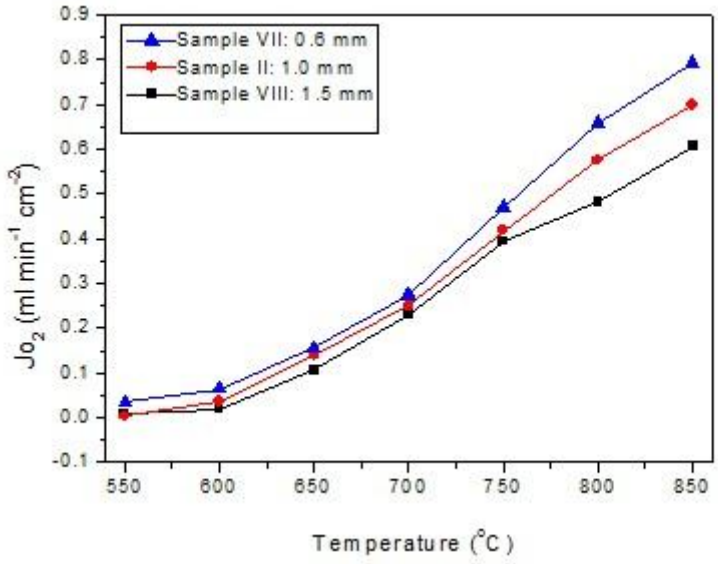

Fig.6-7 The thickness dependence of oxygen permeation fluxes

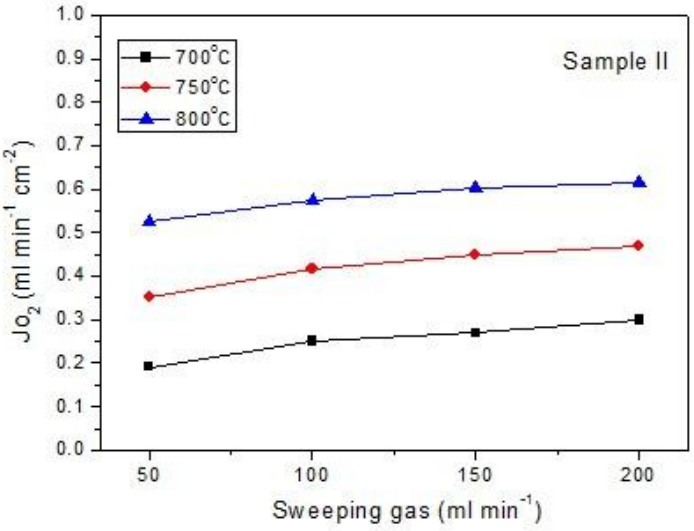

Fig.6-8 The effect of sweep gas rate on oxygen permeation fluxes

6.3.3 Stability Test

The permeation stability of the SDC membrane with internal short circuit was tested at 800°C in the presence of CO_2 or H_2O for more than 900 minutes. As can be seen from **Fig.6-9a**, the O_2 flux was stabilized at 0.5 ml cm^{-2} min^{-1} with pure helium as sweep gas for the first 200 minutes; then slightly reduced to a stable value of 0.4 ml cm^{-2} min^{-1} for the next 200 minutes with addition of 10% CO_2 in the sweep gas. The O_2 flux declined in the presence of CO_2 due to the strong CO_2 chemical adsorption on the membrane surface which inhibited the surface exchange reaction [41, 42]. As the test progressed towards 400 minutes, 3% H_2O was introduced into the sweep gas for another 200 minutes, but O_2 flux decline was no longer observed implying that the presence of steam did not negatively affect the O_2 permeation. This observation is very different from perovskite membranes. Normally, the exposure of perovskite membrane to H_2O will aggravate the CO_2 poison effect and the membrane material undergoes faster formation of carbonate than that under the dry conditions or wet conditions [43, 44]. When the sweep gas finally changed back to the pure helium, the oxygen flux was fully recovered to the original value, which indicates that the influence of CO_2 and H_2O/CO_2 to the SDC membrane under the tested conditions was temporary and there was no permanent damage to the material phase. These results strongly indicated the potential adaptability of this novel design and membrane for real world industrial application.

To make a clear comparison, a typical perovskite $Ba_{0.5}Sr_{0.5}Co_{0.8}Fe_{0.2}O_{3-\delta}$ (BSCF) membrane was also investigated for long term test under the similar atmospheres tested for the SDC membranes. As it was expected, Fig. 9 shows that the BSCF membrane delivered very high initial oxygen fluxes of 2.0 ml cm^{-2} min^{-1}, which is 400% higher than the SDC membranes. However, BSCF membranes could not maintain such a high performance under the same testing conditions as the SDC membranes.

For instance, upon exposure to 10% CO_2, the O_2 flux sharply dropped by 78% in less than 4 hours. When 3% H_2O was introduced, the O_2 flux suffered a further decline. After the sweep gas changed back to the pure He, the O_2 flux of the BSCF membrane could not be recovered because the membrane was permanently damaged, which was attributed to carbonate or metal hydrogen oxide formation as reported elsewhere [45]. Therefore SDC membrane shows strong potential over the perovskite membrane for the deployment in industrial application, particularly to resist these acid gases at high temperatures.

Based on planar design, Air Products and Chemicals has successfully developed and tested the membrane stack at the scale of producing oxygen 1 ton per day (1.0 TPD) for 40 days based on mixed conducting perovskite material operated by high pressurized air feed gas mode [46]. Interestingly, the same planar shaped stack system can be adopted by SDC membrane with one internal short circuit to scale up for oxygen production as schematically proposed in **Fig. 10**. By coupling the proven stability of SDC membranes with their plate design flexibility, the proposed design in this work may offer many engineering process advantages. For instance, it dispenses with CO_2 scrubbing and dehydration for air separation units. Compared with external short circuit structure, this design may reduce process complexity and capital costs by operating with a lower number of unit operations

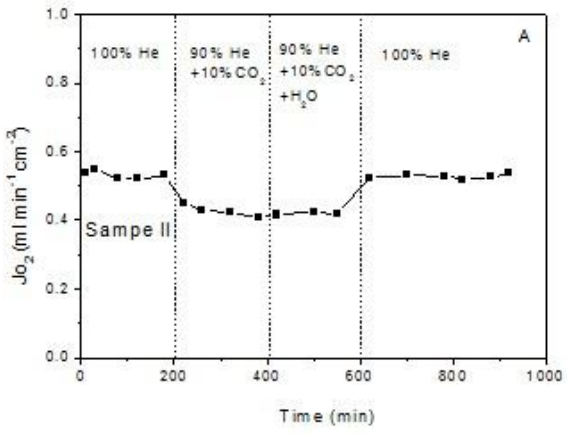

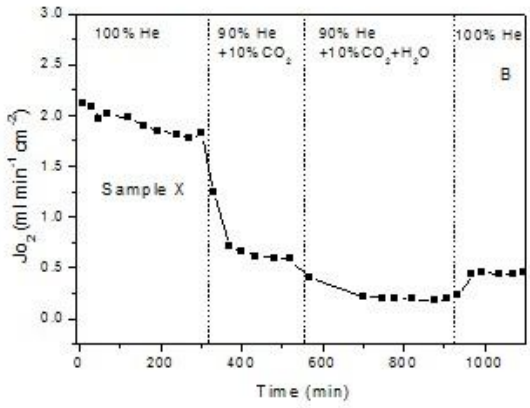

Fig.6-9 Long term oxygen permeation test of A: SDC membrane with internal short circuit (sample II) at 800 ^{o}C and B: BSCF membrane (Sample X: Perovskite) at 850 ^{o}C under He, He+CO_2 or He+CO_2+H_2O mixture.

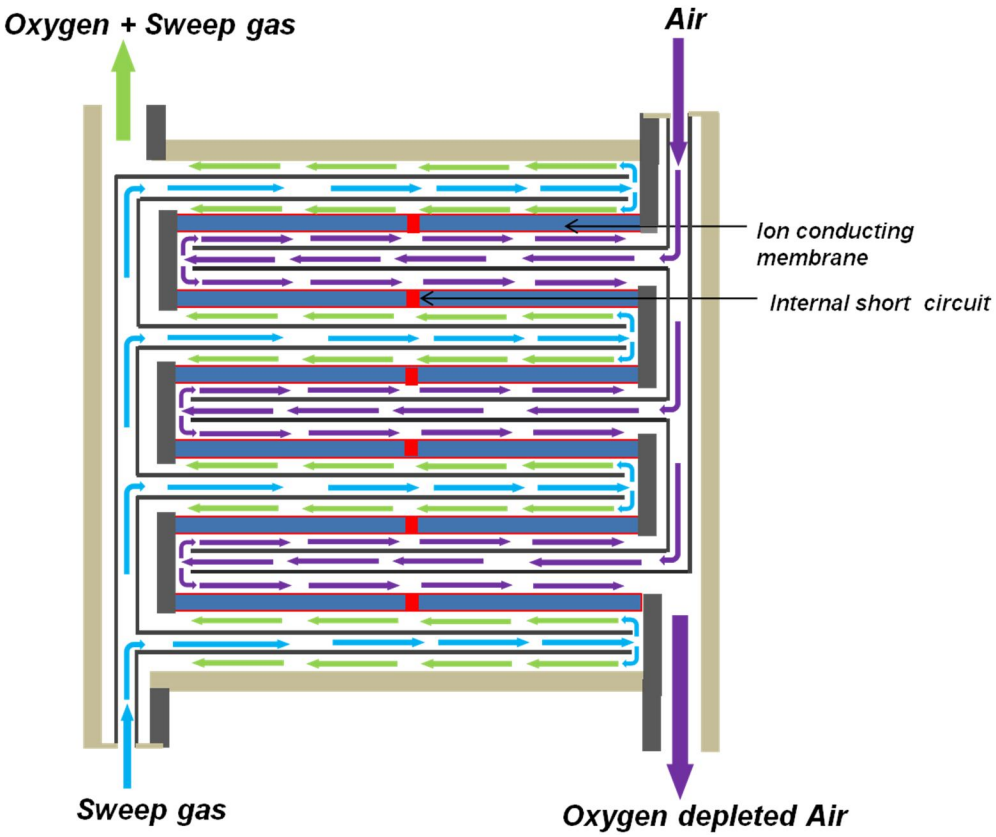

Fig.6-10 Oxygen permeation membrane stack system with the internal short circuit structure

6.4 Conclusions

Based on the working principles of solid oxide fuel cells, a novel ion conducting ceramic membrane configuration with internal short circuit was proposed, designed and experimentally verified in the work. $Sm_{0.2}Ce_{0.8}O_{1.9}$ (SDC) was synthesized and used as the membrane material to demonstrate the novel design. Oxygen permeation results indicated that one internal short circuit in the membrane was sufficient to enable the membrane to function, thus simplifying the planar membrane design for future scaling up. Stability tests provide a sharp contrast between SDC and BSCF membranes. Given that the well-known high stability of the SDC membrane, this work is possibly delivering a solution in the ceramic membrane field of oxygen production for clean energy delivery to resist the high temperature CO_2 attack or poisoning. Such novel membrane design may provide a new way to improve the viability of oxygen separation membranes for clean energy technologies.

6.5 References

1. S. Smart, C.X.C. Lin, L. Ding, K. Thambimuthu and J.C.D. da Costa, *Energy Environ. Sci.*, 2010, **3**, 268-278.
2. K. Jordal, M. Anheden, J. Yan, L. Strömberg, E.S. Rubin, D.W. Keith, C.F. Gilboy, M. Wilson, T. Morria, J. Gale and K. Thambimuthu, *in Greenhouse Gas Control Technologies 7. Elsevier Science Ltd, Oxford*, 2005.
3. G.J. Stiegel, A. Bose and P. Armstrong, *Development of ion transport membrane (ITM), oxygen technology for integration in IGCC and other advanced power generation systems, US Dept. of Energy*, 2006.
4. A. Leo, S. Liu and J.C.D. da Costa, *Int. J. Greenhouse Gas Control*, 2009, **3**, 357-367.
5. J. Sunarso, S. Liu, Y.S. Lin and J.C.D. da Costa, *Energy Environ. Sci.*, 2011, **4**, 2516-2519.
6. Y. Wei, W. Yang, J. Caro and H. Wang, *Chem. Eng. J.*, 2013, **220**, 185-203.
7. X. Dong and W. Jin, Curr. Opin. *Chem. Eng.*, 2012, **1**, 163-170.
8. J. Sunarso, S. Baumann, J.M. Serra, W.A. Meulenberg, S. Liu, Y.S. Lin and J.C.D. da Costa, *J. Membr. Sci.*, 2008, **320**, 13-41.

9. K. Efimov, T. Halfer, A. Kuhn, P. Heitjans, J. Caro and A. Feldhoff, *Chem. Mater.*, 2010, **22**, 1540-1544.
10. Y.Y. Liu, X. Tan and K. Li, Catal. Rev. Sci. Eng., 2006, **48**, 145-198.
11. H. Wang, C. Tablet, A. Feldhoff and J. Caro, *Adv. Mater.*, 2005, **17**, 1785-1788.
12. Y. Liu, X. Zhu, M. Li, H. Liu, Y. Cong and W. Yang, *Angew. Chem. Int. Ed.*, 2013, **52**, 3232-3236.
13. X. Chen, L. Huang, Y. Wei and H. Wang, *J. Membr. Sci.*, 2011, **368**, 159-164.
14. Y. Li, H. Zhao, N. Xu, Y. Shen, X. Lu, W. Ding and F. Li, *J. Membr. Sci.*, 2010, **365**, 460-470.
15. J. Sunarso, S. Liu, Y.S. Lin and J.C.D. da Costa, *J. Membr. Sci.*, 2009, **344**, 281-287.
16. H. Wang, S. Werth, T. Schiestel and J. Caro, *Angew. Chem. Int. Ed.*, 2005, **44**, 6906-1909.
17. X. Zhu, H. Wang and W. Yang, *Chem. Commun.*, 2004, 1130-1131.
18. H. Pan, L. Li, X. Deng, B. Meng, X. Tan and K. Li, *J. Membr. Sci.*, 2013, **428**, 198-204.
19. X. Dong, W. Jin and N. Xu, *Chem. Mater.*, 2010, **22**, 3610-3618.
20. P. Zeng, Z. Chen, W. Zhou, H. Gu, Z. Shao and S. Liu, *J. Membr. Sci.*, 2007, **291**, 148-156.
21. Y. Teraoka, H.M. Zhang, S. Furukawa and N. Yamazoe, *Chem. Lett.*, 1985, **11**, 1743-1746.
22. A. Leo, S. Smart, S. Liu and J.C.D. da Costa, *J. Membr. Sci.*, 2011, **368**, 64-68.
23. S. Baumann, J.M. Serra, M.P. Lobera, S. Escolástico, F. Schulze-Küppers and W.A. Meulenberg, *J. Membr. Sci.*, 2011, **377**, 198-205.
24. H. Jiang, A. Feldhoff, H. Wang and J. Caro, *Angew. Chem. Int. Ed.*, 2011, **50**, 759-763.
25. X. Zhu, H. Liu, Y. Cong and W. Yang, *Chem. Commun.*, 2012, **48**, 251-253.
26. C.S. Chen, H. Kruidhof, H.J.M. Bouwmeester, H. Verweij and A.J. Burggraaf, *Solid State Ionics*, 1996, 86, 569-572.
27. W. Li, T.F. Tian, F.Y. Shi, Y.S. Wang and C.S. Chen, *Ind. Eng. Chem. Res.*, 2009, **48**, 5789-5793.
28. X. Zhu, M. Li, H. Liu, T. Zhang, Y. Cong and W. Yang, *J. Membr. Sci.*, 2012, **394**, 120-130.

29. C.S. Chen, H. Kruidhof, H.J.M. Bouwmeester, H. Verwij and A.J. Burggraaf, *Solid State Ionics*, 1997, **99**, 215-219.
30. S. Li, W. Jin, N. Xu and J. Shi, *J. Membr. Sci.*, 2001, **186**, 195-204.
31. Z. Shao and S.M. Haile, *Nature*, 2004, **431**, 170-173.
32. Z. Zhan and S.A. Barnett, *Science*, 2005, **308**, 844-847.
33. E.D. Wachsman and K.T. Lee, *Science*, 2011, **334**, 935-939.
34. K. Zhang, Z. Shao, C. Li and S. Liu, *Energy Environ. Sci.*, 2012, **5**, 5257-5264.
35. K. Zhang, Y. Zou, C. Su, Z. Shao, L. Liu, S. Wang and S. Liu, *J. Membr. Sci.*, 2013, **427**, 168-175.
36. S. Li, S. Wang, Y. Wang, H. Nie and T.L. Wen, *Fuel Cells*, 2006, **6**, 451-454.
37. L. Zhao, B. He, X. Zhang, R. Peng, G. Meng and X. Liu, *J. Power Sources*, 2010, **195**, 1859-1861.
38. D. Gao, J. Zhao, W. Zhou, R. Ran and Z. Shao, *J. Membr. Sci.*, 2011, **366**, 203-211.
39. Z. Wang, H. Liu, X. Tan, Y. Jin and S. Liu, *J. Membr. Sci.*, 2009, **345**, 65-73.
40. P. Haworth, S. Smart, J. M. Serra and J. C. Diniz da Costa, *Phys. Chem. Chem. Phys.*, 2012, **14**, 9104-9111
41. X. Tan. N. Liu, B. Meng, J. Sunarso, K. Zhang and S. Liu, *J. Membr. Sci.*, 2012, **389**, 216-222.
42. K. Nomurna, Y. Ujihira, T. Hayakawa and K. Tekehira, *Appl. Catal. A: Gen.*, 1996, **137**, 25-36.
43. F. Grillo, M.M. Natile and A. Glisenti, *Appl. Catal. B: Environ.*, 2004, **48**, 267-274.
44. A. Leo, S. Liu and J. C. Diniz da Costa, *Sep. Pur. Technol.*, 2011, **78**, 220–227
45. M. Arnold, H. Wang and A. Feldhoff, *J. Membr. Sci.*, 2007, **293**, 44-52.
46. J.M. Repasky, E.P. Foster, P.A. Armmstrong, V.E. Stein and L.L. Anderson, *ITM oxygen development for advanced oxygen supply, Gasification Technologies Council, San Francisco, Califiornia, USA*, October 12, 2011.

Chapter 7: Highly stable external short circuit assisted-oxygen ionic transport membrane reactor for carbon dioxide reduction coupled with methane partial oxidation

7.2 Introduction

Carbon dioxide (CO_2) is an inevitable product of combustion based energy generation as we rely on fossil fuel resources whilst moving towards more advanced energy conversion and storage technologies [1-3]. Increasing energy demand not only stimulates research and development on these technologies to achieve high efficiency and lower cost but also promotes study on CO_2 mitigation [4-6]. The latter one in particular can be conceptually achieved through CO_2 capture and storage (CCS) e.g. separating CO_2 from other gases and compressing it underground for storage [7,8]. At the moment, this approach is not yet considered economic and practical due to the energy penalty (adding ~40% above the normal energy requirement) into the power plant (e.g. coal combustion plant) in addition to the uncertainty factors on long-term storage stability (e.g. possibility of leakage)[9]. Instead, CO_2 may be directly utilized and/or converted into value-added products at least with the aim to prevent its release to the atmosphere temporarily. CO_2 reduction into CO and O_2 represents such example where the resulting products can be used as reactants for synthesis of other important chemical products [10,11]. The challenge here lies in the fact that this reaction is a highly endothermic reaction and so requires high temperatures (above 1700 ^oC) in addition to thermodynamic equilibrium limited-production [12].

$2CO_2 \rightarrow 2CO + O_2$, ΔH (25 ^oC) =552 kJ mol^{-1} (1)

Membrane reactor technology provides substantial advantages to offset this drawback primarily by the capability allowing for simultaneous reaction and separation [13]. In such reactor, the products are continuously removed from the reaction chamber which leads to the reaction equilibrium being shifted to the right side during reaction e.g. favoring product formation and therefore higher conversion. Membrane reactor configuration and membrane material selection are expected to determine the mechanism and performance of CO_2 reduction [14]. The feasibility of this technology is evident, for example, from National Aeronautics and Space Administration (NASA) development of working CO_2 reduction membrane reactor based on an oxygen ionic conductor for manned space mission into Mars where the major atmosphere component is CO_2 [15] and its CO_2 utilization is of NASA's special interest. CO and O_2 produced in each side of their membrane reactor were utilized to fuel vehicle and life support system, respectively.

Membrane reactor for CO_2 reduction can also be made from perovskite (e.g. ABO_3 compound) mixed ionic-electronic conducting (MIEC) material [16-18]. Since electron transport is allowed in this material, external electrical circuit is not required. Several reports are available which demonstrates perovskite MIEC membrane reactor capability to provide high efficiency during CO_2 reduction reaction in relatively lower temperature e.g. ~ 800-900 ^oC [17,19,20]. Perovskite stability is perhaps the only factor hindering its practical use, especially under the presence of acidic gases such as CO_2, NO_x and H_2S [21-23]. This is to be expected given these high performance perovskites normally containing alkaline earth metal such as Ba and/or Sr in its A-site which are susceptible to the acidic gases [24,25]. In the presence of such gases, the perovskite structure deteriorated over increasing time which in turn, also led to decaying performance. Moreover, during CO_2 reduction, high concentration of CO_2 would be

fed to the membrane reactor, a highly reducing atmosphere. So far, only a handful amount of perovskite membranes can withstand this condition for a short period of time.

The issue of stability would be of paramount importance in real application. Developing membrane reactors featuring high stability in CO_2 (reducing) atmosphere would improve its practical value. In our recent study, an external short circuit concept was introduced to exploit high stability and ionic conductivity of the fluorite oxygen ionic conductor phase (e.g. samarium doped ceria (SDC)) in concomitant with obtaining the high electronic conductivity (from external short circuit) [26]. Here, we extend such concept from oxygen production to membrane reactor. On one side of the membrane e.g. the feed side, the reduction of CO_2 into CO and O_2 was performed on which platinum or silver can be used as a catalyst. The presence of CO_2 and CO here resulted in reducing atmosphere where the oxygen partial pressure is quite low. To attain oxygen transport through the membrane, a partial pressure gradient should exist which necessitates even lower oxygen partial pressure in the other side e.g. permeate side. Therefore, highly reducing atmosphere should be applied to consume the oxygen permeated. We exploited methane for this role. With the inclusion of appropriate catalyst such as $GdNi/Al_2O_3$, methane reacted with the transported oxygen to form syngas e.g. carbon monoxide and hydrogen, both of which are valuable chemicals. In essence, the membrane reactor coupled CO_2 reduction and CH_4 partial oxidation on different sides of the membrane to enable oxygen transport through the membrane. The schematic diagram of the membrane reactor is depicted in **Fig.7-1**.

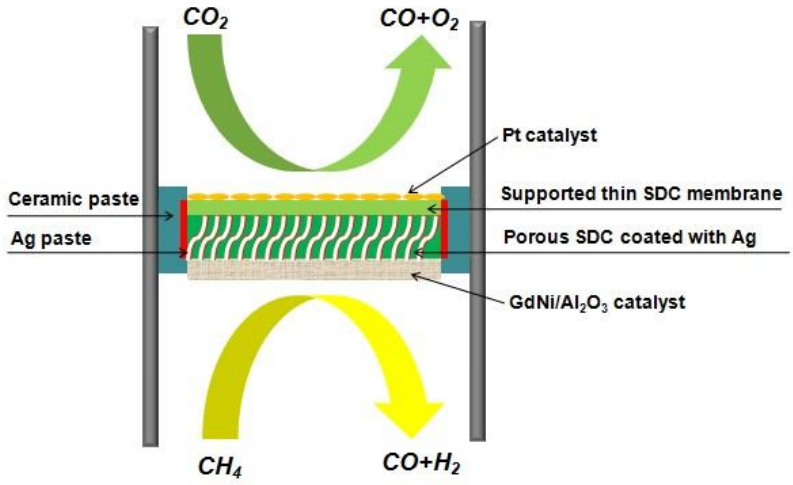

Fig.7-1 Schematic diagrams of the SDC membrane reactor utilizing asymmetric structure, external short circuit, Pt catalyst in the feed side and $GdNi/Al_2O_3$ catalyst in the permeate side.

7.2 Experimental section

Samarium doped ceria-$Sm_{0.2}Ce_{0.8}O_{1.9}$ (SDC) was synthesized using an ethylenediaminetetraaceticacid (EDTA)-citrate complexing sol-gel route. $Ce(NO_3)_2.xH_2O$ and $Sm(NO_3)_3.xH_2O$ (all in analytical reagent (AR) grade) were used as raw materials for the metal-ion sources. To control precisely the stoichiometric amount (of the metal ions), the metal nitrates were first made into their respective aqueous solutions with concentration around 1 M. The real molarity was then determined using EDTA titration technique as detailed elsewhere. The desirable molar ratios were then obtained by mixing required volume of each of the metal ion solution with the known molarity, followed by adding EDTA and citric acid as the complexing agents at the molar ratio of total metal ions: EDTA: citric acid = 1: 1: 2. Ammonia solution, $NH_3(aq)$ was added to control the solution pH to ~6. The solution was stirred afterwards during which the formation of homogeneous mixture was indicated by transparent color. Continuous heating at 90 ^oC led to water evaporation

and later on, a purple gel formation, which was then pre-fired at 250^{o}C, followed by calcination at 1400 ^{o}C in air for 5 h.

The synthesized oxide powders were pressed into disks using a stainless steel die and pellet press set (15.0 mm in diameter) under a hydraulic pressure of ~ 1.5 x 10^{8} Pa. These disks (defined as green disk membranes) (~1.0 mm in thickness) were then sintered in a muffle furnace at 1500 ^{o}C in air for 5 h using a ramping and cooling rate between 1-2 ^{o}C min^{-1}. Silver (Ag) paste was coated throughout the disk circumference to enable electrical conduction between the opposite sides of disk membrane. Likewise, platinum and/or Ag slurry was also coated onto the opposing sides of the disk membrane (the coating was made to cover all surface on both sides so that they are symmetrical). The coated disk membranes were then calcined at 600 ^{o}C in air for 2 h.

Co-pressing technique, which is frequently used to prepare thin-film electrolyte for solid oxide fuel cells was used to fabricate supported thin film disk membranes [27,28]. SDC and NiO powders were mixed and ground at the weight ratio of 2:3, respectively by ball milling in a planetary mill (Pulverisette 5, Fritsch) at a rotation rate of 300 rpm for 6 h. The resultant SDC/NiO (40%SDC) powder was then pressed into disk. This disk acted as a substrate. On top of this disk, SDC powder was added and pressed to form bi-layer disk which was later on sintered at 1350 ^{o}C for 5 h to obtain dense SDC layer on the disk. The resultant disk was then reduced in hydrogen at 500 ^{o}C for 1 h to reduce NiO into Ni and form porous Ni network. Ni was then extracted from the disk by immersing the disk into a diluted nitric acid aqueous solution (HNO_3) at room temperature. At this stage, porous layer containing SDC scaffold was formed on top of dense SDC layer. Silver nitrate ($AgNO_3$) solution was then added to the porous layer until the layer is completely filled with the solution. The disk (containing $AgNO_3$ solution) was then calcined at 500 ^{o}C for 5 h to decompose $AgNO_3$ into the

metallic silver. These silver networks functioned as electron collector to ensure sufficient electronic transport and contact area between the catalyst and membrane.

As a catalyst, $GdNi/Al_2O_3$ with the composition of 5.56 wt% Gd_2O_3, 15 wt% Ni and 79.44 wt% Al_2O_3 was also synthesized using an EDTA-citrate complexing sol-gel route. The procedure repeats the one described above followed by calcination temperature of 850 ^oC in air for 5 h. The resultant $GdNi/Al_2O_3$ catalyst with the amount of ~0.2 g was packed into the porous layer of the SDC membrane and placed facing the permeate side where argon in mixture with methane was fed into.

CO_2 reduction activity of the membranes was measured using gas chromatography technique utilizing high temperature O_2 permeation apparatus. Ceramic paste was used as sealant to fix the disk membrane onto a quartz tube. The effective area for permeation is ~ 0.45 cm^2. Argon in mixture with methane was used as sweep gas in the permeate side to create oxygen partial pressure gradient across the membrane. Helium diluted carbon dioxide (~33 vol. % CO_2 in He) was used as the feed gas. The composition of the permeating gas was characterized using a gas chromatography (Agilent 6890N Network GC system with a thermal conductivity detector (TCD) and Flame Ionization Detector (FID)). A HP-Molecular Sieve (Molsieve) 5A column was employed to separate H_2, O_2, N_2, CH_4 and CO. A PLOT Q column was employed to separate CO_2 and hydrocarbons. The analysis results were verified using carbon mass balance. The experimental error is ~5%. Accordingly, the oxygen permeation flux through the membrane can be calculated using mass balance from known CO_2 and CO flux in the permeate side as well as the known CO_2 amount in the feed side.

The surface morphology of the disk membranes was obtained using scanning electron microscope (SEM, Zeiss Evo 40XVP) at acceleration voltage of 15 kV. The powder x-ray diffraction (XRD) analysis were performed in a powder x-ray diffractometer (Bruker D8 Advances) using a Cu-Kα radiation generated at 40 kV and 30 mA.

7.4 Results and discussion

7.4.1 Membrane reactor performance using 1-mm thick SDC membrane

The catalytic performances of SDC membrane reactor e.g. the CO_2 conversion percentage with and without external short circuit between 700-900 ^oC are shown in **Fig.7-2**; Ar was used as sweep gas here to illustrate the basic case. Here, we use 1-mm thick dense SDC membrane. In general, the CO_2 conversion increased steadily with temperature rise. This is likely the case considering temperature activated nature of catalytic activity of the membrane surface coated with Ag and Pt catalyst as well as oxygen ionic conductivity of SDC. In principle, CO_2 reduction occurred at the surface of the SDC during which CO_2 is effectively converted into CO and O_2. CO was released back to the atmosphere while O_2 was depleted on the membrane. To this end, increasing either the CO_2 reaction rate on the membrane surface or O_2 depletion led to improved CO_2 reduction performance.

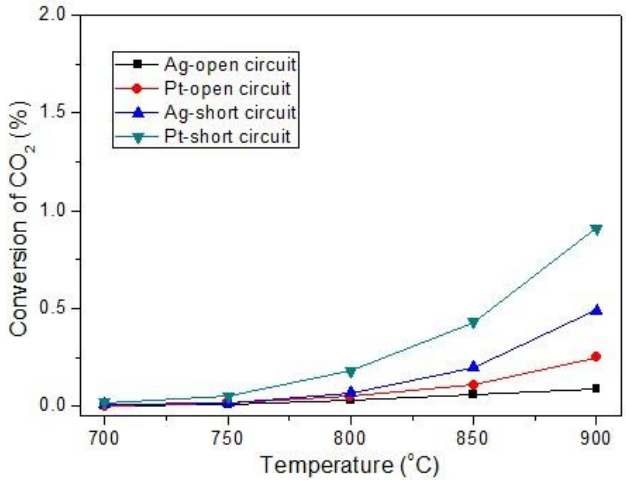

Fig.7-2 Temperature dependent CO_2 conversion; CO_2 with flow rate of 10 ml min^{-1} in mixture with He with flow rate of 30 ml min^{-1} were used as feed gas while Ar with flow rate of 35 ml min^{-1} was used as sweep gas.

As a trend, adding external short circuit enhance the performance by contributing to the higher rate of O_2 depletion through the membrane. In this case, better performance relative to the use of external short circuit can be rationalized in terms of higher electronic conductivity attained via the circuit. SDC is practically an oxygen ionic

conductor which justifies its use as an electrolyte material in solid oxide fuel cell [29]. We can safely say that the electronic conductivity in such compound is substantially lower than the ionic conductivity (neglecting the partial reduction of Ce^{4+} to Ce^{3+} in SDC above 700 ^{o}C due to its low reaction extent) which translates to the electronic conductivity limited oxygen ionic transport [30]. To this end, increasing electronic conductivity would enhance the oxygen transport and thus, the oxygen depletion from the feed side of the membrane. This in turn, brought about enhanced CO_2 reduction. Likewise, Pt improved the performance by acting as a more efficient catalyst for CO_2 reduction. The highest conversion of ~0.91 % at 900 ^{o}C was attained using external short circuit together with Pt catalyst. We speculate that in case of Pt catalyst, CO_2 was coordinated to the transition metal center in such a way that the activation energy required to facilitate the subsequent reduction reactions could be made lower (with respect to Ag) [31].

7.3.2 Membrane reactor performance using asymmetric structured SDC membrane

We probe the extent to which CO_2 conversion can be improved by optimizing the oxygen transport through the disk membrane. This was attained by utilizing asymmetric membrane structure. The asymmetric structure refers to membrane structure containing two layers e.g. dense thin film layer and porous supporting layer. In such membrane, the effective transport layer corresponds to the thin film layer. The porous layer, on the other hand, contributes mechanical strength required to sustain the asymmetric structure while allowing continuous gas transport through its void part besides increasing the area for oxygen surface exchange reactions e.g. oxygen gas dissociation to oxygen ions and oxygen ions association to oxygen gas.

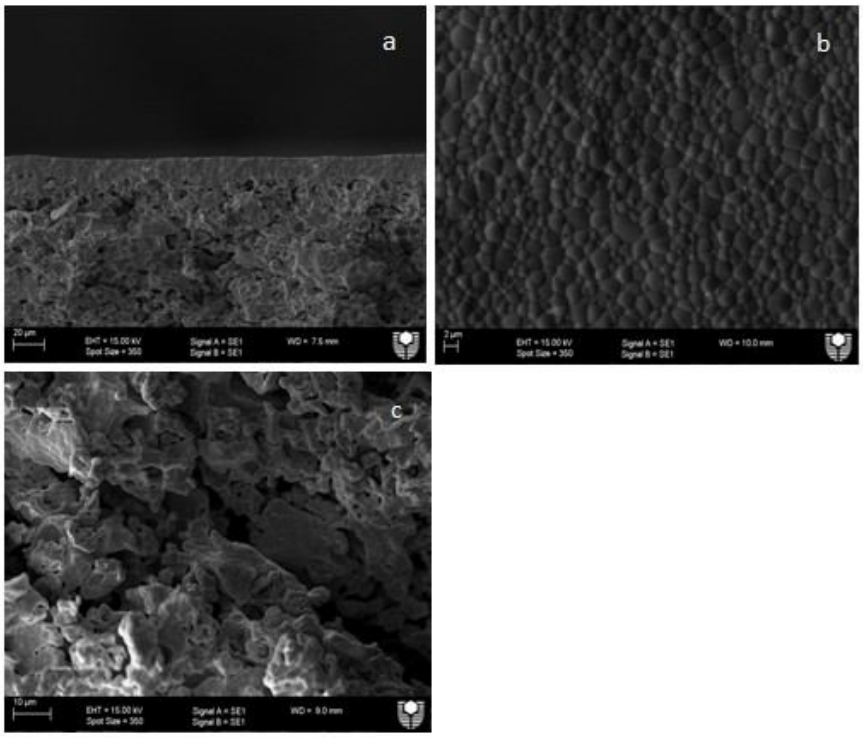

Fig.7-3 SEM images of SDC membrane with asymmetric structure; a. cross-section; b. dense thin layer; c. porous layer.

The prepared asymmetric SDC membrane (preparation details in Experimental) has ~20 μm thick dense layer (**Fig.7-3a**). **Fig.7-3b** displays a snapshot of the dense surface while **Fig.7-3b** shows a snapshot of the porous structure. The very thin layer represents substantial reduction relative to 1 mm-thick membrane utilized in previous section (**3.1**). **Fig.7-4** compares the oxygen fluxes of 1 mm-thick membrane with those of the asymmetric membrane. At the highest temperature of 900 ^{o}C, the flux reached ~1.3 ml cm^{-2} min^{-1} when air was used as feed gas while Ar was used as sweep gas. The oxygen transport through the membrane is also driven by the oxygen partial pressure difference [22]. Therefore, an enhanced transport could be realized by enlarging the partial pressure difference by introducing a highly reducing gas such as CH_4 in the permeate side. In such case, the oxygen which was transported to the permeate side would react with CH_4 to form syngas e.g. CO and H_2; the so-called partial oxidation of methane. In these experiments, CO_2 (flow rate of 10 ml min^{-1}) was

mixed with He (flow rate of 30 ml min^{-1}) and used as feed gas in the feed side of membrane. Accordingly, CH_4 (flow rate of 2 ml min^{-1}) was mixed with Ar (flow rate of 35 ml min^{-1}) and used as sweep gas in the permeate side of membrane (**Fig.7-1**). **Fig.7-5** depicts CO_2 conversion obtained in such configuration with and without the use of external short circuit. It is noteworthy that Pt on the feed side of the membrane was used not only as a catalyst for CO_2 reduction but also as the electronic conducting phase for membrane function. The conversion is substantially improved in comparison with the results shown in **Fig.7-2**, which was obtained through substantial membrane thickness reduction to increase the oxygen permeation rate. External short circuit caused a further performance improvement; consistent with our discussion above. The highest CO_2 conversion of 11 % was achieved at 900 ^oC with the improvement by a factor of 10 comparing to that obtained using 1 mm thick SDC membrane under external short circuit and Ar as sweep gas.

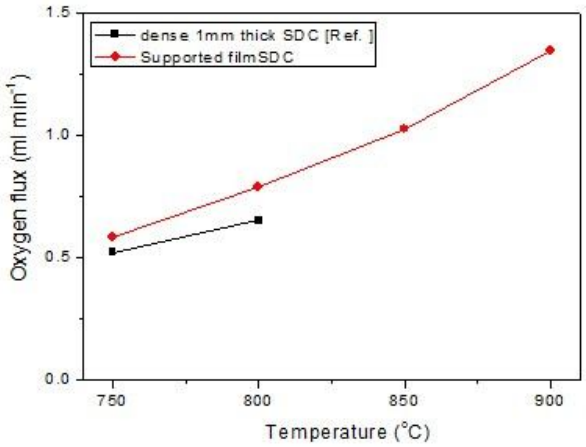

Fig.7-4 Oxygen flux through SDC membrane with asymmetric structure and dense 1 mm-thick SDC membrane; both utilizing external short circuit. Air was used as feed gas while Ar with flow rate of 100 ml min^{-1} was used as sweep gas.

The partial oxidation of methane on the permeate side of the membrane were probed; the results of which were shown in **Fig.7-6**. CH_4 conversion and O_2 flux increased with increasing temperature from 700 ^oC to 900 ^oC. For example, CH_4 conversion

increased from ~10% at 700 °C to ~37% at 900 °C. Likewise, O_2 flux increased from ~0.1 ml cm^{-2} min^{-1} at 700 °C to ~1.12 ml cm^{-2} min^{-1} at 900 °C. CO selectivity, although increased with temperature rise, represent a marginal change with an average value ~84%. During experiments, the permeate side of the membrane contained CH_4, CO, H_2 and very low amount of CO_2 and H_2O. No O_2 was found within the detection limit; mirroring O_2 total consumption by the reaction with CH_4.

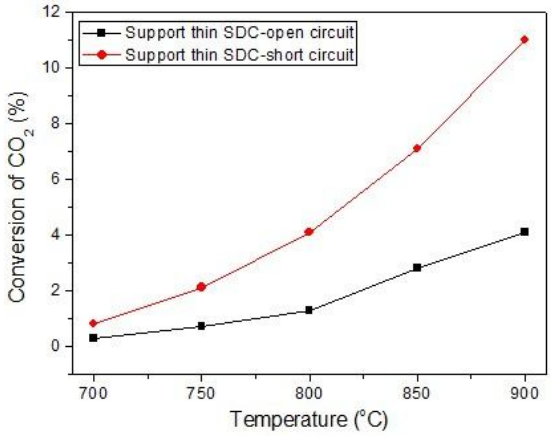

Fig.7-5 Temperature dependent CO_2 conversion; CO_2 with flow rate of 10 ml min^{-1} in mixture with He with flow rate of 30 ml min^{-1} were used as feed gas while CH_4 with flow rate of 2 ml min^{-1} and Ar with flow rate of 35 ml min^{-1} were used as sweep gas.

Upon comparing **Fig.7-4** and **Fig.7-6**, it become apparent that enlarging the oxygen partial pressure difference (by employing sweep gas with much lower oxygen partial pressure in permeate side) did not necessarily translate to higher oxygen fluxes. In fact, the oxygen fluxes in **Fig.7-6** seem to be reduced slightly (relative to those in **Fig.7-4**). Note that for the experiments shown in **Fig.7-4**, air was used as the feed gas. For the experiments shown in Fig. 6, however, CO_2 was used as the feed gas. Accordingly, the discrepancy can then be explained by the fact that breaking O=CO bond requires larger energy (bond enthalpy of 532 kJ mol^{-1}) relative to breaking O=O bond (bond enthalpy of 503 kJ mol^{-1}) [16]. As such, we expected slower surface

exchange reaction in the case of CO_2 which counteracted the positive effect contributed by enlarging the oxygen partial pressure gradient.

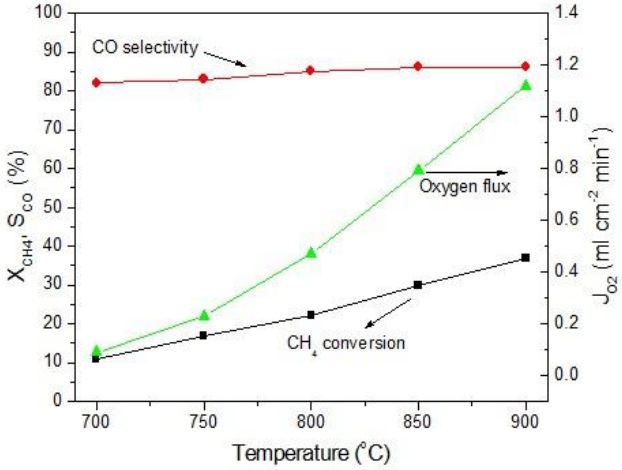

Fig.7-6 Temperature dependent CH_4 conversion on SDC membrane reactor with asymmetric structure utilizing external short circuit; CO_2 with flow rate of 10 ml min^{-1} in mixture with He with flow rate of 30 ml min^{-1} were used as feed gas while CH_4 with flow rate of 2 ml min^{-1} and Ar with flow rate of 35 ml min^{-1} were used as sweep gas.

7.3.3 Effects of CO_2 and CH_4 flow rate

The effect of CO_2 flow rate on the CO_2 reduction reaction in the feed side of SDC membrane reactor was studied at a fixed temperature of 850 ^oC; the results of which is depicted in **Fig.7-7**. During these experiments, in feed side, CO_2 flow rate was varied between 5 to 20 ml min^{-1} whilst the total flow rate of CO_2 and He was kept constant at 40 ml min^{-1}. The CH_4 and Ar flow rate into the permeate side, on the other hand was fixed at 2 ml min^{-1} and 35 ml min^{-1}, respectively. Increasing flow rate brought about reduction in CO_2 conversion from ~8.1% at 5 ml min^{-1} to ~5.6% at 20 ml min^{-1}. This is to be expected considering fixed rate of CO_2 reduction on the membrane surface (e.g. fixed surface area for reaction) and consistent with decreasing CO selectivity (in feed side) with increasing CO_2 flow rate from ~87% at 5 ml min^{-1} to ~85% at 20 ml min^{-1}. Oxygen flux instead increased from ~0.4 ml cm^{-2} min^{-1} at 5 ml min^{-1} to ~0.7 ml min^{-1} cm^{-2} at 10 ml min^{-1}. Beyond 10 ml min^{-1}, the oxygen flux was marginally

increased to 1.0 ml min^{-1}. It is highly plausible that larger amount of CO_2 in feed side led to less driving force for transport given the fixed oxygen partial pressure in permeate side. Furthermore, CH_4 conversion was slightly increased from ~28% at 5 ml min^{-1} to ~33% at 20 ml min^{-1}; in agreement with increasing oxygen flux trend. We expected that the permeated oxygen was directly consumed in the permeate side by the reaction with CH_4.

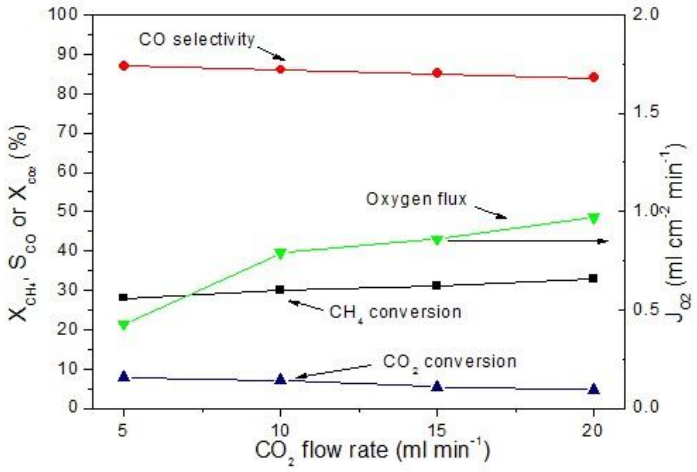

Fig.7-7 The effect of CO_2 flow rate on the membrane reactor performance at 850 ^oC; CO_2 with flow rate of 5-20 ml min^{-1} in mixture with He with flow rate of 35-20 ml min^{-1} were used as feed gas (total flow rate was fixed at 40 ml min^{-1}) while CH_4 with flow rate of 2 ml min^{-1} and Ar with flow rate of 35 ml min^{-1} were used as sweep gas.

Fig.7-8, in turn, depicts the effect of CH_4 flow rate in the permeate side under other similar conditions of **Fig.7-7**. During these experiments, in the feed side, CO_2 and He flow rate was fixed at 10 ml min^{-1} and 30 ml min^{-1}, respectively. In the permeate side, nonetheless, the CH_4 flow rate was varied between 1 to 5 ml min^{-1} whilst the total flow rate of CH_4 and Ar was kept at 37 ml min^{-1}. With the exception of CH_4 conversion, CO_2 conversion, oxygen flux and CO selectivity (in feed side) were of increasing trends with CH_4 flow rate. These trends can be rationalized in terms of the enlarged oxygen partial pressure difference at increasing CH_4 flow rate. At higher driving force, more oxygen would be transported through the membrane which is

equivalent to the faster oxygen transport rate. For this to occur, more CO_2 would be consumed during similar reaction time period which is also reflected by the faster CO_2 reduction rate (in feed side). Accordingly, more CO would be produced per CO_2. Moreover, given that there is a fixed rate of CH_4 partial oxidation on the permeate side of the membrane (e.g. fixed surface area for reaction), putting more CH_4 would only result in more left-over amount of CH_4 thus decreasing its conversion.

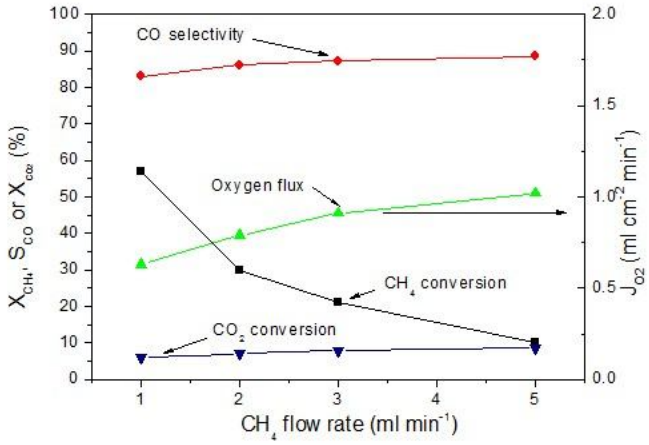

Fig.7-8 The effect of CH_4 flow rate on the membrane reactor performance at 850 ^oC; CO_2 with flow rate of 10 ml min^{-1} in mixture with He with flow rate of 30 ml min^{-1} were used as feed gas while CH_4 with flow rate of 1-5 ml min^{-1} and Ar with flow rate of 36-32 ml min^{-1} were used as sweep gas (total flow rate was fixed at 40 ml min^{-1}).

7.3.4 Long-term stability

As previously mentioned, long-term stability forms a key indicator to reflect the practical value of certain membrane reactor. **Fig.7-9** shows the performance of SDC membrane reactor utilizing external short circuit at 850 ^oC. CO_2 and He flow rate in the feed side was fixed at 10 ml min^{-1} and 30 ml min^{-1}, respectively while CH_4 and Ar flow rate in the permeate side was fixed at 2 ml min^{-1} and 35 ml min^{-1}, respectively. In the first 2 hour period, transient behavior was observed for oxygen flux and CH_4 conversion during which the both variables demonstrate quite substantial increase to their steady values. Arguably, the typical equilibrium response period for this system

is 2 hour. Beyond this period up to 100 hour after the start, very stable response was evident on CO selectivity, CH_4 conversion, CO_2 conversion and O_2 flux. Albeit its apparent scattering, O_2 flux shows relatively stable trend e.g. scattering around a well-defined median value of ~0.75 ml min^{-1} cm^{-1}.

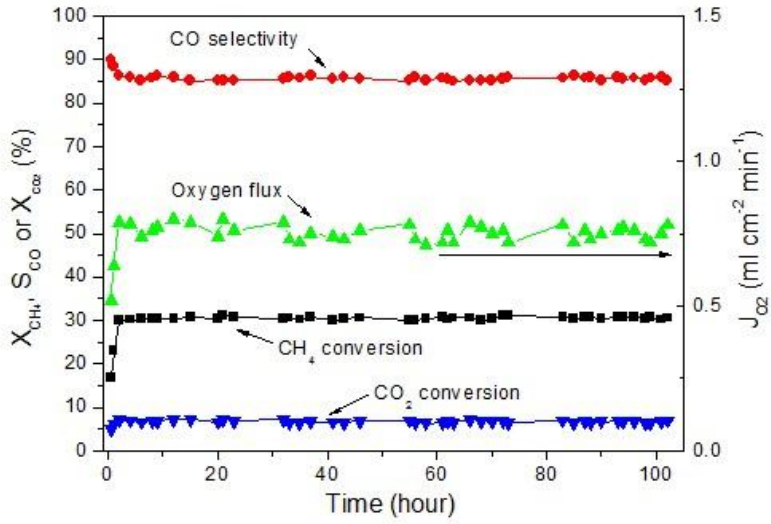

Fig.7-9 Long term performance of the membrane reactor at 850 ^oC; CO_2 with flow rate of 10 ml min^{-1} in mixture with He with flow rate of 30 ml min^{-1} were used as feed gas while CH_4 with flow rate of 2 ml min^{-1} and Ar with flow rate of 35 ml min^{-1} were used as sweep gas.

Considering the exposure of the membrane to the highly reducing atmosphere in both sides for 100 hours, the observed stability is quite remarkable. Such performance may not be attained using perovskite based membranes. Moreover, after the test, SDC membrane maintained the original structure without cracking presence on the membrane surface. **Fig.7-10** further confirmed SDC stability by comparing the powder x-ray diffraction patterns of as prepared fresh membrane with those of membranes exposed to CO_2 and CH_4 at 850 ^oC for 100 h. The original characteristic peaks which correspond to the crystal structure of SDC were retained after exposure with no noticeable deterioration and formation of additional peaks; ruling out structure alteration after exposure.

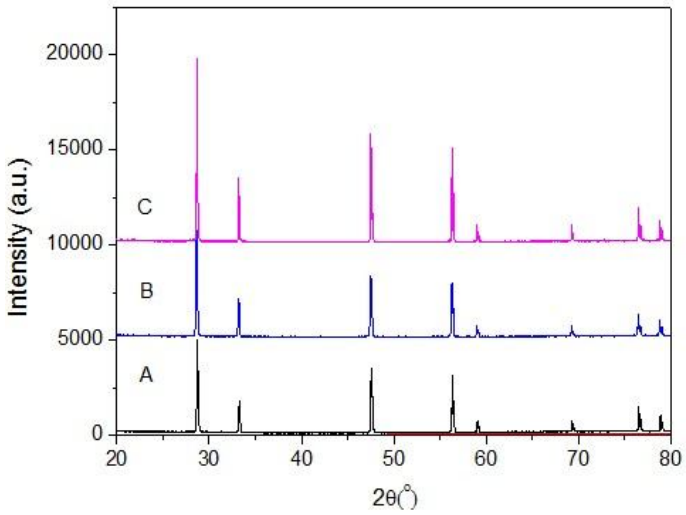

Fig.7-10 Powder XRD patterns of the SDC membranes; A. as prepared; B. after 100 h under CO_2 at 850 ^oC, C. after 100 h under CH_4 at 850 ^oC.

It is also worthwhile to mention that in reactions involving CH_4, conventional Nicatalyst suffers from coking e.g. carbon deposition which deteriorates its catalytic activity over time due to the coverage of catalyst's active sites. In this membrane reactor, there is no evidence of such phenomena (**Fig.7-11**). This highlights the resistance of $GdNi/Al_2O_3$ towards coking probably associated with the synergistic interaction between GdNi and Al_2O_3 substrate [32].

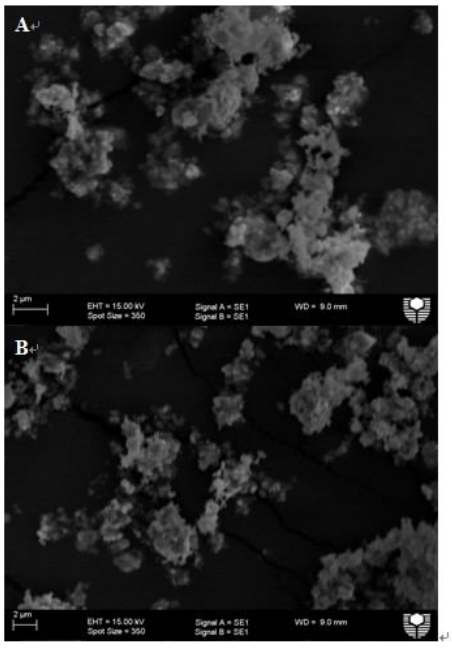

Fig.7-11 SEM images of the $GdNi/Al_2O_3$ catalyst; A. before test; B. after test.

7.4 Conclusions

We have shown that SDC membrane utilizing external short circuit can be applied as membrane reactor to couple the carbondioxide reaction in the feed side with the methane partial oxidation in the permeate side. To optimize the performance of such membrane reactor, we have applied asymmetric structure to reduce the ionic transport resistance through the membrane. Further on, we also showed the interplay between the controlled variable e.g. gas flow rate in the feed and permeate side and the catalytic performances. The practical value of the membrane reactor was also verified by subjecting it to 100-hour testing during which the membrane retained very stable performances following 2-hour transient period. Moreover, the structure of the membrane was not altered after the test.

7.5 Reference

1 United Nations. 2006. 2004 Energy Statistics Yearbook. United Nations Department for Economic and Social Information and Policy Analysis, Statistics Division, New York.

2 S. Kaneco, H. Katsumata, T. Suzuki and K. Ohta, *Energy Fuels*, 2006, **20**, 409-414.

3 R.J. Andres, D.J. Fielding, G. Marland, T.A. Boden and N. Kumar, *Tellus*, 1999, **1751**, B:759-765.

4 K. Paustian, C.V. Cole, D. Sauerbeck and N. Sampson, *Climatic Change*, 1998, **40**, 135-162.

5 A. Yamasaki, *J. Chem. Eng. Jap.*, 2003, **36**, 361-375.

6 A.J. Plantinga and T. Mauldin, *Climatic Change*, 2001, **49**, 21-40.

7 C.A. Scholes, *Int. J. Greenhouse Gas Control*, 2010, **4**, 739-755.

8 D.M. D'Alessandro, B. Smit and J.R. Long, *Angew. Chem. Int. Ed.*, 2010, **49**, 6058-6082.

9 M.B. Hägg and A. Lindrathen, *Ind. Eng. Chem. Res.*, 2005, **44**, 7668-7675.

10 S. Kaneco, H. Katsumata, T. Suzuki and K. Ohta, *Energy Fuels*, 2006, **20**, 409-414.

11 K. Xie, Y. Zhang, G. Meng and J.T.S Irvine, *Energy Environ. Sci.*, 2011, **4**, 2018-2222.

12 H. Shin, S. Choi, K. Jung and S. Han, *Chem. Mater.*, 2001, **13**, 1238-1242.

13 N. Itoh, M.A. Sanchez, W. Xu, K. Haraya, M. Hongo, *J. Membr. Sci.*, 1993, **77**, 245-253.

14 M. Bracht, P.T. Alderliesten, R. Kloster, R. Pruschek, G. Haupt, E. Xue, J.R.H. Ross, M.K. Koukou and N. Papayannakos, *Energy Convers. Manage.*, 1997, **38**, S159-S164.

15 B.M. Frankie and R. Zubrin, *Chem. Eng. Prog.*, 1999, **95**, 45-54.

16 W. Jin, C. Zhang, X. Chang, Y. Fan, W. Xing and N. Xu, *Environ. Sci. Technol.*, 2008, **42**, 3064-3068.

17 W. Jin, C. Zhang, P. Zhang, Y. Fan and N. Xu, *AIChE J.*, 2006, **52**, 2545-2550.

18 D.A. Slade, A.M. Duncan, K.J. Nordheden and S.M. Stagg-Williams, *Green Chem.*, 2007, **9**, 577-581.

19 Y. Fan, J.Y. Ren and W. Onstor, *Ind. Eng. Chem. Res.*, 2003, **42**, 2618-2626.

20 C. Zhang, X. Chang, Y. Fan, W. Jin and N. Xu, *Ind. Eng. Chem. Res.*, 2007, **46**, 2000-2005.

21 M.A. Peña and J.L.G. Fierro, *Chem. Rev.*, 2001, **101**, 1981-2017.

22 J. Sunarso, S. Baumann, J.M. Serra, W.A. Meulenberg, S. Liu, Y.S. Lin and J.C. Diniz da Costa, *J. Membr. Sci.*, **2008**, 320, 13-41.

23 W. Yang, H. Wang, X. Zhu and L. Lin, *Topics Catal.*, 2005, **35**, 155-167.

24 Y. Liu, X. Tan and K. Li, *Catal. Rev.*, 2006, **48**, 145-19.

25 X. Dong and W. Jin, *Curr. Opin. Chem. Eng.*, 2012, **1**, 163-170.

26 K. Zhang, Z. Shao, C. Li and S. Liu, *Energy Environ. Sci.*, 2012, **5**, 5257-5264.

27 L. Zhao, B. He, Y. Ling, Z. Xun, R. Peng, G. Meng and X. Liu. *Int. J. Hydrogen Energy*, 2010, **35**, 3769-74.

28 L. Zhao, B. He, B. Lin, H. Ding, S. Wang, Y. Ling, R. Peng, G. Meng and X. Liu, *J Power Sources*, 2009, **194**, 835-7.

29 Z. Shao and S.M. Haile, *Nature*, 2004, **431**, 170-173.

30 H. Daisuke, T. Atsuko, T. Shinya, H. Takashi and S. Mitsuru, *Solid State Ionics*, 2005, **176**, 881-887.

31 K. Hara, A. Kudo, T. Sakata and M. Watanabe, *J. Electrochem. Soc.*, 1995, **142**, L57-L59.

32 Z. Shao, C. Zhang, W. Wang, C. Su, W. Zhou, Z. Zhu, H.J. Park and C. Kwak, *Angew. Chem. Int. Ed.*, 2011, **50**, 1792-1797.

Chapter 8: External short circuit-assisted proton conducting ceramic membrane for H_2 permeation

8.1 Introduction

Clean and high efficiency energy conversion technology is highly relevant towards resolving our universal energy problem in a sustainable way e.g. how to meet constantly increasing energy demand with lowest impact to the environment. Fuel cell is one such technology which converts chemical energy into electrical energy via chemical reactions (on electrodes) and ionic transport (in electrolyte) [1,2]. Among various fuel cells, proton exchange membrane fuel cells (PEMFCs) and solid oxide fuel cells (SOFCs) are perhaps the most practical ones for stationary and transport applications [3-5]. As a fuel for these devices, hydrogen is rendered an excellent candidate given its high energy density and non-polluting reaction products (e.g. water) [6-8]. This, of course, is based solely on a perspective of hydrogen as an energy carrier. At the moment, hydrogen cannot be sustainably produced or freely found in nature in useful quantities, not to mention these daunting problems in its distribution and storage [9,10]. While hydrogen can be obtained from water using electrochemical or photochemical water splitting technologies, these processes are not practical due to the associated energy penalty and/or efficiency issue. At present, most hydrogen is produced through methane steam reforming with the reaction below [11]:

$$CH_4\,(g) + 2H_2O \rightarrow 3H_2\,(g) + CO_2\,(g) \qquad (1)$$

The drawback of this process lies in the production of carbon dioxide which should be separated from the other gases and properly treated to counteract its greenhouse effects.

Membrane technology has drawn much attention because of its numerous attractive characteristics such as low capital investment, operating and maintenance costs, simple installation and operation and more importantly, the potential of enabling simultaneous separation and reaction capability (e.g. membrane reactors) [12,13]. Therefore, direct dehydrogenation reaction without carbon dioxide emission can be achieved. Palladium (Pd) based metal membrane was widely employed and studied as a hydrogen permeation membrane due to its relatively high permeability and catalytic activity (to dissociate molecular hydrogen) [14]. However, its high cost and poor mechanical stability towards hydrogen embrittlement have hindered its widespread use [15,16]. Proton conducting perovskite oxide is an attractive alternative of membrane reactor material for hydrogen production [17,18]. Numerous proton conducting materials have been developed since the first finding of $SrCeO_3$ by Iwahara et al which features proton conductivity at high temperatures [19-34]. To be applied as hydrogen permeation membrane, the materials should exhibit mixed proton and electron conducting capability [35]. Accordingly, the downside of these perovskites is in their much lower electronic conductivity relative to their proton conductivity, which rather favors their use as an electrolyte than as a hydrogen membrane [36-38]. As a consequence, the hydrogen permeation rate through these proton conducting membranes are mainly determined by electron transport across the membrane. Toward this, the electronic conductivity may be enhanced by introducing multivalent cations into $BaCeO_3$-based oxides or by adding a pure electron conducting phase (e.g. metal) into the original proton conducting perovskite phase. Indeed, enhanced hydrogen permeation fluxes were achieved in the latter case e.g. by using dual-phase

mixed conducting membrane [40-44]. In dual-phase case however electronic conductivity improvement was obtained at the expense of a certain reduced amount of proton conductivity.

In this work, the purpose was to examine the hypothesis that an external short circuit structure based on the $BaZr_{0.1}Ce_{0.2}Y_{0.7}O_{3-\delta}$ and $BaZr_{0.3}Ce_{0.6}Y_{0.1}Zn_{0.05}O_{3-\delta}$ proton conducting membrane would facilitate the electron transport between the opposite sides of the membrane without altering (or reducing) the intrinsic proton conductivity. More details into this concept for oxygen separation are available elsewhere [45, 46] and now we apply it to hydrogen separation. To this end, we systematically studied the hydrogen permeation properties of the resultant proton conducting membranes.

8.2 Experimental section

$BaZr_{0.1}Ce_{0.2}Y_{0.7}O_{3-\delta}$ (BZCY) and $BaZr_{0.3}Ce_{0.6}Y_{0.1}Zn_{0.05}O_{3-\delta}$ (BZCYZn) perovskite oxides were synthesized using a combined ethylenediaminetetraaceticacid (EDTA)-citrate complexing route. $Ba(NO_3)_2.xH_2O$, $Ce(NO_3)_2.xH_2O$, $Zr(NO_3)_4.xH_2O$, $Y(NO_3)_3.xH_2O$ and $Zn(NO_3)_2.xH_2O$ (all in analytical reagent grade), were applied as raw materials for the metal-ion sources. To control precisely the stoichiometric amount (of the metal ions), the metal nitrates were first made into their respective aqueous solutions (~1 M). The real molarity was then determined using EDTA titration technique as detailed elsewhere [20]. The desirable molar ratios were obtained by mixing the required volume of each of the metal ion solution with the known molarity, followed by adding EDTA and citric acid as the complexing agents at the molar ratio of total metal ions: EDTA: citric acid = 1: 1: 2. Ammonia solution, $NH_3(aq)$ was added to control the solution pH to ~6. The solution was stirred afterwards during which the formation of homogeneous mixture was indicated by transparent color. Continuous heating at 90 ^oC led to water evaporation and later on, a

transparent purple gel formation, which was then pre-fired at 250 ^{o}C, followed by calcination at 1000 ^{o}C in air for 5 h.

The synthesized oxide powders were pressed into disks using a stainless steel die and pellet press set (15.0 mm in diameter) under a hydraulic pressure of ~ 1.5 x 10^{8} Pa. These disks (defined as green disk membranes) (~1.0 mm in thickness) were then sintered in a muffle furnace at 1500 ^{o}C in air for 5 h using a ramping and cooling rate between 1-2 ^{o}C min^{-1}. Silver (Ag) paste was coated throughout the disk circumference to enable electrical conduction between the opposite sides of disk membrane. Platinum slurry was also coated on the opposing sides of the disk membrane. The coated disk membranes were then calcined at 800 ^{o}C in air for 2 h to increase the adherence. The disk membrane setup for hydrogen permeation e.g. external short circuit-assisted membrane is depicted in **Fig.8-1**.

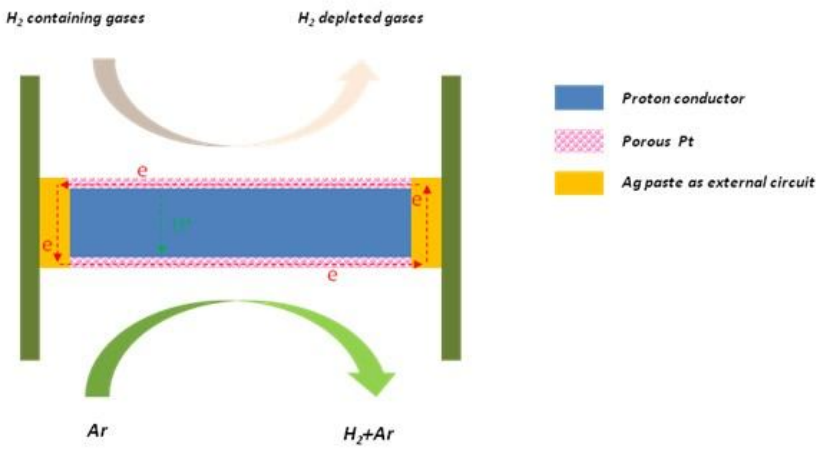

Fig.8-1 Schematic of the hydrogen permeation membrane utilizing external short circuit

The surface morphology of the disk membranes was obtained using scanning electron microscope (SEM, Zeiss Evo 40XVP) at acceleration voltage of 15 kV. The powder x-ray diffraction (XRD) analysis were performed in a powder x-ray diffractometer (Bruker D8 Advances) using a Cu-Kα radiation generated at 40 kV and 30 mA.

The hydrogen permeation properties of the disk membranes were measured using gas chromatography (GC) technique utilizing high temperature H_2 permeation apparatus. Ceramic paste was used as sealant to fix the disk membrane onto a quartz tube. The effective area for permeation is ~ 0.45 cm^2. Argon was used as sweep gas in the permeate side to create hydrogen partial pressure gradient across the membrane. Nitrogen diluted hydrogen (50 vol. % H_2 in N_2) was used as feed gas. The composition of the permeating gas was characterized using gas chromatography (Agilent 6890N Network GC system with a thermal conductivity detector (TCD) and Flame Ionization Detector (FID)). The hydrogen permeation flux could then be calculated according to:

$$J_{H_2} = \frac{F}{S}(y_{H_2} - y_{N_2}) \qquad (2)$$

Where F, S, y_{H2} and y_{N2} are the flow rate of the permeate, the effective membrane area, the hydrogen and nitrogen mole fraction in the permeate, respectively.

8.3 Results and discussion

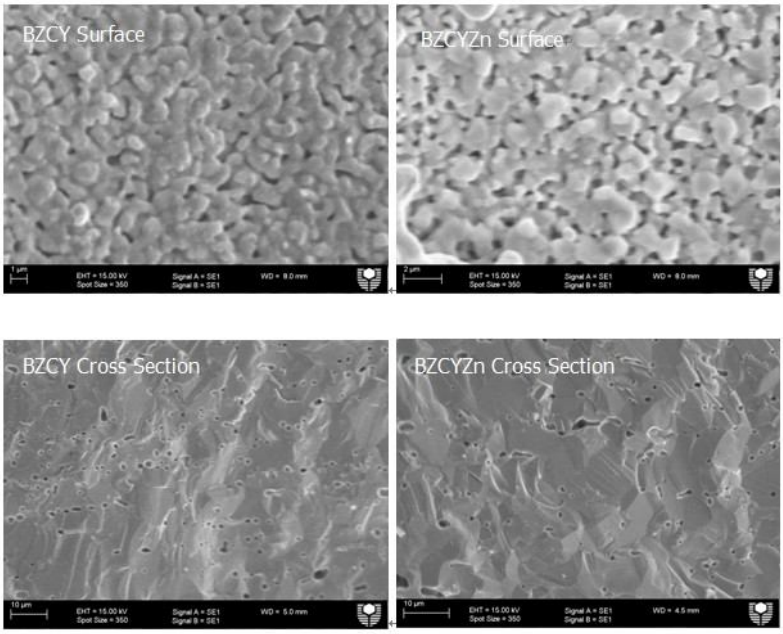

Fig. 8-2 SEM images of the surface and the cross-section of BZCY and BZCYZn membranes.

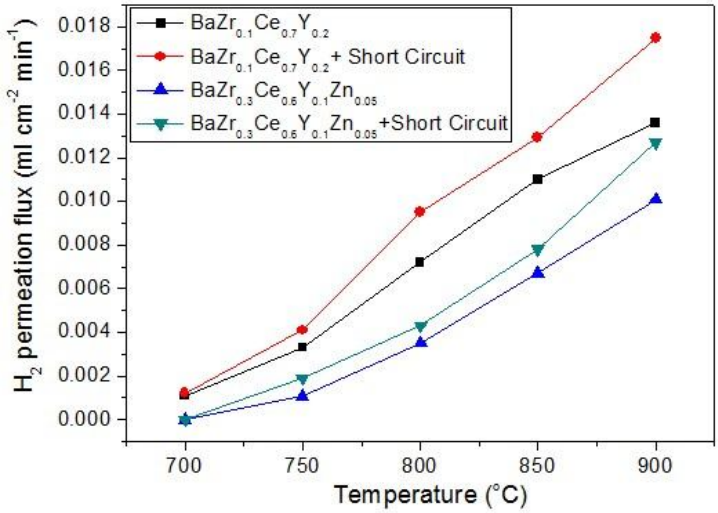

Fig.8-3 Temperature dependent hydrogen permeation fluxes through basic and external short circuit-assisted BZCY and BZCYZn membranes. Feed gas: 40 ml min^{-1} H_2 + 40 ml min^{-1} N_2; Sweep gas: 100 ml min^{-1} Ar.

The surface and cross-section morphology of $BaZr_{0.1}Ce_{0.2}Y_{0.7}O_{3-\delta}$ (BZCY) and $BaZr_{0.3}Ce_{0.6}Y_{0.1}Zn_{0.05}O_{3-\delta}$ (BZCYZn) disk membranes is depicted in **Fig.8-2,** all of which demonstrate the formation of dense structures containing small amount of closed pores. Noteworthy is that such a porous structure in the bulk is not favorable for ion diffusion. Hydrogen permeation performances of 1-mm thick disk membranes of BZCY and BZCYZn between 700-900 ^oC using 50 vol. % of H_2 in N_2 as feed gas and Ar as sweep gas is depicted in **Fig.8-3**. As a reference for comparison, the performance of the basic BZCY and BZCYN disk membranes without external short circuit e.g. silver coating in circumference and platinum coating on both opposing disk surfaces was also displayed. The temperature activated nature of the hydrogen permeation process is evident from the steady increase of all hydrogen permeation fluxes with temperature rise due to enhanced hydrogen reduction and/or oxidation on membrane surface as well as accelerated proton diffusion in bulk membrane. BZCY has high proton conductivity and is regarded as one of the best proton conductors among perovskite type-$BaCeO_3$ and $BaZrO_3$ based materials. Nonetheless, the

observed hydrogen flux through basic BZCY membrane was quite low e.g. only ~0.013 ml cm^{-2} min^{-1} at 900°C. We speculate that this low flux is ascribed to the low electronic conductivity of BZCY. During hydrogen permeation, electrons are continuously depleted or generated when the proton was converted to hydrogen (and vice versa). As a result, the low electronic conductivity may limit the hydrogen permeation flux if it is not sufficiently high. In BZCY case, the presence of transition metal Ce allows partial reduction of some Ce^{4+} to Ce^{3+} and therefore promotes electron transfer by increasing the electronic transporting carriers, i.e., electron hole.

Accordingly, the hydrogen permeation flux is also observed through BZCYZn membrane, although at a lower value of ~0.010 ml cm^{-2} min^{-1} at 900 °C. This lower hydrogen flux is mainly due to the relative weak proton conducting ability of BZCYZn oxide. However, the advantage of BZCYZn is not in terms of its permeation flux but rather about the stability as the presence of more Zr content has been associated with enhanced structure stability on the perovskite oxides [47-49]. It is worthwhile to trade-off some flux values with stability so that the materials can operate longer, which translates to high reliability and low maintenance cost.

Upon utilizing external short-circuit, the hydrogen fluxes through BZCY increased by ~38% to 0.018 ml cm^{-2} min^{-1} at 900 °C whereas that through BZCYZn increased by ~20% to 0.012 ml cm^{-2} min^{-1} at 900 °C. This, to some extent, might be taken as supporting evidence towards our thinking of electronic conductivity limiting transport. External short circuit, in this respect, contributed to the enhancement of the electronic conductivity which in turn, improved the hydrogen transport rate.

Fig.8-4 shows the hydrogen permeation flux through external short circuit-assisted BZCY and BZCYZn disk membrane at 950 °C as a function of argon sweep flow rate between 50-200 ml min^{-1}. Hydrogen fluxes were very slightly increased with increasing sweep flow rate considering the higher partial pressure driving force across

the membrane due to lower hydrogen partial pressure at the permeate side (at higher sweep flow rate). The very slight nature of increase implies less dependence of hydrogen transport towards sweep gas flow rate. For example at 950 ^{o}C, when the sweep flow rate was raised by 400% from 50 ml min^{-1} to 200 ml min^{-1}, the flux through BZCY was only improved by 25% (from 0.0112 ml cm^{-2} min^{-1} to 0.0141 ml cm^{-2} min^{-1}) while the flux through BZCYN was only improved by 26% (from 0.0072 ml cm^{-2} min^{-1} to 0.0091 ml cm^{-2} min^{-1}).

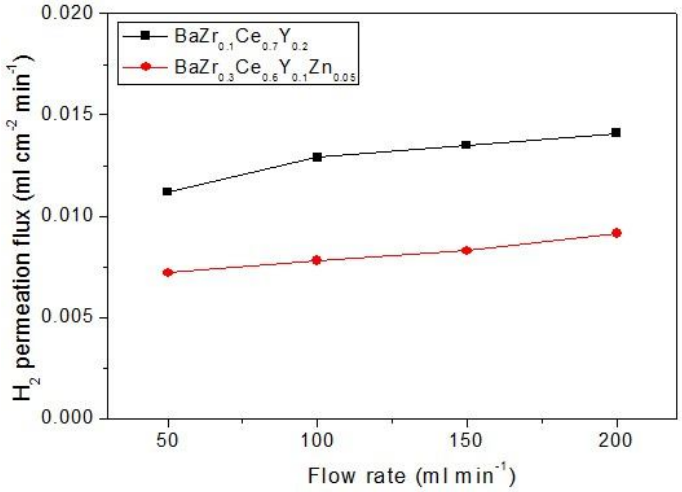

Fig. 8-4 Hydrogen permeation fluxes through external short circuit-assisted BZCY and BZCYZn membranes at 950 ^{o}C and different sweep gas flow rate.

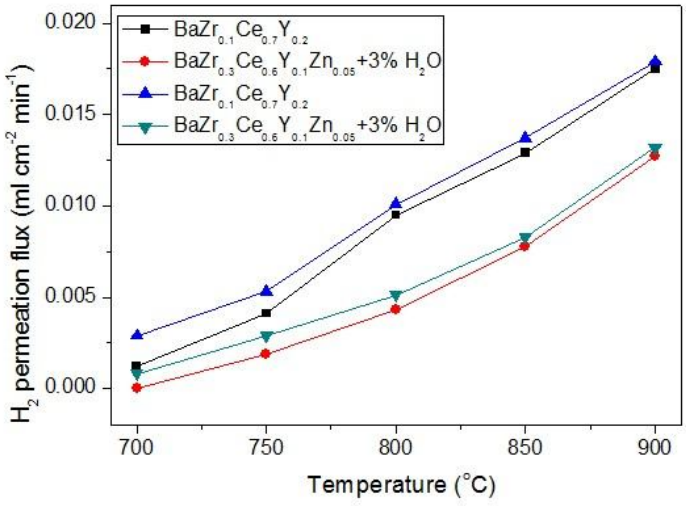

Fig.8-5 Temperature dependent hydrogen permeation fluxes through external short circuit-assisted BZCY and BZCYZn membrane on both membrane sides with and without water vapor (3 vol. % H_2O).

The effect of water vapor on the hydrogen permeation transport between 700-900°C was probed by the addition of 3% of water vapor into both sweep gas and feed gas; the results of which is depicted in **Fig.8-5**. The hydrogen fluxes of external short circuit-assisted BZCY and BZCYZn disk membranes are slightly increased with addition of water vapor. This implies reduced hydrogen transport resistance within the membrane system. The presence of water vapor is likely to reduce the activation energy for proton transformation to hydrogen atom (and vice versa) by activating the oxide surface [21]. In addition, water may also increase proton conductivity through membrane and enhance interfacial reaction kinetics [50]. To further test the possible mechanism of water effect on the hydrogen permeation through the ceramic membranes, 3 vol. % H_2O was added into both sides of the membrane reactor while hydrogen flow was stopped e.g. resulting in that there was no hydrogen flux that can be detected in both sides of the membrane reactor. This highlights the fact that water vapor by itself without proper catalyst could not dissociate into hydrogen ions and associated into hydrogen gas. The possible reaction mechanism in the presence of water vapor is proposed as follows:

1) at the feed side of the membrane

$$H_2(g) + H_2O(g) \rightarrow H_3O^+ + H^+ + 2e^- \quad (3)$$

2) at the permeate side of the membrane

$$2H^+ + 2H_2O(g) + 2e \rightarrow 2H_3O^+ + 2e \rightarrow H_2(g) + 2H_2O(g) \quad (4)$$

Water vapor role is therefore to facilitate hydrogen adsorption or association process.

For practical applications, stability is critical. Most perovskite type proton conducting membranes are very sensitive and reactive in the presence of acidic gases such as CO_2 due to their intrinsic alkaline composition. The stability of the permeation fluxes of the external short circuit-assisted BZCY and BZCYZn disk membranes in the presence of CO_2 is tested by adding 10 vol. % of CO_2 in Ar as sweep gas after 4 h of

normal testing; the results of which is displayed in **Fig.8-6**. The permeation flux profile was quite stable in the initial 4 h when Ar was used as sweep gas. Sudden rapid decline of hydrogen flux occurred on both membranes when 10 vol. % CO_2 was introduced. Later on, when the sweep gas was switched to Ar again, the hydrogen flux of BZCY slightly increased, but far less than its original value. BZCYZn disk membrane, in contrast, recovered almost all of its original flux value before CO_2 introduction; denoting its superior stability to resist CO_2. On the some cases of the oxygen permeation membranes with the existence of CO_2 gas, the similar phenomena were observed as well. It has been proven that the physical adsorption of CO_2 effect on the oxygen vacancies of the membrane surface, rather than chemical reaction with membrane surface to form carbonate, could lead to the decrease in oxygen flux [51,52]. Therefore, here the decline of hydrogen flux through BZCYZn may be also due to the absorption effect of CO_2 on the membrane surface, which occupies the active sites around the oxygen vacancies, i.e., inhibiting hydrogen association and desorption. As further evidence, **Fig.8-7** shows the powder XRD patterns of BZCY and BZCYZn disk membranes before and after stability test. In case of BZCY, it is evident that after the test, the original characteristic peaks from the fresh sample were no longer preserved with the main one (e.g. the one at 28 ^{o}) shifted to lower angle accompanied by the presence of extra peaks distinct to those before the test. These observations suggest the deterioration and/or substantial modification of the original crystal structure as well as the formation of cabonate (barium caborante) due to reaction with CO_2. In case of BZCYZn, the characteristic peaks from before the test was retained after the test.

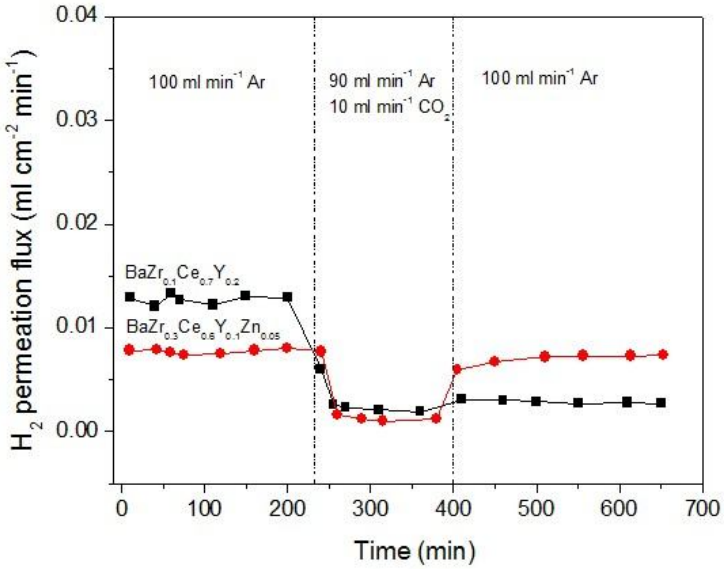

Fig.8-6 Long term hydrogen permeation fluxes through $BaZr_{0.1}Ce_{0.2}Y_{0.7}O_{3-\delta}$ (BZCY) and $BaZr_{0.3}Ce_{0.6}Y_{0.1}Zn_{0.05}O_{3-\delta}$ membrane (with external short circuit) using different sweep gas at 850 °C.

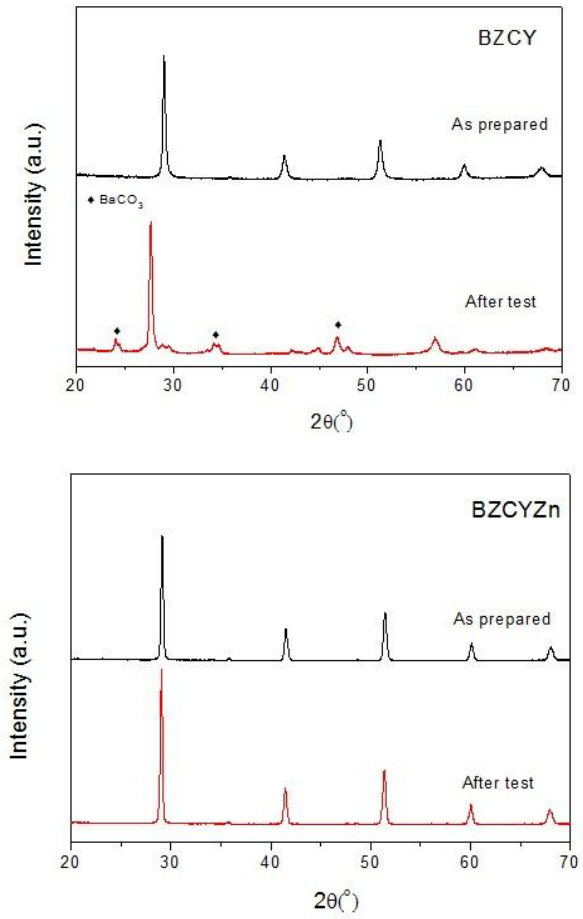

Fig.8-7 Powder XRD patterns of $BaZr_{0.1}Ce_{0.2}Y_{0.7}O_{3-\delta}$ (BZCY) and $BaZr_{0.3}Ce_{0.6}Y_{0.1}Zn_{0.05}O_{3-\delta}$ membrane before/after the stability test under 20 ml min^{-1} pure CO_2 for 10 h at 850°C.

8.4 Conclusions

$BaZr_{0.1}Ce_{0.2}Y_{0.7}O_{3-\delta}$ (BZCY) and $BaZr_{0.3}Ce_{0.6}Y_{0.1}Zn_{0.05}O_{3-\delta}$ (BZCYZn) disk membranes have been prepared using EDTA-citrate route and sintering at 1500 ^{o}C. Utilizing external short circuit concept, the performances of these membranes for H_2 permeation were studied. H_2 permeation fluxes through BZCY and BZCYZn membranes assisted with external short circuit were higher than those through basic BZCY and BZCYZn ones. Addition of water vapor into the sweep gas led to slight increase of H_2 permeation fluxes for both membranes, most likely due to water vapor role to facilitate hydrogen adsorption and/or association process. In the presence of CO_2, BZCYZn demonstrated superior structure and permeation fluxes stability e.g. retaining the original structure from before the test and recovering the original fluxes from the normal test before introduction of CO_2. Further studies into BZCYZn are thus warranted with the aim to optimize its H_2 fluxes using thin film technology.

8.5 References

1. E.D Washsman and K.T Lee, *Science*, 2011, **334**, 935-939.

2. B.C.H. Steele and A. Heinzel, *Nature*, 2001, **414**, 345-352.

3. Z.L. Zhan and S.A. Barnett, *Science*, 2005, **308**, 844-847.

4. Z. Shao and S.M. Haile, *Nature*, 2004, **43**, 170-173.

5. M.K. Debe, *Nature*, 2012, **486**, 43-51.

6. M.Z.Jacobson and W.G. Colella, *Science*, 2005, **308**, 1901-1905.

7. D.L. Trimm and Z.I. Önsan, *Catal. Rev.*, 2001, **43**, 31-84.

8. J.M. Ogden, M.M. Steinbugler and T.G. Kreutz, *J. Power Sources*, 1999, **79**, 143-148.

9. D.K. Ross, *Vacuum*, 2006, **80**, 1084-1089.

10. J.A. Turner, *Science*, 2004, **305**, 972-974.

11. L. Barelli, G. Bidini, F. Gallorini and S. Servili, *Energy*, 2008, **33**, 554-570.

12. Y. Wei, W. Yang, J. Caro and H. Wang. *Chem. Eng. J.*, 2013, **220**, 185-203.

13. S. Liu, X. Tan, K. Li and R. Hughes, *Catal. Rev.*, 2001, **43**, 147-198.

14. E. Kikuchi, *Catal. Today*, 2000, **56**, 97-101.

15. J. Tong, H. Suda, K. Haraya and Y. Matsumura, *J. Membr. Sci.*, 2005, **260**, 10-18.

16. S. Yun, S.T. Oyama, *J. Membr. Sci.*, 2011, **375**, 28-45.

17. H. Iwahara, Y. Asakura, K. Katahira and M. Tanaka, *Solid State Ionics*, 2004, **168**, 299-310.

18. H. Iwahara, *Solid State Ionics*, 1995, **77**, 289-298.

19. H. Iwahara, T. Yajima, T. Hibino and H. Ushida, *J Electrochem Soc* 1993, **140**, 1687-1691.

20. C. Zuo, S. Zha, M. Liu, M. Hatano and M. Uchiyama, *Adv. Mater.*, 2006, **18**, 3318-3320.

21. K.D. Kreuer, *Annu. Rev. Mater. Res.*, 2003, **33**, 333-359.

22. Y. Lin, R. Ran, Y. Guo, W. Zhou, R. Cai, J. Wang and Z. Shao, *Int. J. hydrogen energy*, 2010, 35, 2637-2642.

23. Y. Lin, W. Zhou, J. Sunarso, R. Ran and Z. Shao, *Int. J. hydrogen energy*, 2012, **37**, 484-497.

24. F. Zhao, S. Wang, L. Dixon and F. Chen, *J. Power Sources*, 2011, **196**, 7500-7504.

25. F. Zhao, Q. Liu, S. Wang, K. Brinkman and F. Chen, *Int. J. hydrogen energy*, 2010, **35**, 4258-4263.

26. G. Meng, G. Ma, Q. Ma, R. Peng and X. Liu, *Solid State Ionics*, 2007, **178**, 697-703.

27. K. Xie, R. Yan, Y. Jiang, X. Liu and G. Meng, *J. Membr. Sci.*, 2008, **325**, 6-10.

28. Z. Sun, E. Fabbri, L. Bi and E. Traversa, *J. Am. Ceram. Soc.*, 2012, **95**, 627-635.

29. Y. Liu, Y. Guo, R. Ran and Z. Shao, *J. Membr. Sci.*, 2012, **415**,391-398.

30. X. Tan, J. Song, X. Meng and B. Meng, *J. Eur. Ceram. Soc.*, 2012, **32**, 2351-2357.

31. A. Thursfield, A. Murugan, R. Franca and I.S. Metcalfe, *Energy. Environ. Sci.*, 2012, **5**, 7421-7459.

32. Y. Liu, X. Tan and K. Li, *AIChE J.*, 2006, **52**, 1577-1585.

33. L. Malavasi, C.A.J. Fisher and M.S. Islam, *Chem. Soc. Rev.*, 2010, **39**, 4370-4387.

34. G.C. Mather, D. Poulidi, A. Thursfield, M.J. Pascual, J.R. Jurado and I.S. Metcalfe, *Solid State Ionics*, 2010, **181**, 230-235.

35. T. Norby and Y. Larring, *Solid State Ionics*, 2000, **136**,139-148.

36. L. Zhao, B. He, Y. Ling, Z. Xun, R. Peng, G. Meng and X. Liu, *Int. J. Hydrogen Energy*, 2010, **35**, 3769-3774.

37. L. Zhao, B. He, B. Lin, H. Ding, S. Wang, Y. Ling, R. Peng, G. Meng and X. Liu, *J. Power Sources*, 2009, **194**, 835-837.

38. L. Bi, S. Zhang, S. Fang, L. Zhang, H. Gao, G. Meng and W. Liu, *J. Am. Ceram. Soc.*, 2008, **91**, 3806-3809.

39. L. Yang, S. Wang, K. Blinn, M. Liu, Z. Liu, Z. Cheng and M. Liu, *Science*, 2009, **326**,126-129.

40. M. Cai, S. Liu, K. Efimov, J. Caro, A. Feldhoff, H. Wang, *J. Membr. Sci.*, 2009, **343**, 90-96.

41. X. Meng, J. Song, N. Yang, B. Meng, X. Tao, Z. Ma and K. Li, *J. Membr. Sci.*, 2012, **401**,300-305.

42. C. Zuo, S.E. Dorris, U. Balachandran and M. Liu, *Chem. Mater.*, 2006, **18**, 4647-50.

43. C. Zuo, T.H. Lee, S.E. Dorris, U. Balachandran and M. Liu, *J. Power Source*, 2006, **159**, 1291-1295.

44. X. Qi, Y.S. Lin, *Solid State Ionics*, 1999, **120**, 85-93.

45. K. Zhang, Z. Shao, C. Li and S. Liu, *Energy Environ. Sci.*, 2012, **5**, 5257-5264.

46. K. Zhang, Y. Zou, C. Su, Z. Shao, L. Liu, S. Wang and S. Liu, *J. Membr. Sci.*, 2013,**427**,168-175.

47. S. Li, W. Jin, P. Huang, N. Xu, J. Shi, M.Z.C. Hu, A. Payzant and Y.H. Ma. *.AIChE J.*, 2009, **45**, 276-284.

48. H. Jiang, F. Liang, O. Czuprat, K. Efimov, A. Feldhoff, S. Schirrmeister, T. Schiestel, H. Wang and J. Caro, *Chem. Eur.*, *J*., 2010, **16**, 7898-7903.

49. E. Fabbri, A. D'Epifanio, E.D. Bartolomeo, S. Licoccia and E. Traversa, *Solid State Ionics* 2008, **179**, 558-564.

50. S.J. Song, E.D. Wachsman, J. Rhodes, S.E. Dorris and U. Balachandran, *Solid State Ionics*, 2004, **167**, 99-105.

51. X. Tan, N. Liu, B. Meng, J. Sunarso, K. Zhang and S. Liu, *J. Membr. Sci.*, 2012, **389**,216-222.

52. J. Wang, Y. Wei, L. Zhou, Z. Li and H. Wang, *AIChE J*. 2012, **58**, 2473-2478.

Chapter 9: High performance BSCF membranes shelled by SDC film

9.1 Introduction

In the 21st century, the energy consumption is increasing yearlyto satisfy the growth of world economy. Our contemporary society is facing a serious dilemma between energy requirement and environmental conservation. The current energy delivery infrastructure is based on the fossil fuel combustion power system. However, these natural fossil fuel resources like coal, oil or gas are not infinite and gradually running out. Moreover, the over-consumption of these fossil fuels is polluting our planet by releasing the huge amounts of greenhouse gases to the atmosphere, which is causing severe climate change and may result to catastrophic disaster to human being. As an alternative to these fossil fuels energy, much faith has been placed onto renewable sources of energy to absolutely solve the energy and environmental issues. However, the fact may be contrary to good public perception as renewable energy is not the silver bullet to immediately solve all our problems. Instead of the great conversion to wind power or solar power, the world has to be forced into great use of fossil fuels with higher CO_2 emission to meet the scale of the growth in demand, especially from developing countries. It is forecasted that even with major technological breakthrough, renewable energy could only make up for 30% energy supply by the middle of this century.[1-2] Therefore, it is urgent to improve energy efficiency and lower the waste streams, especially for energy-intensive chemical industry. As it seems, there is no easy way to this problem which must be challenged with a clever combination of several means. Membrane reactors combining the reaction and separation in one unit hold many advantages for chemical reaction process [3-10]. The production process can

be intensified by the in-situ separation effect from the membrane reactor, which can cause higher conversion of reactants and higher selectivity of products. With the help of this membrane technology, the energy efficiency can be dramatically improved with low emission due to the increased selectivity for desired products.

Among the various membrane reactors, dense mixed conducting oxygen permeation ceramic membrane reactors [11-15], which can be used in coal gasification or oxy-fuel combustion power station system with CO_2 sequestration, have received much more interest due to their great potential in clean energy delivery. By integrating these ceramic membranes which exhibit both ionic and electronic conducting ability to obtain pure oxygen from air into coal power station can reduce energy cost by 35% or more as conventional oxygen processes [16-18]. In these membrane reactor processes, ceramic membranes usually have to be exposed into certain extremely hostile operating conditions, such as erosive environments and high temperatures and pressures. Therefore, the development of highly efficient and stable oxygen permeation membrane materials is the main task for the practical application. Pioneering work on $La_{1-x}Sr_xCoO_{3-\delta}$ by Teraoka et al [19] provided the first example that high oxygen permeation fluxes could be achieved from these mixed conducting perovskite membranes. In the following several decades, many membrane materials with different oxygen transport properties have been reported due to major research efforts by the scientific community. In these previous works, an exciting $Ba_{0.5}Sr_{0.5}Co_{0.8}Fe_{0.2}O_{3-\delta}$ (BSCF) membrane has been developed [20,21], which shows surprising high oxygen transport ability reflected by its high oxygen permeation flux at intermediate-high temperatures. This material is extensively applied as the oxygen separation membranes and membrane reactors for CH_4 conversion to value-added products [22-25]. However, it is hard for pervoskite containing alkaline-earth elements

to survive from the attack of CO_2 or SO_2 erosive gas due to the carbonate formation on its basic surface of perovskite oxide.

In this work, we propose a novel method to design a $Sm_{0.2}Ce_{0.8}O_{1.9}$ (SDC) function layer on BSCF membrane. The SDC function shell can be made on the BSCF membrane surface using the precursor solution followed by the thermal treatment, which can greatly strengthen BSCF membrane stability against CO_2 acid gas, while with improved oxygen permeation flux.

9.2 Experimental section

$Ba_{0.5}Sr_{0.5}Co_{0.8}Fe_{0.2}O_{3-\delta}$ (BSCF) composites oxides were synthesized by a combined EDTA-citrate complexing sol-gel process. $Ba(NO_3)_2.xH_2O$, $Sr(NO_3)_2.xH_2O$, $Co(NO_3)_3.xH_2O$ and $Fe(NO_3)_3.xH_2O$(all in A.R. grade) were applied as the raw materials for the metal-ion sources. For the precise controlling of the doping level, the metal nitrates were first made into aqueous solutions (~1M) separately with their precise concentrations determined by standard EDTA titration technique. Necessary amounts of metal nitrates in the state of aqueous solution were then prepared into a mixed solution according to the aimed composition, followed by the introduction of EDTA and citric acid as the complexing agents at the mole ratio of total metal ions: EDTA: citric acid=1:1:2. The pH value of the system was controlled at ~ 6 with the help of $NH_3.H_2O$. Continuous heating at 90 ^oC resulted in evaporating water from the solution until a transparent purple gel was obtained, which was pre-fired at 250 ^oC and followed by calcined at various temperatures in air for 5 h to get the products with the final composition and phase structure.

For the fabrication of dense membranes, the as-synthesized BSCF oxide powders were pressed into disk-shape membranes in a stainless steel mold (15.0 mm in diameter) under a hydraulic pressure of approximately 1.5×10^8 Pa. These green

membranes were further sintered in an electrical box furnace at 1100 ^{o}C in air for 5 h at a heating /cooling rate of 1-2 ^{o}C min^{-1}. $Sm_{0.2}Ce_{0.8}O_{1.9}$ (SDC) was introduced onto the surface of BSCF membrane with a dip-coating process using nitrate solutions, which were prepared from individual nitrates. The concentration was 0.3 M of the total metal ions. The coating was carried out by dipping the BSCF membrane into the solution, drawing slowing up and sintering at 800^{o}C for 2 h.

Scanning Electron Microscopy (SEM) images were obtained using a Zesis EVO 40XVP at an accelerating voltage of 15kV. The XRD analysis was carried out on a Bruker D8 Advances X-ray diffractometer using Cu Ka radiation generated at 40 kv and 30 mA. The ECR test was conducted by measuring the conductivity in a process of an abrupt step change in oxygen partial pressure around the samples, which can be created by introducing mixtures of N_2 and O_2 of known oxygen content. To obtain good quality samples for the microstructual analysis, the prepared membranes were embedded by platinum and then cut into slices with a thickness of ~100 nm in a focused ion beam (FIB) workstation with a voltage of 15kV. The as-prepared slices were observed by using a high resolution transmission electron microscopy (HRTEM) operated at an accelerating voltage of 300 kV.

Permeation properties of the membranes were investigated by the gas chromatography (GC) method using a high-temperature oxygen permeation apparatus. A silver paste or non-conductive ceramic paste was used as the sealant to fix the membrane disk onto a dense quartz tube and exposed an effective area of ~ 0.45 cm^2 at the sweep side for permeation study. Helium was applied as the sweep gas to create an oxygen partial pressure gradient across the membrane, which also acted as the carrier gas to bring the permeated oxygen to a Shimadzu 2014A equipped with a 5Å capillary molecule column and thermal conductivity detector for quantitative oxygen concentration analysis.

The oxygen permeation flux was calculated by:

$$Jo_2\ (ml\ cm^{-2}\ \min^{-1}) = [C_{O_2} - C_{N_2} \times \frac{0.21}{0.79} \times \left(\frac{28}{32}\right)^{\frac{1}{2}}] \times \frac{F}{S}$$

Where C_O and C_N are the measured concentrations of oxygen and nitrogen in the gas on the sweep side, respectively (mol ml^{-1}), F is the flow rate of the exit gas on the sweep side (ml s^{-1}), and S is the membrane geometric surface area of the sweep side (cm^2).

9.3 Results and discussion

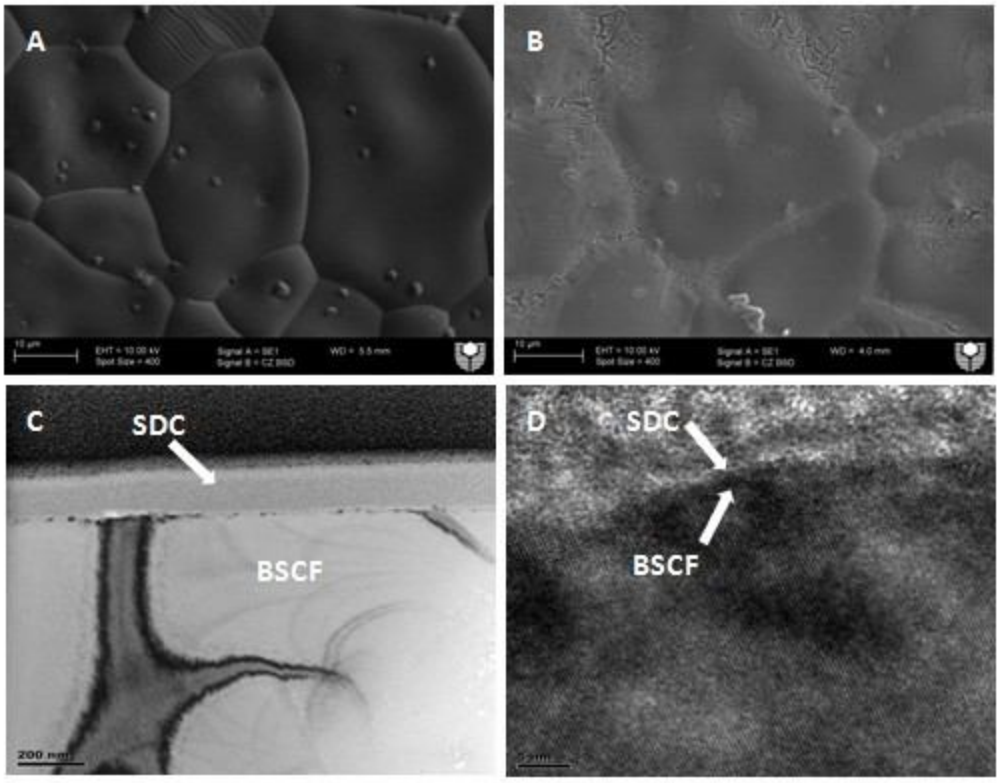

Fig.9-1 SEM and TEM images for BSCF membrane with SDC protective layer, A: SEM image of pure BSCF membrane surface; B: SEM image of BSCF membrane surface with SDC layer; C and D: TEM images of BSCF membrane cross section with SDC layer.

It can be seen from Fig.9-1 that the dense pure BSCF membrane was fabricated by sintering at 1100°C for 5h. The grain sizes vary from 5 um to 10um. Meanwhile, the morphology of BSCF membrane surface loaded with SDC thin layer was obtained by

dip coating SDC precursor nitrate followed by thermal treatment at 800°C for 2 h. As shown in SEM picture, an obvious SDC shell covering on the surface of BSCF membrane can be observed. Viewed from the surface, the grain boundary of BSCF membrane can still be clearly identified, which implies that the SDC shell has very thin thickness. According to TEM image, the thickness of the SDC shell can be controlled at 100 nm. Noteworthy is that SDC shell tended to crack after the thermal treatment evidenced by the grain boundary area in the SEM image. It is difficult to form an uniform SDC layer covering the entire BSCF membrane surface without of defects or pinholes due to the mismatch of thermal expansion between the two differenct material phases of SDC and BSCF. However, it is interesting to find that the every single BSCF grain on the sintered membrane surface was fully covered by the SDC shell leaving cracks along the grain boundary on the BSCF membrane surface.

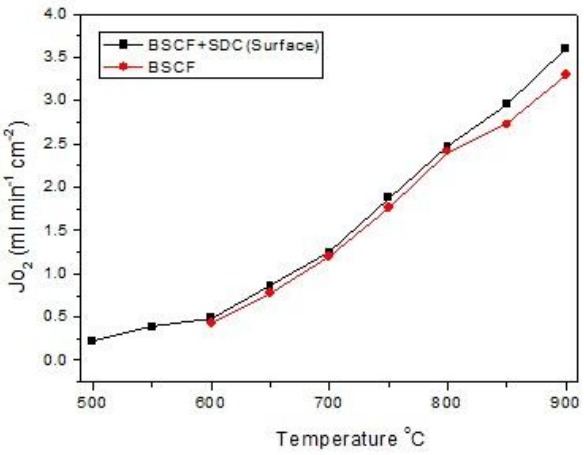

Fig.9-2 Oxygen flux through BSCF membrane with/without SDC layer

Fig.9-2 demonstrates the oxygen permeation fluxes through 1 mm thick BSCF membrane with SDC function shell. Oxygen partial pressure on the oxygen rich sidewas maintained at 0.21 atm by applying air as the feed gas, while a constant helium sweep rate of 100 ml min^{-1} was applied to the other side of the membrane

surface to create a medium oxygen pressure gradient across the membrane. After applying the SDC thin layer on the membrane surface, the oxygen flux through BSCF membrane experienced an obvious increase from ~3.2 ml cm^{-2} min^{-1} to 3.7 ml cm^{-2} min^{-1} at 900^{o}C. Over the whole test temperature range between 600 and 900 ^{o}C, there is a steady increase of oxygen flux through BSCF membrane with SDC shell as compared to pure BSCF membrane. This improvement shows that bringing the SDC thin layer on the BSCF membrane surface may have has a positive effect on its oxygen permeation cability. As well known, SDC is a typical oxygen ion conducting oxide widely used as the electrolyte for solid oxide fuel cell due to its excellent pure oxygen ion transport ability at intermediate-low temperatures. For oxygen permeation materials, it is necessary to have a matched sufficiently high electronic conducting ability for oxygen reduction on the membrane surface. Therefore, it seems an impossible mission for pure oxygen ion conductors to play as oxygen permeation membranes without the extra phase for electron transport. However, certain electronic conductivity can be observed on SDC with the operation temperatures above 600 ^{o}C due to the thermal reduction from Ce^{4+} to Ce^{3+}. [26] This thermal-sensitive electronic conductivity provides SDC the possibility that it can be used as surface modification material for the mixed conducting BSCF oxygen permeation membrane at high temperatures (>600^{o}C). On the other hand, the SDC film applied on the BSCF membrane is very thin less than one hundred nano-meter. It was found that the electronic conductivity could be enhanced with reducing the grain size of SDC oxide down to a few nanometers[27]. As a result, it is reasonable to believe that this thin SDC shell can offer sufficient electrons for the oxygen reduction on the BSCF membrane at high temperatures. Meanwhile, it was reported that SDC shows the fast oxygen transport ability at relative lower temperatures, which is the reason for the electrolyte membrane with high ionic conductivity to be operated at the temperatures down to

500 ^{o}C. Therefore, the introduction of SDC thin shell would not impede the oxygen permeation process through BSCF dense membrane.

It is well known that oxygen permeation ability of a dense ceramic membrane is closely related to its oxygen bulk transport rate and surface exchange kinetics. In our case, the improvement of oxygen flux through BSCF membrane with SDC thin layer may be resulted from enhanced oxygen exchange rate on the membrane surface. To further investigate the oxygen surface reaction occurring on the shell, electrical conductivity relaxation (ECR) technique was applied to identify the surface exchange coefficients of BSCF membrane with SDC shell. **Fig.9-3** exhibits the typical transient conductivity response between 600 ^{o}C and 800 ^{o}C upon abruptly changing the oxygen partial pressure from 0.5 to 0.25 atm and the temperature dependence of the fitted k_{ex} of BSCF membrane with SDC shell. As can be clearly seen in **Fig.9-3**, the BSCF membrane with SDC shell has much faster oxygen exchange reaction process as compared to pure BSCF membrane. From the temperature dependence of surface exchange coefficients, a steady rise of k_{ex} of BSCF membrane with SDC shell was observed within the investigated temperature range. For example, at 750^{o}C, the value of k_{ex} increased from 0.007cm s^{-1} to 0.015 cm s^{-1}. This result explains that the fast oxygen surface exchange process account for the improved oxygen flux through the BSCF membrane surface with SDC shell.

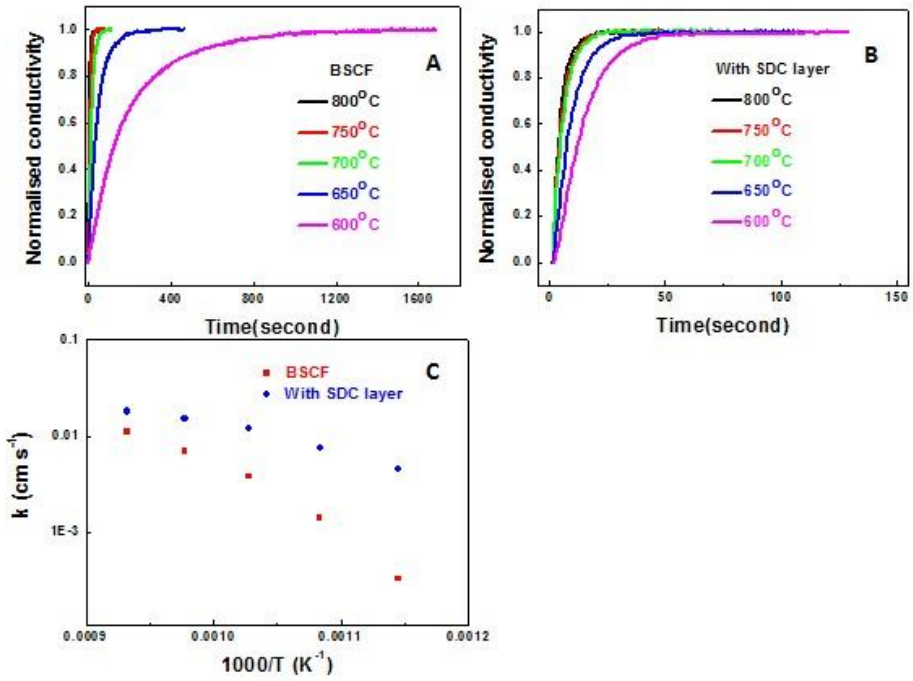

Fig.9-3 ECR response curves of BSCF membrane with/without SDC layer at various temperatures after sudden change of oxygen partial pressure from 0.05 to 0.2 atm (A&B), and the temperature dependence of the fitted k_{ex} (C).

Because of the nature of the contained alkaline earth elements, perovskite type mixed conducting membranes are very sensitive to react with acidic gases such as CO_2. Many perovskite membranes possessing high oxygen permeation flux, such as $Ba_{0.5}Sr_{0.5}Co_{0.8}Fe_{0.2}O_{3-\delta}$ (BSCF) and Ba(Co, Fe, Nb)$O_{3-\delta}$, tends to suffer from decomposition of the structure and hence partial or even completely loss of the oxygen permeation ability in the CO_2 containing atmosphere. To test the permeation stability of the SDC shell protecting BSCF membrane in the presence of CO_2, the oxygen permeation experiment was conducted using the gas mixture with CO_2 and He as the sweep gas. As seen in **Fig.9-4**, during the examination time around 5 h, both BSCF membrane with SDC shell and pure BSCF membrane have relative stable oxygen flux under 100% pure He as the sweep gas. After switching the sweep gas from the pure He to the 10% CO_2 containing mixture gas, the flux through pure BSCF membrane had a sharp decrease, leveling off at only 1.2 ml cm^{-2} min^{-1}. After changing

back to pure He sweep gas, the flux could not be recovered to its original value, which is consistent with the observation reported in previous works [28]. Interestingly, it can be observed that after experiencing a slight oxygen flux decline, the BSCF membrane with SDC shell could be fully restored to its origin oxygen permeation value with the sweep gas switching back to pure He. Such temporary oxygen flux decrease on perovskite membranes exposed to CO2 containing gas has been observed by other researchers as well [29,30]. It was believed that it may be caused by the adsorptive effect of CO_2 on the membrane surface, but not by the poison effect from the reaction between CO_2 and membrane material to form carbonate. Therefore, this CO_2 stability test result shows that the BSCF membrane with SDC shell has a strong tolerance against acidic CO_2 gas. As well known, SDC is a very robust material to resist most of acidic gases even including concentrated nitric acid. Therefore, the introduction of SDC shell on the BSCF membrane is favorable for its stability against acidic CO_2. However, this SDC shell is not continuously or totally covering the surface of BSCF membrane. As can be seen from SEM image (**Fig.1**), there are some cracks or pinholes along the BSCF grain boundary area, leaving part of the BSCF membrane area susceptible to CO_2 erosion. However, our experimental results implied that despite of these cracks, the SDC shell could still protect the BSCF membrane well from erosive CO_2. As aforementioned, SDC shell can greatly enhance the oxygen surface exchange rate on the BSCF membrane. Thus, the oxygen surface reaction on the cracking area without SDC protection was very slower than that area covered by SDC.Due to the different oxygen releasing rates from different membrane area, the molecular oxygen may diffuse from these locations (SDC) with faster oxygen permeating rate to these cracking areas (BSCF) with less oxygen permeated; thus a stagnant layer of oxygen gas was formed on top of the BSCF surface. This stagnant oxygen film can prevent the exposed BSCF membrane from acidic CO_2 erosion.

Another possible mechanism is the formation of continuous and dense carbonate film fully covering these cracking locations from CO_2 attack. Why the cracked SDC film can still protect the BSCF membrane is an interesting topic definitely deserving further investigation in the future.

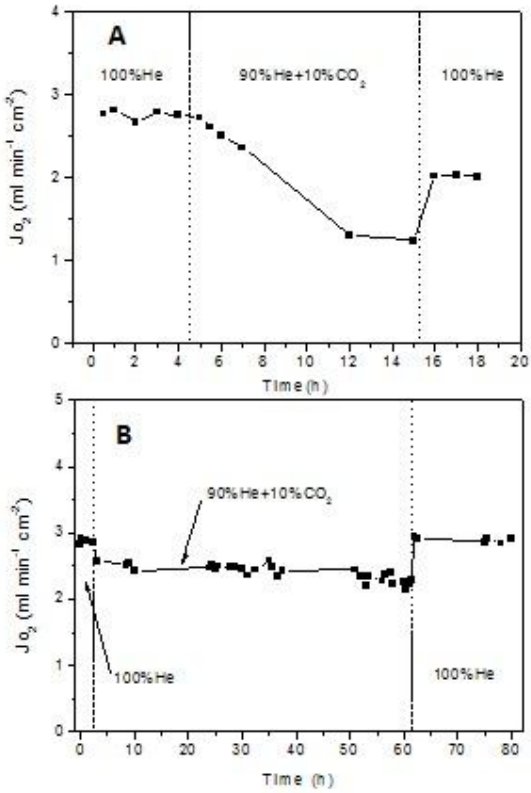

Fig.9-4 Long term oxygen permeation test under CO_2 at 850°C, A: pure BSCF membrane; B: BSCF membrane with SDC layer.

9.4 Conclusions

The fluorite $Sm_{0.2}Ce_{0.8}O_2$ (SDC) protective layer was successfully developed on the perovskite $Ba_{0.5}Sr_{0.5}Co_{0.8}Fe_{0.2}O_{3-\delta}$ membrane by using precursor solution with thermal treatment. The SEM and TEM results show that SDC layer can cover most of BSCF membrane surface but leaving some cracks along the grain boundary of the BSCF membrane. The oxygen flux through the BSCF membrane was improved due to the faster oxygen surface exchange rate from the SDC layer. More interesting, the SDC protective layer afforded the BSCF membrane with improved chemical stability to

resist the CO_2 erosion at high temperatures evidenced by its stable oxygen permeation operation under CO_2 atmosphere over 70 hours.

9.5 Reference

1. M. Asif and T. Muneer, *Renew. Sustain. Energy Rev.*, 2007, **11**, 1388-1413.
2. M.G. Salameh, *Appl. Energy*, 2003, **75**, 33-42.
3. A. Thursfield and I.S. Metcalfe, *J. Mater. Chem.*, 2004, **14**, 2475-2485.
4. K. Xie,Y. Zhang, G. Meng and J.T.S. Irvine, *Energy Environ. Sci.*, 2011, **4**, 2218-2222.
5. X. Dong, G. Zhang, Z. Liu, Z. Zhong, W. Jin and N. Xu, *J. Membr. Sci.*, 2009, **340**, 141-147.
6. H. Jiang, H. Wang, F. Liang, S. Werth, T. Schiestel and J. Caro, *Angew. Chem. Int. Ed.*, 2009, **48**, 2983-2983.
7. H. Jinag, Z. Cao, S. Schirmeister, T. Schiestel and J. Caro, *Angew. Chem. Int. Ed.*, 2010, **49**, 5656-5660.
8. H. Jiang, H. Wang, S. Werth, T. Schiestel and J. Caro, *Angew. Chem. Int. Ed.*, 2008, 47, 9341-9344.
9. S. Sun, M.R. Dassonneville, X. Zhu, W. Chu and W. Yang, *Catal. Today*, 2010, **149**, 167-171.
10. Q. Li, X. Zhu, Y. He and W. Yang, *Catal. Today*, 2010, **149**, 185-190.
11. J. Sunarso, S. Baumann, J.M. Serra, W.A. Meulenberg, S. Liu, Y.S. Lin and J.C. Diniz da Costa, *J. Membr. Sci.*, **2008**, 320, 13-41.
12. W. Yang, H. Wang, X. Zhu and L. Lin, *Topics Catal.*, 2005, **35**, 155-167.
13. Y. Liu, X. Tan and K. Li, *Catal. Rev.*, 2006, **48**, 145-19.
14. X. Dong and W. Jin, *Curr. Opin. Chem. Eng.*, 2012, **1**, 163-170.
15. X. Dong, W. Jin and N. Xu, *Chem. Mater.*, 2010, **22**, 3610-3618.
16. G. J. Stiegel, A. Bose and P. Armstrong, *Development of ion transport membrane (ITM) oxygen technology for integration in IGCC and other advanced power generation systems*, US Dept. of Energy, 2006.
17. E. Kakaras, A. Doukelis, D. Glannakopoulos and A. Koumanakos, *6th European Meeting on Coal Research and Its Applications, Canterbury, England*, 2006.

18. S. Smart, C. X. C. Lin, L. Ding, K. Thambimuthu and J. C. Diniz da Costa, *Energy Environ. Sci.*, 2010, **3**, 268-278.

19. Y. Teraoka, H. Zhang and N. Yamazoe, *Chem. Lett.*, 1985, **9**, 1367-1370.

20. Z. Shao, W. Yang, Y. Cong, H. Dong, J. Tong and G. Xiong, *J. Membr. Sci.*, 2000, **172**,177-188.

21. Z. Shao, G. Xiong, Y. Cong and W. Yang, *Sep. Purif. Technol.*, 2001, **25**, 419-429.

22. Z. Shao, H. Dong, G. Xiong, Y. Cong and W. Yang, *J. Membr. Sci.*, 2001, **183**, 181-192.

23. P. Zeng, Z. Chen, W. Zhou, H. Gu, Z. Shao and S. Liu, J. Membr. Sci., 2007, **291**, 148-156.

24. L. Ge, W. Zhou, R. Ran, S. Liu, Z. Shao, W. Jin and N. Xu, *J. Membr. Sci.*, 2007, **306**, 318-328.

25. L. Ge, R. Ran, K. Zhang, S. Liu and Z. Shao, *J. Membr. Sci.*, 2008, **318**, 182-190.

26. H. Daisuke, T. Atsuko, T. Shinya, H. Takashi and S. Mitsuru, *Solid State Ionics*, 2005, **176**, 881-887.

27. W.C. Chueh, Y. Hao, W. Jung and S.M. Haile, *Nat. Mater.*, 2012, **11**, 155-161.

28. K. Zhang, Z. Shao, C. Li and S. Liu, *Energy Environ. Sci.*, 2012, **5**, 5257-5264.

29. X. Tan. N. Liu, B. Meng, J. Sunarso, K. Zhang and S. Liu, *J. Membr. Sci.*, 2012, **389**, 216-222.

30. K. Nomurna, Y. Ujihira, T. Hayakawa and K. Tekehira, *Appl. Catal. A: Gen.*, 1996, **137**, 25-36.

Chapter 10: Conclusions and Recommendations

10.1 Conclusions

In this thesis, various ceramic membranes with novel configurations including the external short circuit, internal short circuit and surface protective layer by shell structure were designed and experimentally verified for oxygen (or hydrogen) permeation aiming to improve the membrane stability to withstand the acid gases like CO_2 or reducing gases like CH_4 at high tempertaures. With detailed structural and property characterizations, the permeation performances and stability of these ceramic membranes were carefully investigated. Through these studies, several general conclusions can be made as below.

10.1.1 Novel CO_2-tolerant ion-transporting ceramic membranes with external short circuit for oxygen separation at intermediate temperatures

- An external short circuit structure was added on these robust ion conducitng fluorite oxide of $Sm_{0.2}Ce_{0.8}O_2$ (SDC) membranes to realize the mixed electronic and oxygen ion conducting function for oxygen separation. The SDC membrane with external short circuit structure showed high oxygen fluxes, especially at lower temperature.
- Significant oxygen performance stability was observed during the long term test under CO_2 containing atmosphere.

10.1.2 Enhanced oxygen permeation performance of CO_2 tolerant ion conducting membrane with easily sintered bismuth-based oxide

- Based on this novel membrane configuration with the external short circuit, fluorite oxide $Y_{0.25}Bi_{0.75}O_2$ (YSB) with higher ionic conductivity was used as the membrane bulk material for better oxygen permeation performance.
- The improved oxygen flux through the external short circuiting YSB membrane was achieved.

- The YSB membrane showed excellent permeation stability under the CO_2 and H_2O environment.

10.1.3 CO_2-tolerant ceramic membrane driven by electrical current for oxygen production at intermediate temperatures

- The external electrical current was applied on the SDC membrane to drive the high oxygen flux. Super-high oxygen fluxes could be achieved by simply adjusting the external electrical current.
- Stable oxygen flux could be obtained within the CO_2 containing atmosphere due to high resistance from the robust SDC membrane.

10.1.4 Robust ion-transporting ceramic membrane with an internal short circuit for oxygen production

- Another novel membrane design with the internal short circuit for oxygen separation under the mixed conducitng function was studied.
- The internal short circuit structure improved the oxygen flux through SDC membrane with high stability against CO_2 atmosphere.
- The internal short circuit structure shows the advantage to scale up the oxygen permeation membrane system in plannar stack design one membrane configuration currently being tested by Air Products.

10.1.5 Highly stable external short circuit assisted-oxygen ionic transport membrane reactor for carbon dioxide reduction coupled with methane partial oxidation

- The external short circuiting SDC membrane was successfully applied as membrane reactor for CO_2 reduction coupled with methane partial oxidation.
- CO_2 reduction efficiency achieved as high as 10% by optimizing membrane structure with supported thin film.

- The membrane reactor with the modified SDC membrane maintained its stable performance during 100 h long term operation.

10.1.6 External short circuit-assisted proton conducting ceramic membrane for H_2 permeation

- The concept of external short circuit was expanded to proton conducting membrane like $BaZr_{0.1}Ce_{0.2}Y_{0.7}O_{3-\delta}$ (BZCY) and $BaZr_{0.3}Ce_{0.6}Y_{0.1}Zn_{0.05}O_{3-\delta}$ (BZCYZn) for H_2 separation. .
- The hydrogen permeation fluxes have been improved due to the faster electronic conduction realized by external short circuit structure.
- The introduction of water vapour in the down stream could increase the hydrogen flux through the membranes.
- The BZCYZn membrane possessed more stable hydrogen flux under CO_2 atmosphere.

10.1.7 High performance BSCF membranes shelled by SDC film

- The fluorite SDC layer was successfully coated on the perovskite BSCF membrane surface;
- The oxygen flux was increased due to the faster oxygen exchange rate taking place on SDC membrane surface;
- The BSCF membrane coated with the SDC protective layer had an excellent permeation stability under CO_2 gas.

10.2 Recommendations

1. This study was mainly focused on developing novel membrane configurations with high stability and permeation flux on the basis of the well-known fluorite oxide of SDC. Other efforts such as developing new membrane materials or

tailoring membrane material composition can be considered to further improve membrane permeation performances.

2. In addition to the membrane development with high stability, lowering its operation temperature is also another target for future work. If operated at low temperatures (<400^{o}C), the usage of cheap stamped stainless steel interconnects and polymeric seals is possible. In addition, rapid start-up and repeated thermal cycling becomes allowable. These are critical important for the realization of membrane permeation system applications. Therefore, further studies on developing new membranes that can be operated at lower temperature becomes more and more imperative.
3. Other promising applications of these robust ceramic membranes lie in the areas of gas production and conversion. Combined with various industrial processes, these membranes have potentials to do many taskes including CO_2 capture and hydrocarbon conversions. Therefore, to develop membranes with good stability not only against CO_2 but also against other gases like SO_2, and coke formation is highly needed for our environmental sustainable development by re-balancing our carbon cycle.
4. Except from the direct oxygen separation or production, the ceramic membranes can play a lot of games as the membrane reactors for various chemical conversions and reactions. Therefore, for further study, it is worthy a shot to use these tough ceramic membranes into valuable chemicals conversion, such as C_2H_x synthesis from CH_4 or even from H_2O and CO_2, and pollution control, such as NO_x reduction to N_2 and O_2.
5. Computational simulation and calculation can be employed to further understand the effects on oxygen transport through the membrane to give some clues and guideline towards the membrane material composition and structure design.